Theory of Explosions and Detonations for a Three-Step Chain-Branching Chemistry Model

by

Nabeil Maflahi

A thesis submitted to
The University of Birmingham
for the degree of
Doctor of Philosophy

School of Mathematics
The University of Birmingham
August 2005

Abstract

A three-step kinetics scheme is used to model chain-branching reactions but also thermal reactions that are traditionally modelled using a one-step scheme. The chain-branching crossover temperature T_B is adjusted to accommodate for the different reaction types. Two main scenarios are considered: a homogeneous reactive gas in a closed vessel, and the initiation of detonation waves in a tube induced by a shock that is driven either by a piston or a contact. In the homogeneous scenario, the reaction behaves more and more like a chain-branching reaction the smaller T_B is below the initial temperature (unity in our non-dimensionalized scales). For $T_B > 1$ however, heat is released from the outset, and the reaction proceeds in a thermal manner similar to what occurs with one-step schemes. It is shown how the three-step scheme can be matched to widely used two-step and one-step models in the cases $T_B < 1$ and $T_B > 1$ respectively. With piston-driven shock-induced detonations and for $T_B - 1$ sufficiently large, we reproduce situations similar to those which occur with one-step thermal schemes. For $T_B \sim 1$, both thermal and chain-branching effects are witnessed. With T_B sufficiently below unity, chain-branching is very prominent from the outset, and since no secondary shock is formed, the situation is unlike what usually occurs with one-step thermal schemes, but is in good agreement with predictions of a simplified two-step chain-branching model. The major qualitative difference when using an acoustically permeable contact discontinuity to drive the shock instead of a piston occurs when $T_B - 1$ is sufficiently large, where we witness the temperature maximum and the fuel minimum move away from the driving surface.

To My Wife and Family

Acknowledgements

My greatest appreciation goes to my supervisor, Gary Sharpe, who has been a constant support throughout my research, no matter how frivolous my questions were. I am also grateful to my co-supervisor John Billingham for providing guidance with the asymptotics. Acknowledgement is also due to the EPSRC and the University of Birmingham School of Mathematics for funding this research. Finally, thank you to my wife and family who have had to put up with my awkward working hours.

Contents

List of Figures

Chapter 1

INTRODUCTION

1.1 Thermal and Chain-Branching Explosions

When talking about explosions, one usually envisages a chemical reaction of utmost brevity, ignited by an external device (e.g. electric spark, flame) and resulting in a large release of thermal energy. Spontaneous explosions, however, occur without the aid of external initiating devices. These are either thermal explosions (whereby the heat generated is the main contributor in the increase of the rate of reaction, thereby generating more heat, and so on) or branched-chain explosions. Although the main focus of this work is on branched-chain explosions, I will also consider situations, using the same model, where very little chain-branching occurs and so the reaction is actually thermal.

A branched-chain explosion is one where the fuel is converted into stable products via intermediary reactions (known as propagation reactions). Fuel is transformed into chain carriers (sometimes referred to as radicals) in the initiation reaction, which are then either involved in propagation and branching reactions which create more chain carriers, or are converted into stable products via termination or recombination reactions. It is the competition between these propagation and termination reactions that determines the type of explosion. If the conditions are right for propagation to be dominant, then we end up with a branched-chain explosion, otherwise we may well witness a thermal explosion

instead.

Probably the most common example used when describing branched-chain reactions is that of Hydrogen-Oxygen combustion. The most important steps of which are

1. Initiation

$$H_2, O_2, M \rightarrow H, O \text{ or } OH \tag{1.1}$$

2. Propagation and Branching

$$H + O_2 \rightarrow OH + O \tag{1.2}$$

$$O + H_2 \rightarrow OH + H \tag{1.3}$$

$$OH + H_2 \rightarrow H_2O + H \tag{1.4}$$

3. Termination

$$H + H + M \rightarrow H_2 + M \tag{1.5}$$

$$H + OH + M \rightarrow H_2O + M \tag{1.6}$$

$$H + O_2 + M \rightarrow HO_2 + M \tag{1.7}$$

(M is any of the other species present) [1].

The *initiation* reaction converts fuel into chain carriers (in the above example this corresponds to H_2 and O_2 molecules being converted into H and O atoms and the hydroxyl radical OH in equation (1.1)). The *propagation* reaction then combines these chain carriers with remaining fuel to produce more chain carriers. If, as in hydrogen-oxygen combustion, there is a net increase in the number of chain carriers, then we call this a *branching* propagation reaction. In one cycle of the above branching reactions, one H atom results in two H atoms (i.e. a net increase of one), and hence in a chain of only fifty cycles each original H atom grows to 2^{50} or about 10^{15} H atoms! Of course there

must be an inhibitor to this growth in chain carriers, and this is partly achieved by the *termination* reaction which converts chain carriers into stable products (such as H_2O in equation (1.6)). Branching is of course also inhibited by the amount of fuel left, but which process of inhibition is most dominant or which one starts first will depend on the parameters in the problem.

Prior to 1965, thermal and chain-branching explosions were treated quite independently [2]. Thermal reactions were regarded as driven strictly by the self-heating produced by the exothermicity of the reactions. On the other hand, chain-branching explosions were modelled as isothermal phenomena, and autocatalysis occurred strictly because of the formation of highly reactive chain carriers which can react to produce more such species. Neither type models most chemical reactions in fuels such as Hydrogen-Oxygen and hydrocarbon mixtures very well, and in 1965 Gray and Yang [2] initiated the modern studies of a unified theory which recognizes that when branching reaction rates become appreciable, some self-heating is inevitable. Their work concentrated on criticality issues rather than the time histories of the reactants and the temperature, and contained a phase plane analysis which was used to study singular points in the temperature-chain carrier plane. Nowadays, when chain-branching reactions are considered, the termination reaction is regarded as highly exothermic and dependant upon chain carrier concentration, as is the case in reality [1, 3, 6, 7, 11, 13].

It is characteristic that the rate coefficients for chemical reactions depend strongly and nonlinearly on the temperature. According to the Arrhenius law [3], this temperature dependence is described by

$$k = A \exp\left(-\frac{E}{RT}\right), \tag{1.8}$$

where A is a *pre-exponential frequency factor*, R is the universal gas constant, and E is the *activation energy* of the reaction and corresponds to an energy barrier which has to be overcome. Although in general, A is actually a function of the temperature T, it is sufficient for most purposes in combustion to regard it as a constant [3]. E tends to be

very large for initiation and branching reactions, and so much work on combustion (including part of this work) exploits this fact by tackling the equations using high activation energy asymptotics. Termination reactions on the other hand tend to have a very small temperature dependence, and as such k is either made a constant or is made to depend algebraically on T rather than exponentially for such reactions [4].

Thermal reactions are typically modelled using one-step Arrhenius kinetics, which sees fuel F being converted into stable products P in a single first-order reaction

$$F \rightarrow P. \tag{1.9}$$

Most work in the field of combustion theory has, especially in the past, concentrated on the one-step scheme. Such work was, and still is, instrumental in the advancement of the theory of combustion and in the development of diagnostic tools to help analyse the results, such as the use of 'pressure against specific volume' phase planes [5] which we use to classify the evolution to detonation. In practise however, most chemical reactions which are of interest cannot be accurately modelled using one-step kinetics, but require some type of chain-branching mechanism to capture the essential features of these reactions. The initiation, branching and termination steps of chain-branching reactions mentioned above are typically modelled using the following general three-step scheme [6, 7, 8] , which I too shall use.

1. Initiation

$$F \xrightarrow{R_I} Y \tag{1.10}$$

2. Branching

$$F + Y \xrightarrow{R_B} 2Y \tag{1.11}$$

3. Termination

$$Y \xrightarrow{R_C} P \tag{1.12}$$

Here Y represents chain carriers and R_I, R_B and R_C represent the specific reaction rates for the reaction steps (1.10), (1.11) and (1.12), respectively. Initiation and termination are represented by first order equations, whereas branching requires a second order equation since it can only occur with the collision of fuel and chain carrier particles. We notice a net increase of one chain carrier in the branching reaction.

Probably the most important feature in most chemical explosions is the existence of an *ignition-delay time* or *induction time* which is the time it takes for a spontaneous explosion to occur for given initial values of temperature, pressure and chemical composition. This time can be as long as several hours or as short as microseconds, during which there is a slow buildup of chain carriers formed by the initiation reaction from fuel. Part of this work will be concerned with determining induction times for various values of the *chain-branching crossover temperature* T_B, which is the temperature at which the chain-branching reaction rate is of the same order as the termination reaction rate. If enough chain carriers are produced to kick-start the branching reaction and the termination reaction cannot consume the chain carriers at a fast enough rate, then a chain-branching explosion occurs which sees the fuel being converted into chain carriers at an exponentially large rate. Unlike thermal explosions though, this branching explosion does not release significant amounts of heat. Practically all the heat release occurs after the branching explosion in a zone dominated by the strongly exothermic termination reaction which converts the chain carriers into stable products. See figure 1.1.

The initiation and branching reactions are roughly thermally neutral, but some heat is still released in the induction and branching zones by the termination reaction (1.12). This heat release however is very small compared to that which occurs after the chain-branching explosion when chain carrier concentration reaches its peak.

As mentioned earlier, it is the competition between the branching and termination reactions which determines the outcome of the reaction. If branching dominates (at least for a while) then a chain-branching explosion may well occur. If it is weak, then

Figure 1.1: Time behaviour of a typical chain-branching explosion in an adiabatic system

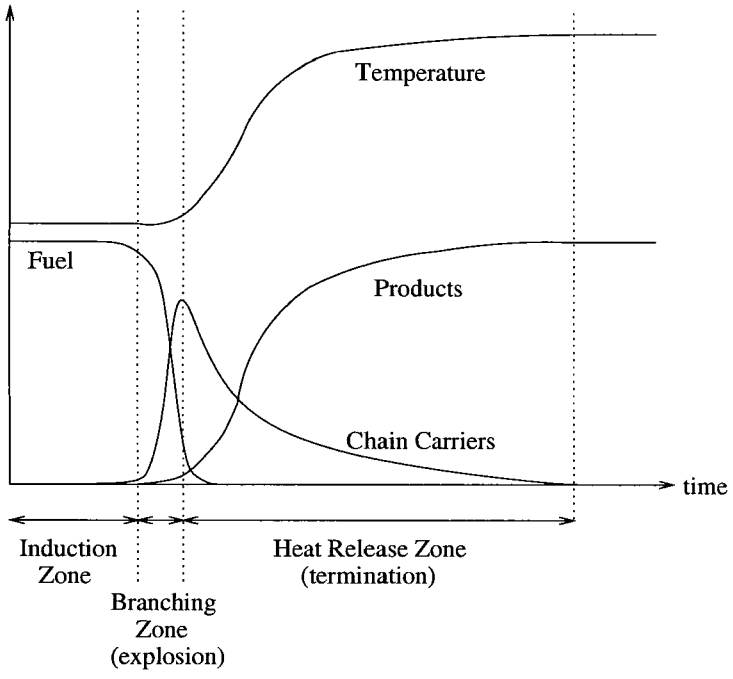

the termination reaction will simply consume any chain carriers as soon as they are produced. The result will then be that the chain-branching explosion is suppressed, delayed or eliminated altogether. If the branching reaction is very weak, then a chain-branching explosion will not occur, and the outcome will be more like a thermal explosion as in figure 1.2. Here, we no longer have the three distinct zones typical of chain-branching explosions. Instead, the induction zone is now releasing heat, and the explosion (i.e. the rapid consumption of fuel) results not in the buildup of chain carriers but in the rapid buildup of products and in the associated rapid heat release.

The T_B parameter described earlier will potentially allow me to describe reactive systems varying from the nearly purely chain-branching to the nearly purely thermal.

This thesis will investigate chain-branching explosions in three parts: the homogeneous, closed vessel scenario, piston-driven shock-induced initiation of detonation waves, and contact-driven shock-induced initiation of detonation waves.

Figure 1.2: Time behaviour of a typical thermal explosion in an adiabatic system

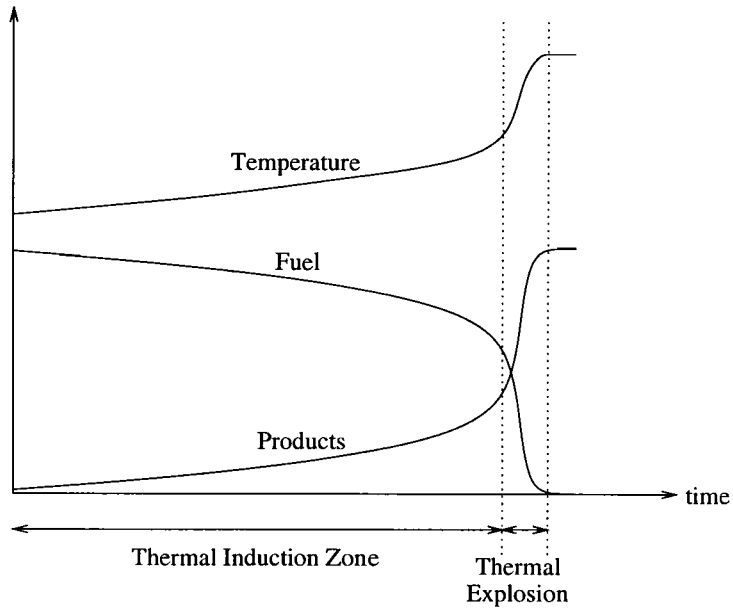

1.2 Homogeneous explosions

To best understand how chain-branching explosions develop, I shall begin by investigating them in a spatially homogeneous reactive mixture inside a constant volume closed adiabatic vessel. The notion of a well-stirred closed vessel implies that the whole volume is simultaneously involved and hence we can disregard propagating combustion waves [3]. Such setups but with heat loss to the cooler vessel wall were first considered for thermal explosions by Semenov [9] in 1935, and later by Frank-Kamenetskii [10] in 1955. Semenov's work assumed uniform (i.e. homogeneous) temperatures throughout the vessel and a Newtonian heat transfer law, whereas Frank-Kamenetskii considered the more realistic law of Fourier that allows for diffusion of heat to the vessel wall, and hence non-uniform temperatures.

Homogeneous chain-branching explosions were dealt with in 1978 by Kapila [11] in an attempt to develop a theory analogous to that of Kassoy's [12] complete solution to the thermal explosion problem two years earlier. Both pieces of work treated the problem asymptotically in the realistic limit of high activation energy. Kapila's work

gave a complete time history of the chain-branching explosion and also derived a critical value of a parameter based on the branching rate relative to the termination rate, below which a fizzle reaction occurs and beyond which an explosion occurs. The time history of the explosion is shown to consist of the three temporal zones described earlier. Kapila, however, does not use the three-step scheme already mentioned but does away with the initiation reaction after assuming that a small concentration of chain carriers is already present in the starting mixture.

The effects of *dissociation* (breaking up of the stable species produced by the propagation reactions) and the effects of the subsequent *recombination* (reverse of dissociation) were included by Birkan and Kassoy [1] in a five-step kinetic scheme. In Hydrogen-Oxygen combustion, these added reactions can be written as

$$H_2O, H_2, M \leftrightarrow H, OH, HO_2, \tag{1.13}$$

where dissociation is the forward reaction and recombination the reverse. Using data from a typical Hydrogen-Oxygen system at a temperature of 500K, they calculate from their results a long induction time of about 0.3ms, a brief chain-branching explosion time of about 0.06μs and a heat release zone of about 1.2μs. Major dissociation only comes into effect about 20μs after the temperature reaches nearly its maximum value, owing to the very high activation energy of the dissociation reaction. The recombination process only becomes important when the temperature approaches the final equilibrium state, which is found to be much less than the maximum attainable temperature due to the endothermicity of the dissociation reaction.

More recently in 2000, Bonilla et al. [13] investigated chain-branching explosions using the ratio ε of the characteristic chemical time of the short branching zone to that of the long termination zone as an asymptotically small parameter. They argue that this is a more natural choice than Kapila's high activation energy analysis (where the small parameter is scaled directly with the initial temperature) when dealing with initial temperatures

sufficiently above the branching crossover temperature. Like Kapila's approach, they use a two-step scheme by assuming an arbitrarily small initial chain carrier concentration ν, but explain that for more accuracy in the limit $\varepsilon \to 0$ they need an additional straining of the time coordinate when ν is very small.

Currently in review, is a paper by Blythe, Kapila and Short [14] that considers the full three-step homogeneous problem for various values of the T_B parameter in the asymptotic limit of high activation energy. Although focus is primarily on values of T_B at and close to the initial temperature (i.e. $T_B = 1,\ 1+\epsilon,\ 1+\epsilon\ln(\epsilon)$, where ϵ is the inverse activation energy of the branching reaction), they also consider the two more general cases, $T_B - 1 = O(1) < 0$ and $T_B - 1 = O(1) > 0$ as $\epsilon \to 0$, that we have also considered here. A basic conclusion that can be drawn from their work is that both thermal and chain-branching effects are witnessed in the explosion region of the solution for values of T_B close to unity. For T_B sufficiently far below or above unity, both this thesis and Blythe et al. find that the reaction proceeds in a predominantly chain-branching or predominantly thermal manner, respectively. All the homogeneous problem asymptotics presented in this thesis were carried out independently before the Blythe et al. paper was submitted.

In chapter 2, I shall investigate homogeneous explosions from initiation up until termination when the temperature reaches its maximum, using a combination of numerics and asymptotics. I shall give complete time histories of the reactions, determine the time to explosion and compare my numerical results with the asymptotics where they exist. Like Kapila [11], I shall use the large activation energy of the branching reaction as an asymptotically large parameter. However, since I will be using a three-step scheme (as opposed to Kapila's two-step scheme) I will use the large activation energy of the initiation reaction as another asymptotically large parameter, but one that is much larger than that of the branching reaction (as tends to be the case in reality [3]). Like Kapila [11] but unlike Birkan and Kassoy [1], I shall disregard the effects of dissociation and recombina-

tion. Both these reactions have activation energies which are so large that by the time the temperature becomes sufficiently high the chain explosion (if any) will have already occurred.

An important aspect of this present work, as already mentioned, is the ability to accommodate for different reactions which vary from the nearly purely chain-branching to the nearly purely thermal. As we shall see, this can be done by adjusting the branching crossover temperature T_B appropriately. A matching procedure will also be carried out to match parameters from our three-step model to those from the widely used one-step and two-step models where it is appropriate to do so.

1.3 Shock-induced initiation of detonations

A shock wave, as the term suggests, is a wave where there are sudden and large changes across the wave front. These changes are in the temperature, pressure, density and fluid velocity of the supporting medium which in our case is a reactive gas, but is just as applicable in condensed phase explosives. Shock waves are very different to ordinary sound or acoustic waves, for which there are only small amplitude longitudinal displacements of molecules, no net flow of gas and where any physical changes in the gas are small and reversible. The velocity of such acoustic waves, termed the local sound speed of the gas, is determined by the collision rate between the gas molecules and so is primarily determined by the temperature of the gas [15].

A different situation arises when a disturbance is driven through the gas at a speed larger than the local molecular velocity. Analogous to the formation of a bow-wave in front of a ship, pressure, temperature and density all build up ahead of the disturbance or wave front. Such a wave is known as a shock wave. The driving mechanism might be a solid piston travelling at some constant velocity into the gas (chapter 3) or a contact discontinuity (chapter 4). Ahead of the shock wave, the reactive gas is motionless and spatially uniform, and is at a low enough temperature such that we can regard the gas

as chemically inert. As the shock wave passes through the gas, it immediately heats the gas in its wake to a temperature that is high enough for the gas to begin reacting at a noticeable rate, thus igniting, or detonating, the gas as it moves.

Since we are concerned with shock-induced ignition it makes sense to clarify the two main combustion processes associated with gas flow: slow combustion and detonation [16]. With these waves, the combustion of the gas is necessarily accompanied by motion of the gas. Hence the process of combustion here is not only a chemical phenomenon but also one of gas dynamics, and so the outcome has to be determined by solving simultaneously the nonlinearly coupled equations describing the chemical kinetics of the reaction and the gas dynamics of the mixture. On the other hand, the homogeneous closed vessel situation only requires us to solve the equations describing the chemical kinetics of the reaction.

In slow combustion, the velocity of propagation of combustion in the gas depends on the amount of heat transfer from the combustion zone to the unburnt gas mixture. The main mechanism of heat transfer is ordinary conduction [16], hence such combustions waves, known as deflagrations or flames, travel subsonically. The pressure and density across a deflagration both decrease, and hence this type of combustion wave is expansive.

Detonations, however, are more violent in nature, but based on the number of papers written, have probably not been studied as much as deflagrations. In simple one dimensional theory, a (strong) detonation wave can be regarded as a very strong shock wave closely followed by an exothermic reaction capable of providing enough energy to sustain the wave. It is generally far more destructive than the original shock wave used to ignite it owing to the presence of more energy from the reaction, and the continuous initiation of chemical combustion by the adiabatic compression and heating of the gas behind the shock front [17]. Unlike a flame or deflagration, a detonation wave travels supersonically with respect to the fuel ahead of the wave. Also, whereas flames and deflagrations are expansive, (strong) detonation waves, by virtue of the integral shock wave, are necessarily highly compressive.

In chapter 3, I shall be investigating piston-driven shock-induced ignition in a reactive gas using the three-step chain-branching scheme as in our study of the homogeneous closed vessel scenario. Several different cases will be considered based on different values of the chain-branching crossover temperature T_B. This crucial parameter, which as we shall see in the homogeneous problem controls the ratio of the induction length to the termination zone, will determine how the detonation wave will develop. Short and Quirk [7] used T_B as a bifurcation parameter in studying the nonlinear stability of a detonation wave for the three-step chain-branching reaction, and also determined a detonability limit value of T_B beyond which the detonation fails.

In 1982, Abouseif and Toong [18] carried out numerical studies using a one-step thermal model in a piston-tube setup. They were able to predict threshold values of energy necessary for the direct initiation of detonations, and they did this by stopping the piston after a finite time and seeing whether the shock decayed or developed into a detonation. Jackson and Kapila [19] mention that their work in 1985 appears to be the first to apply a systematic asymptotic procedure to shock-induced ignition with the one-step thermal model. The main purpose of their work was to describe the state of the gas between the piston and the shock and to determine how much the chemical heat release accelerates the shock, up to the instance of thermal runaway at the piston.

Dold, Kapila and Short [20] presented, based on large activation energy asymptotic arguments, the evolution of detonations for the one-step model subsequent to runaway at the piston. The reaction wave begins as a shockless 'weak detonation' that travels supersonically at every point in its structure. They place emphasis on the correct use of the term "propagation" of reaction waves, and stress that these weak detonations are not self-propagating since characteristics cannot travel faster than the local sound speed and hence cannot travel faster than the weak detonation. However, as soon as this weak detonation wave slows down to and below the *Chapman-Jouget* (CJ) speed (the speed at which a point at the rear of the wave - the CJ point - becomes sonic), information

can then begin to travel faster than the wave giving rise to a shock wave near the CJ point. The shock wave overtakes and engulfs the weak detonation, and since it increases the sound speed of the material in its trail it is able to sustain genuine propagation. The reaction wave is thus transformed from a weak detonation to a 'strong', self-propagating, *Zeldovich-von Neumann-Döring* (ZND) detonation.

Since a large majority of chemical reactions are actually chain-branching, an asymptotic study by Dold and Kapila [6] was conducted to compare the already well known theoretical evolution to detonation under a one-step model with the evolution to detonation under a three-step chain-branching scheme. Although they only investigated the very early time behaviour under these two schemes, they were able to highlight fundamentally different types of reaction waves that can emerge at the end of an induction period for the different models. Such results are verified by some experimental observations carried out for example by Strehlow [4]. The asymptotic study showed that the reaction wave which emerges travels subsonically away from the piston. Hence, in contrast with the one-step results, disturbances are able to overtake the reaction wave from the outset, and thus the reaction wave is self-propagating from the outset.

A far more comprehensive piston study to determine the differences between shock ignition in one-step thermal and chain-branching models was conducted recently by Sharpe [21] using a combination of numerical and asymptotic techniques. Since the main aim was to establish the major qualitative differences, Sharpe used a simple, but widely used, two-step model rather than the more elaborate three-step model used in this thesis. Chain-initiation and chain-branching are represented in the induction step, which is isothermal but temperature sensitive, and which ends with a complete and instantaneous transformation of fuel into chain carriers rather than the finite (but exponentially thin in the limit of high activation energy) explosion time one gets with the three-step model. The second step then represents the exothermic termination reaction. The transition or ignition point is defined as the point which marks the end of the induction zone and the start of the

termination zone. He considers three cases: when the rate of heat release in the termination reaction is slow, comparable and fast as compared to the initial induction time (i.e., when the termination zone is long, comparable and short as compared to the initial induction time, respectively). To achieve these different cases, he uses different values of a parameter k, which he defines to be the ratio of the termination reaction rate to that of the induction step, and hence plays a similar role to our T_B. In all cases, and as Dold and Kapila [6] previously revealed, the transition point is found to initially travel at a subsonic speed. In the case of fast heat release, a secondary shock forms quickly near the piston (without involving a weak detonation, as it does in the one-step model) and develops into a strong detonation. With a moderate heat release, the secondary shock forms much closer to the leading shock and only develops into a strong detonation after it collides with the leading shock. For low rates of heat release, although the reaction wave or transition point is continually accelerated, a secondary shock cannot form quickly enough before the pressure disturbances catch up with the leading shock, a situation completely unlike what occurs with the one-step model, unless the initiating shock is sufficiently strong [22].

Varying T_B will allow me to accommodate for situations which are truly chain-branching and also situations which bear resemblance to one-step thermal models. But since T_B, as we shall see, also controls the ratio of the induction zone to the termination zone, we can compare our results with those of Sharpe's two-step study.

In all the above cited cases of shock-induced ignition, the driving force has been a piston (or some equivalent system such as shock reflection off a rear wall). This entails a symmetric boundary condition at the piston face which reflects all acoustic disturbances back into the reactive mixture, thus enhancing chemical reaction. The situation is different when, rather than a solid piston, we have a contact surface driving the shock wave through the reactive material. This can be seen in some cases of deflagration-to-detonation

transition (DDT), where an accelerated flame produces two shocks that merge to generate a strong transmitted shock and a driving contact surface [23]. It is also known that the rupture of a diaphragm, which initially separates two gases of very different densities, results in the generation of a strong shock and a driving contact surface [15].

Being a gas-dynamical phenomenon, the contact surface is acoustically permeable, allowing acoustic disturbances emanating from the reaction zone ahead to be transmitted through the contact surface. This undoubtedly means that, depending on how permeable the contact is, the exothermic reaction ahead cannot be as vigorous as in the piston case. Furthermore, according to numerical [24] and analytical [25] findings for the one-step case, both in the high activation energy asymptotics limit, ignition is found to take place away from the contact surface, whereas with piston driven situations ignition always begins at the piston face owing to the intuitive reason that this is where the gas has been hottest for longest. The reason Short and Dold [24] and Parkins [25] give for the offset of the ignition point in contact-driven systems is that the temperature maximum moves off the contact surface and into the gas ahead owing to acoustic leakage through the permeable contact surface. Both these papers link the acoustic permeability, α_0, of a contact surface to its strength (i.e. the ratio of densities across the contact), and allow the piston problem to be recovered by taking $\alpha_0 \to \infty$. For finite $\alpha_0 > 1$, there will always be some transmission of disturbances through the contact, and for $\alpha_0 = 1$ there is no reflection and all disturbances pass through the contact (note then that here a density and temperature discontinuity no longer exists). The case $\alpha_0 < 1$ is physically unattainable with a contact arising out of a shock-merging setup (as is the case in [24], [25] and in this thesis too).

Contact-driven shock-induced detonations can also occur in condensed phase (solid or liquid) explosives. These scenarios are relevant to the issue of safe storage and handling of highly reactive materials, and have been studied using various experimental techniques. Gustavsen, Sheffield, Alcon and Hill [26], for example, fire a planar projectile from a gas gun at high speed into an initially stationary solid explosive sample in order to compare

the shock sensitivity of newly pressed explosive with explosive pressed 17 years earlier. In a similar experiment, Gustavsen, Sheffield and Alcon [27] compare the shock sensitivity of two different formulations of the same explosive. The resulting Riemann problem in these types of experiments involves the transmission of a planar shock wave into the explosive as well as a planar shock wave back into the projectile, with the contact surface generated at the impact (material) interface.

The aforementioned papers on contact-driven gaseous systems ([24] and [25]) assume one-step Arrhenius chemistry, and involve high activation energy asymptotic studies up to thermal runaway (Short and Dold [24] use a numerical method to solve the leading order asymptotic equations). However, it does not appear that highly resolved numerical simulations of the full evolution for finite activation energies have been performed, even for the one-step model. In chapter 4, we will perform a numerical investigation into how the same contact-driven system would evolve under the three-step Arrhenius model, for various values of the T_B parameter. It is expected that for values of T_B which lead to one-step behaviour in the homogeneous vessel scenario, we will see some of the effects from [24] and [25] appearing in our three-step model. Also, a high activation energy asymptotic study using the chain-branching two-step model is conducted in order to provide insight into what may be expected in the three-step model when using chain-branching values of T_B. The asymptotic results can then also be compared with Sharpe's asymptotic study of the two-step *piston*-driven shock case [21] in order to determine the differences when we use a contact as opposed to a piston to drive the shock.

Chapter 2

HOMOGENEOUS CLOSED VESSEL EXPLOSIONS

2.1 The mathematical model

Consider a well-stirred, insulated, constant volume vessel filled with a single reactant (fuel), F (figure 2.1). The *well-stirred* condition ensures we have a diffusionless, spatially homogeneous vessel so that the concentrations of reactants do not depend on position. Temperature is also the same throughout the reactive mixture. Hence we are dealing with ordinary differential equations rather than partial differential equations.

We shall make the following additional assumptions:

1. Although the initiation reaction has a high activation energy, it is assumed to be thermally neutral (it is actually very slightly endothermic) [1].

Figure 2.1: The mechanically stirred, closed vessel.

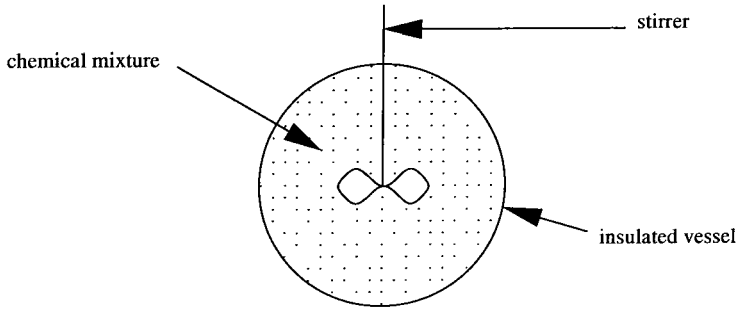

2. The propagation reaction is also assumed to be thermally neutral. This is a realistic assumption since for example in Hydrogen-Oxygen systems, the propagation reactions only contribute five percent of the total heat release. It also has a high activation energy, but much smaller than that of the initiation reaction. [1, 11]

3. Termination is strongly exothermic, and is assumed to have a zero activation temperature. In reality, it is very weakly dependent on temperature. [1, 3, 11]

Attempting to model a real chain-branching reaction exactly, such as the Hydrogen-Oxygen combustion example given in (1.1)–(1.7), would not only be extremely cumbersome but the results would be particular to the specific fuel and initial conditions. Instead, I shall use the generic three-step kinetic scheme (1.10)–(1.12) which models the essential physical characteristics of a chain-branching explosion. The non-dimensionalized reaction rates, modelled using the Arrhenius law, are:

$$R_I = k_I f \exp\left(\frac{-1}{\varepsilon_I T}\right), \tag{2.1}$$

$$R_B = k_B \rho f y \exp\left(\frac{-1}{\varepsilon_B T}\right), \tag{2.2}$$

$$R_C = k_C y, \tag{2.3}$$

where f and y are the mass fractions of fuel and chain carriers respectively, ε_I and ε_B are the inverse activation temperatures of initiation and branching respectively, ρ is density (which is constant) and k_I, k_B and k_C are the rate constants. Mass conservation tells us that

$$f + y + z \equiv 1$$

where z is the mass fraction of product.

Our equations are non-dimensionalized using the scalings

$$\begin{aligned} \rho = \frac{\tilde{\rho}}{\tilde{\rho}_0}, \quad T = \frac{\tilde{T}}{\tilde{T}_0}, \quad t = \tilde{k}_C \tilde{t}, \quad \varepsilon_I = \tilde{T}_0 \tilde{\varepsilon}_I, \quad \varepsilon_B = \tilde{T}_0 \tilde{\varepsilon}_B, \\ k_I = \frac{\tilde{k}_I}{\tilde{k}_C}, \quad k_B = \frac{\tilde{k}_B}{\tilde{k}_C}, \quad k_C = \frac{\tilde{k}_C}{\tilde{k}_C} = 1, \quad Q = \frac{\tilde{\mu}}{\tilde{R}\tilde{T}_0}\tilde{Q}, \end{aligned} \tag{2.4}$$

where symbols with a tilde denote dimensional quantities, a '0' subscript denotes initial values, Q is the total amount of heat released, R is the universal gas constant and μ is the mean molecular weight. We note that $k_C = 1$, and that $T = 1$ at $t = 0$. We assume that $\rho \equiv 1$.

It is convenient to redefine the rate constants k_I and k_B by defining two new constants T_I and T_B by

$$k_I = \exp\left(\frac{1}{\varepsilon_I T_I}\right), \tag{2.5}$$

$$k_B = \exp\left(\frac{1}{\varepsilon_B T_B}\right), \tag{2.6}$$

so

$$R_I = f \exp\left[\frac{1}{\varepsilon_I}\left(\frac{1}{T_I} - \frac{1}{T}\right)\right], \tag{2.7}$$

$$R_B = fy \exp\left[\frac{1}{\varepsilon_B}\left(\frac{1}{T_B} - \frac{1}{T}\right)\right]. \tag{2.8}$$

The convenience of these two new constants is clear when we look at the orders of R_I and R_B as the temperature T passes though T_I and T_B. Since we are assuming that the overall reaction is exothermic (and hence T is a monotonically increasing function of time) then R_I balances with R_C when $T = T_I$ since the exponential factor in R_I becomes unity - i.e. initiation balances termination. In fact as T passes through T_I, the exponential in R_I changes from being exponentially small to exponentially large. Similarly, and more importantly, R_B balances with R_C when $T = T_B$ i.e. the branching rate balances the

termination rate[1]. For these reasons, T_I and T_B are known as the chain-initiation and chain-branching crossover temperatures respectively [7], and we assume that

$$T_B < T_I. \tag{2.9}$$

Setting $T_I = 3$, as in [7], and assuming that the temperature cannot exceed this value implies that the initiation rate is always exponentially small. This is in physical agreement with typical chain-branching reactions where chain-initiation reactions are energetically inhibited because they have an activation energy greater than the bond dissociation energy [3].

2.1.1 Governing equations

$$\frac{df}{dt} = -f \exp\left[\frac{1}{\varepsilon_I}\left(\frac{1}{T_I} - \frac{1}{T}\right)\right] - fy \exp\left[\frac{1}{\varepsilon_B}\left(\frac{1}{T_B} - \frac{1}{T}\right)\right] \tag{2.10}$$

$$\frac{dy}{dt} = f \exp\left[\frac{1}{\varepsilon_I}\left(\frac{1}{T_I} - \frac{1}{T}\right)\right] + fy \exp\left[\frac{1}{\varepsilon_B}\left(\frac{1}{T_B} - \frac{1}{T}\right)\right] - y \tag{2.11}$$

$$\frac{dT}{dt} = \beta y \tag{2.12}$$

Initial conditions are

$$f(0) = 1, \quad y(0) = 0, \quad T(0) = 1, \tag{2.13}$$

and so initially the reactive mixture consists purely of fuel. The rate of change of fuel (2.10) is governed by the rate at which fuel is consumed by the initiation reaction (first term on the right-hand side) and the rate at which it is consumed by the branching reaction (last term). In the chain carrier equation (2.11), the first two terms on the right-hand side describe the rate at which chain carriers are produced by the initiation and branching reactions, whereas the final term gives the rate at which chain carriers are consumed by the termination reaction.

[1]This is of course assuming that T can ever reach T_I or T_B. e.g. T can never become equal to T_B if $T_B < 1 =$ initial temperature.

To clarify the temperature equation (2.12), suppose initiation, branching and termination release or absorb a total amount of heat Q_I, Q_B and Q_C respectively. Then

$$\frac{1}{(\gamma-1)}\frac{dT}{dt} = Q_I f \exp\left[\frac{1}{\varepsilon_I}\left(\frac{1}{T_I}-\frac{1}{T}\right)\right] + Q_B f y \exp\left[\frac{1}{\varepsilon_B}\left(\frac{1}{T_B}-\frac{1}{T}\right)\right] + Q_C y \qquad (2.14)$$

where γ is the ratio of specific heats (1.4 for air). Now in reality, and in accordance with assumptions (1) and (2), Q_I and Q_B are small. So we assume that $Q_I = Q_B = 0$ and let $Q_C \stackrel{def}{=} Q$, i.e. all heat release occurs in the termination step. Letting

$$\beta \stackrel{def}{=} Q(\gamma-1) \qquad (2.15)$$

then gives (2.12). Another assumption commonly made in this area of work is that γ is constant, i.e. the gas is polytropic. Polytropic equations of state are also actually often used for modelling solid or liquid explosives, but with a value of $\gamma \approx 3$ [28].

One notes that it is possible to deal with the temperature equation straight away as follows:

Adding (2.10) and (2.11) gives

$$\frac{df}{dt} + \frac{dy}{dt} = -y$$

so that (2.12) gives

$$\frac{dT}{dt} = \beta\left(-\frac{df}{dt} - \frac{dy}{dt}\right)$$

which can be integrated to give

$$T = \beta(-f-y) + const.$$

Initial conditions (2.13) give that $const = 1+\beta$ and hence

$$T = 1 + \beta(1-f-y) = 1+\beta z \qquad (2.16)$$

and thus we can eliminate T, leaving us with only two coupled ordinary differential equations in two dependent variables, f and y. This representation may appear to make the process of obtaining a solution (either numerical or asymptotic) simpler, but unfortunately we come across certain difficulties when defining new regions in the asymptotic solution. Hence I shall stick to the original set of equations defined above. What (2.16) does tell us however is the maximum attainable temperature (T_M) in our system. Since the final (burnt) state of our system corresponds to $f = y = 0$, $z = 1$ and $T = T_M$, then

$$T_M = 1 + \beta \tag{2.17}$$

Equation (2.16) also tells us that the temperature T increases linearly with the amount of product z produced.

2.2 Strategies for finding a solution

Looking at our governing equations, the nonlinearities (algebraic and exponential) give us a big hint that attempting to look for an analytic solution would be futile. This is not a surprise though, since in chemically reactive systems, nonlinear problems are more the rule than an exception. This leaves us with two obvious routes: numerics and asymptotics. Getting a computer to solve a system of equations numerically is common practice, but unfortunately, as with many problems in chemical combustion, stiffness problems make the numerics all the more difficult and delicate. These problems arise when "zones of rapid variation occur in the solution due to the presence of several widely disparate spatial and/or temporal scales" [29]. The culprits in our system are the small values of ε_I and ε_B which occur inside the exponentials - resulting in exponentially small or exponentially large values. Modern computing technology has however lessoned the impact of such problems, and numerical solutions are now very commonly produced. Minor underflow problems did still occur when experimenting with very small values of ε_I and ε_B, but

Figure 2.2: Fuel ignition time for various values of T_B, using $\varepsilon_I = \frac{1}{15}$, $\varepsilon_B = \frac{1}{5}$, $Q = 4$, $\gamma = 1.4$, $T_I = 3$.

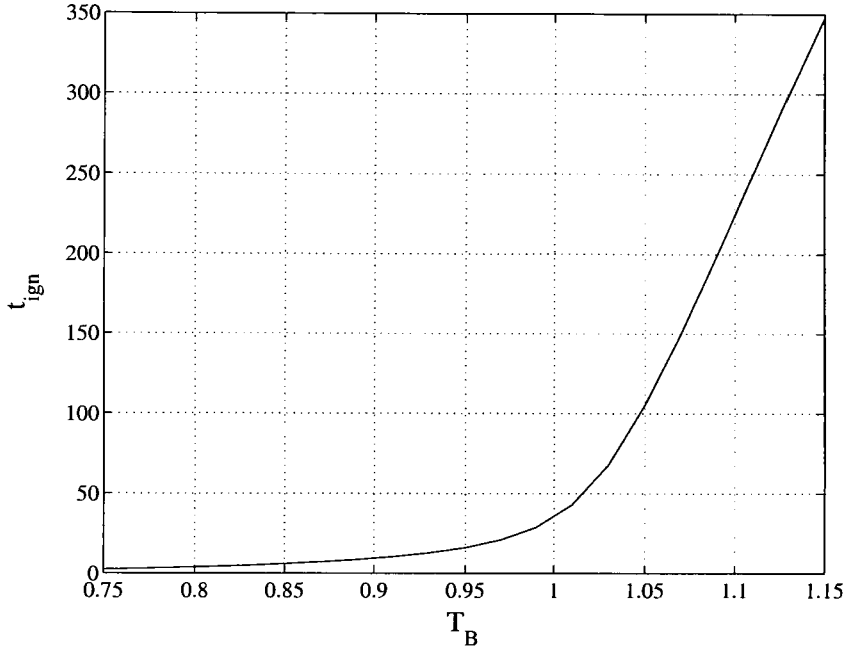

more importantly, no overflow problems were encountered.

Keeping asymptotics in mind, it makes sense to tackle this problem by considering the orders of the exponential factors in (2.10) and (2.11). Since our assumption is that T_I is fixed, our critical factor becomes T_B. At $t = 0$, $T = 1$ and so initially $\exp\left[\frac{1}{\varepsilon_I}\left(\frac{1}{T_I} - \frac{1}{T}\right)\right]$ is exponentially small while $\exp\left[\frac{1}{\varepsilon_B}\left(\frac{1}{T_B} - \frac{1}{T}\right)\right]$ is initially exponentially large, of order one, and exponentially small for $T_B < 1$, $T_B = 1$ and $T_B > 1$ respectively[2]. This critical value of T_B is emphasised in figure 2.2 which was obtained numerically (the ignition time, t_{ign}, in our numerical solutions, is defined as the time it takes for half the fuel, f, to be consumed). Hence, it makes sense to split the problem into at least two categories: $T_B < 1$ and $T_B > 1$.

Whereas the smallness of ε_I and ε_B may be a problem in numerical work, this is precisely what is required for valid asymptotics, hence the numerics and asymptotics

[2]I use the terms "exponentially large" and "exponentially small" loosely here, since for $T_B \approx 1$, $\exp\left[\frac{1}{\varepsilon_B}\left(\frac{1}{T_B} - \frac{1}{T}\right)\right]$ is actually order one.

should complement one another in some respects.

I shall define two new constants which, as we shall see, are ubiquitous in our asymptotic work:

$$e_I \stackrel{def}{=} \exp\left[\frac{1}{\varepsilon_I}\left(\frac{1}{T_I}-1\right)\right], \qquad e_B \stackrel{def}{=} \exp\left[\frac{1}{\varepsilon_B}\left(\frac{1}{T_B}-1\right)\right],$$

where e_I is exponentially small while e_B is exponentially large, of order one, and exponentially small for $T_B < 1$, $T_B = 1$ and $T_B > 1$ respectively.

Where I give numerical results, these will correspond to the following parameter values (unless stated otherwise):

$$\varepsilon_I = \frac{1}{15}, \qquad \varepsilon_B = \frac{1}{5}, \qquad Q = 4, \qquad \gamma = 1.4, \qquad T_I = 3.$$

The algorithm used to numerically solve the equations, is a general fourth order Runge-Kutta routine with adaptive time stepping.

2.3 Exponentially-large branching factor ($T_B < 1$)

In this case, the branching reaction exponential factor $\exp\left[\frac{1}{\varepsilon_B}\left(\frac{1}{T_B}-\frac{1}{T}\right)\right]$ is not only exponentially large initially, but owing to the monotonically increasing temperature T, continues to be so throughout the entire reaction. The whole branching rate term (R_B, or second term in (2.10) and (2.11)) however is initially zero since $y(0) = 0$, and it ultimately dies off as the fuel f is depleted.

2.3.1 Numerical results

The plots in figures 2.3–2.6 are for $T_B = 0.9,\ 0.8,\ 0.6$ and 0.3. As is clearly visible, the solution consists of three distinct temporal regions: an induction region, a very brief explosion region and a thermal region in which all species approach the stable equilibrium. Each figure resembles figure 1.1 of a typical chain-branching explosion in an adiabatic

Figure 2.3: Histories of species and temperature for $T_B = 0.9$.

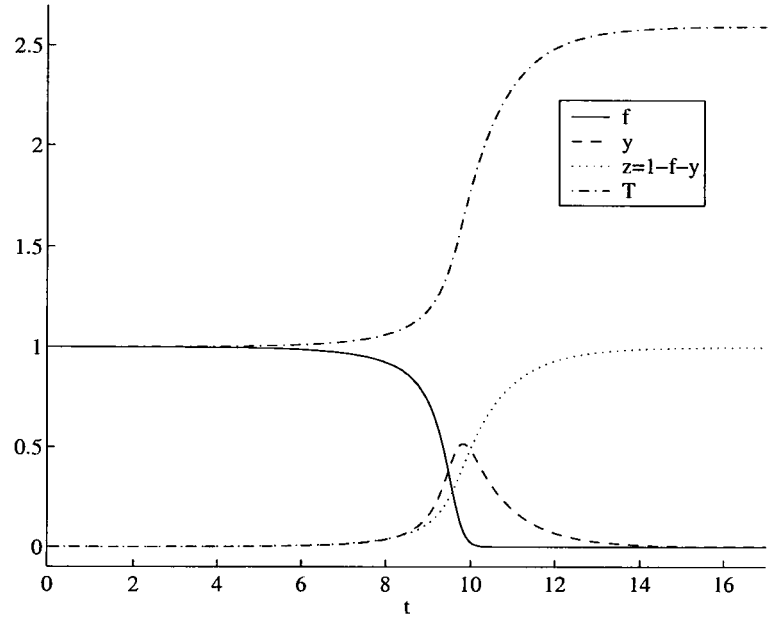

vessel.

The induction region represents a period of time where there is very little perturbation in all dependent variables (f, y, z and T) from the initial state. This region is shorter for smaller T_B (ranging from a time of 1.5×10^{-4} for $T_B = 0.3$ to about a time of 8 for $T_B = 0.9$). The only reaction at work here is the initiation reaction, which is producing chain carriers from fuel at an exponentially small rate. The fact that there are no chain carriers in the system to begin with means that R_B is forced to remain negligible for a period of time. The termination reaction also is dormant in this region for the same reason. As soon as just enough chain carriers have been produced to kick start the branching reaction, we witness a chain-branching explosion marked by a very rapid depletion of fuel, most of which is immediately converted into chain carriers. Again, this region is shorter for smaller T_B. One notes that even by the end of the explosion, there is little or no increase in temperature owing to branching being thermally neutral. Any heat released in this zone (observable for the larger values of T_B) is due to the exothermic termination reaction converting some of the chain carriers into products. This is not

Figure 2.4: Histories of species and temperature for $T_B = 0.8$.

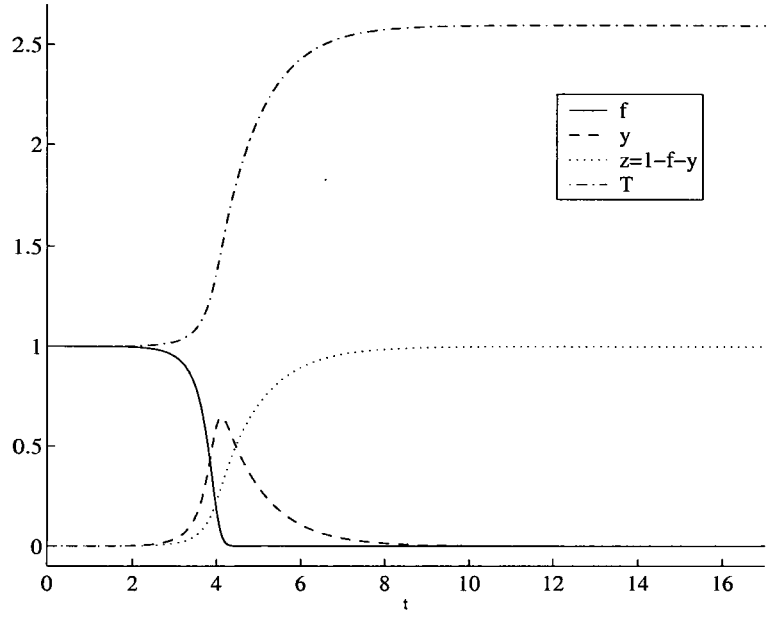

observed for $T_B = 0.3$ as the branching rate is simply too fast to allow for the buildup of products. Once most of the fuel is depleted, the chain carrier concentration reaches its maximum value, y_M. This value is larger for smaller T_B since smaller T_B means a larger branching rate R_B, and hence the explosion occurs too fast for the $O(1)$ termination rate to have much effect. As soon as y_M is reached, there is no more fuel and hence the only reaction occurring is that of termination which converts all the chain carriers to products over a long time scale. It is also in this region that we begin to witness the temperature significantly increase until it reaches its maximum, T_M (= 2.6 here, and as predicted by (2.17)). According to equation (2.12) the rate of change of T is directly proportional to y, and this is expressed in our graphs by the inflection points in T and z occurring at the time when $y = y_M$. Whereas the lengths of the induction and branching zones vary considerably with T_B, the termination zone operates on the same time scale since the termination reaction is insensitive to temperature and so is unaffected by the value of T_B. Figures 2.3–2.6 clearly show that starting at the time when $y = 0.5$ it takes a time

Figure 2.5: Histories of species and temperature for $T_B = 0.6$ (top: full display, below: zoomed in at explosion).

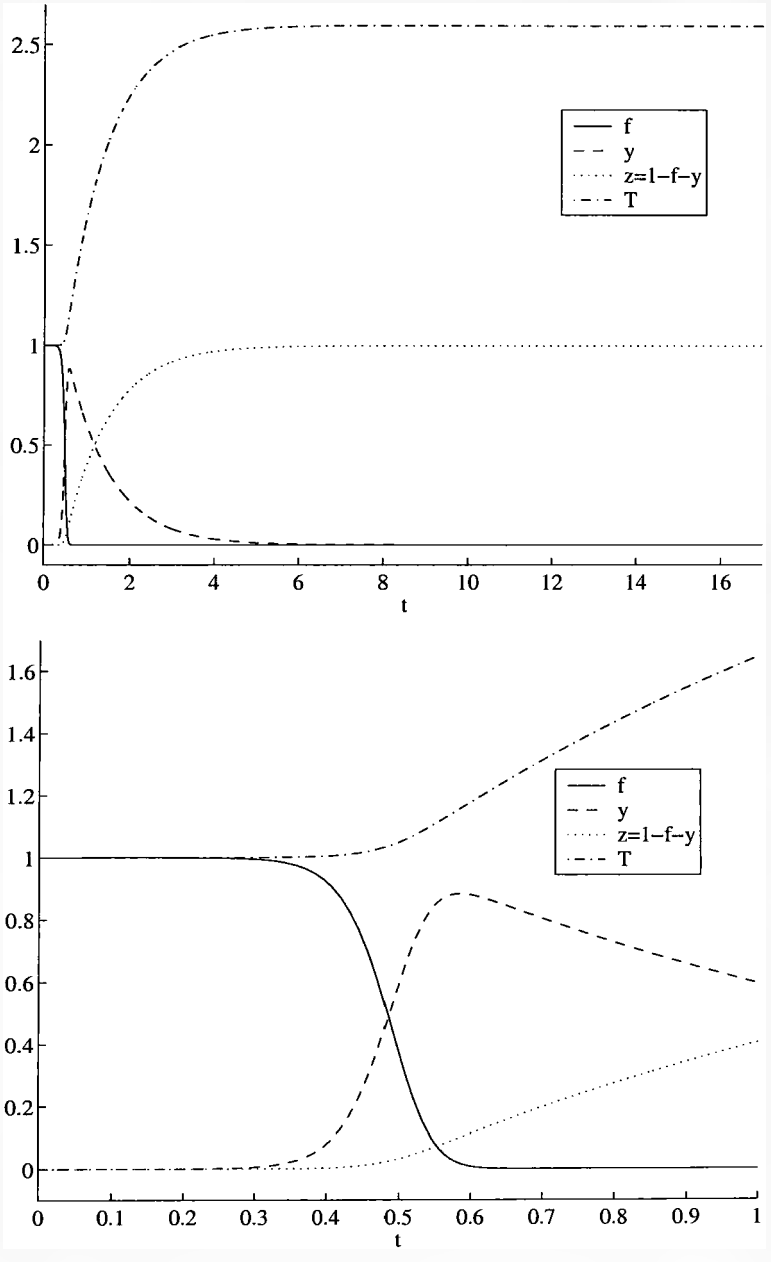

Figure 2.6: Histories of species and temperature for $T_B = 0.3$ (top: full display, below: zoomed in at explosion).

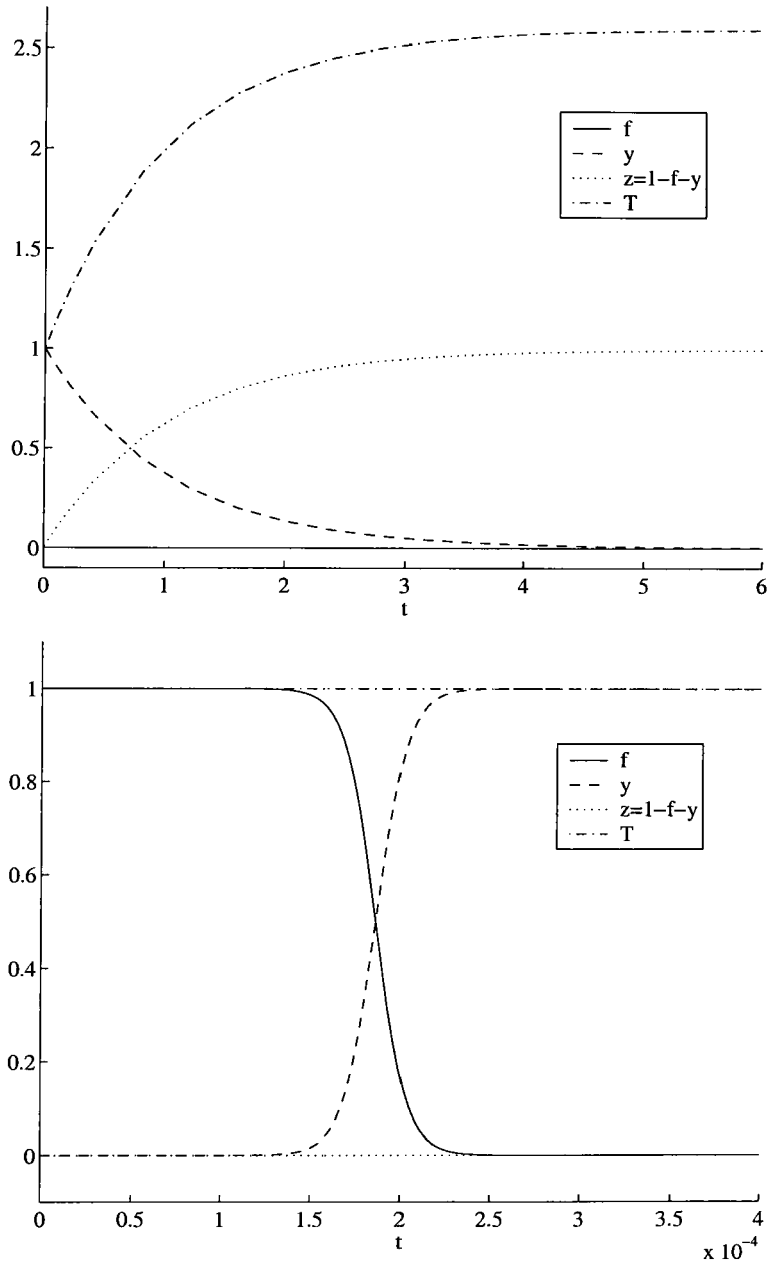

of 4 units for the termination reaction to exhaust most of the chain carriers[3]. Hence, the ratio of the length of the induction zone to that of the termination zone decreases with decreasing T_B, starting out at a value of approximately 2 for $T_B = 0.9$, becoming 1 for $T_B = 0.8$ and tending to zero very rapidly after that.

The chain-branching explosion is more dramatic for smaller values of T_B, in that not only does it occur very rapidly but it also occurs very suddenly, taking only a time of 1.5×10^{-4} to begin for $T_B = 0.3$ (figure 2.6). The graphs also look more and more like purely chain-branching explosions the smaller T_B is, in the sense that the three temporal regions are more well-defined, y_M is closer to 1 and the branching zone has a small or negligible buildup of products and a small or negligible heat release. Taking the $T_B = 0.3$ example again (figure 2.6), fuel is converted into chain carriers in a symmetric fashion (i.e. a decrease in f is marked by a virtually equivalent increase in y) and the branching region is well defined and void of products and heat release. Then y_M reaches exponentially close to the maximum possible value of one, and so for some time the chemical mixture consists almost only of chain carriers.

2.3.2 Asymptotic analysis

From assumptions (1) and (2) on p. 17 we have that

$$0 < \varepsilon_I \ll \varepsilon_B \ll 1. \tag{2.18}$$

Since $T_B < 1$ here, e_B is exponentially large (e_I is always exponentially small since $T_I = 3$). We shall use these facts to construct leading order asymptotic solutions to the governing equations (2.10)-(2.13).

[3]Formally, it takes an infinite amount of time to deplete *all* chain carriers.

Region I - Induction

It may make sense to try an expansion of the form

$$f = 1 + \varepsilon_I f_1, \qquad y = 0 + \varepsilon_I y_1, \qquad T = 1 + \varepsilon_I \theta_1,$$

$$f_1,\ y_1,\ \theta_1 = O(1),$$

since the very small perturbation in this region is caused almost exclusively by the initiation reaction. However, such an expansion fails since a balance in the equations is not achievable.

A leading order balancing act (see appendix A.1) to determine the correct gauge functions to use shows that the correct expansion is

$$f = 1 + \frac{e_I}{e_B} F, \qquad y = 0 + \frac{e_I}{e_B} Y, \qquad T = 1 + \frac{e_I}{e_B^2}\theta, \qquad t = \frac{1}{e_B}\tau, \tag{2.19}$$

$$F,\ Y,\ \theta,\ \tau = O(1).$$

Our governing equations (2.10)–(2.13) now become

$$\begin{aligned}
\frac{dF}{d\tau} &= -\left(1 + \frac{e_I}{e_B}F\right) \exp\left[\frac{1}{\varepsilon_I}\left(1 - \frac{1}{1 + \frac{e_I}{e_B^2}\theta}\right)\right] \\
&\quad - \left(1 + \frac{e_I}{e_B}F\right) Y \exp\left[\frac{1}{\varepsilon_B}\left(1 - \frac{1}{1 + \frac{e_I}{e_B^2}\theta}\right)\right], \qquad (2.20) \\
\frac{dY}{d\tau} &= \left(1 + \frac{e_I}{e_B}F\right) \exp\left[\frac{1}{\varepsilon_I}\left(1 - \frac{1}{1 + \frac{e_I}{e_B^2}\theta}\right)\right] \\
&\quad + \left(1 + \frac{e_I}{e_B}F\right) Y \exp\left[\frac{1}{\varepsilon_B}\left(1 - \frac{1}{1 + \frac{e_I}{e_B^2}\theta}\right)\right] - \frac{1}{e_B}Y, \qquad (2.21) \\
\frac{d\theta}{d\tau} &= \beta Y. \qquad (2.22)
\end{aligned}$$

Initial conditions are

$$F(0) = Y(0) = \theta(0) = 0. \tag{2.23}$$

To leading order, the exponential factors can be written as

$$\begin{aligned}\exp\left[\frac{1}{\varepsilon_I}\left(1-\frac{1}{1+\frac{e_I}{e_B^2}\theta}\right)\right] &\sim \exp\left[\frac{1}{\varepsilon_I}\left(1-1+\frac{e_I}{e_B^2}\theta\right)\right] \\ &= \exp\left(\frac{e_I}{\varepsilon_I e_B^2}\theta\right) \sim 1+\frac{e_I}{\varepsilon_I e_B^2}\theta \sim 1,\end{aligned} \tag{2.24}$$

assuming $\theta = o\left(\frac{e_B^2}{e_I}\right)$ and $\theta = o\left(\frac{\varepsilon_I e_B^2}{e_I}\right)$, and

$$\begin{aligned}\exp\left[\frac{1}{\varepsilon_B}\left(1-\frac{1}{1+\frac{e_I}{e_B^2}\theta}\right)\right] &\sim \exp\left[\frac{1}{\varepsilon_B}\left(1-1+\frac{e_I}{e_B^2}\theta\right)\right] \\ &= \exp\left(\frac{e_I}{\varepsilon_B e_B^2}\theta\right) \sim 1+\frac{e_I}{\varepsilon_B e_B^2}\theta \sim 1,\end{aligned} \tag{2.25}$$

assuming $\theta = o\left(\frac{e_B^2}{e_I}\right)$ and $\theta = o\left(\frac{\varepsilon_B e_B^2}{e_I}\right)$.

Hence we arrive at the following leading order approximation to equations (2.20)–(2.22)

$$\frac{dF}{d\tau} = -1-Y, \tag{2.26}$$

$$\frac{dY}{d\tau} = 1+Y, \tag{2.27}$$

$$\frac{d\theta}{d\tau} = \beta Y. \tag{2.28}$$

Solving and applying the initial conditions (2.23) give the leading order solutions

$$\boxed{\begin{aligned} F &= 1-e^{\tau}, && (2.29)\\ Y &= -1+e^{\tau}, && (2.30)\\ \theta &= \beta\left(e^{\tau}-\tau-1\right). && (2.31)\end{aligned}}$$

Possible non-uniformities in these solutions occur when

1. $F = O\left(\frac{e_B}{e_I}\right)$, i.e. when there is significant fuel consumption. (2.29) tells us this occurs when $\tau = O\left(\ln\left(\frac{e_B}{e_I}\right)\right)$.

2. $\theta = O\left(\frac{e_B^2}{e_I}\right)$, i.e. when the temperature is high enough. (2.31) tells us that this occurs when $\tau = O\left(\ln\left(\frac{e_B^2}{e_I}\right)\right)$.

3. $\theta = O\left(\frac{\varepsilon_B e_B^2}{e_I}\right)$, i.e. when the temperature is high, but not as high as in number 2. (2.31) tells us that this occurs when $\tau = O\left(\ln\left(\frac{\varepsilon_B e_B^2}{e_I}\right)\right)$.

4. $\theta = O\left(\frac{\varepsilon_I e_B^2}{e_I}\right)$, i.e. when the temperature is high, but not as high as in number 3. (2.31) tells us that this occurs when $\tau = O\left(\ln\left(\frac{\varepsilon_I e_B^2}{e_I}\right)\right)$.

The earliest non-uniformity is obviously number 1. This makes sense since, in this case, a significant increase in temperature can only occur after significant fuel consumption, so that chain-termination can begin.

Region II - Chain-Branching Explosion

The orders of F, Y and θ at $\tau = O\left(\ln\left(\frac{e_B}{e_I}\right)\right)$ are

$$F = O\left(\frac{e_B}{e_I}\right), \qquad Y = O\left(\frac{e_B}{e_I} - 1\right) = O\left(\frac{e_B}{e_I}\right),$$

$$\theta = O\left(\frac{e_B}{e_I} - \ln\left(\frac{e_B}{e_I}\right) - 1\right) = O\left(\frac{e_B}{e_I}\right),$$

and so we rescale the variables as follows:

$$F = \frac{e_B}{e_I}\hat{F}, \qquad Y = \frac{e_B}{e_I}\hat{Y}, \qquad \theta = \frac{e_B}{e_I}\hat{\theta}, \qquad \tau = \ln\left(\frac{e_B}{e_I}\right) + \hat{\tau}, \tag{2.32}$$

$$\hat{F},\ \hat{Y},\ \hat{\theta},\ \hat{\tau} = O(1).$$

With respect to our original variables f, y, T and t, we have

$$f = 1 + \hat{F}, \qquad y = \hat{Y}, \qquad T = 1 + \frac{1}{e_B}\hat{\theta}, \qquad t = \frac{1}{e_B}\left[\ln\left(\frac{e_B}{e_I}\right) + \hat{\tau}\right], \tag{2.33}$$

hence we expect to see $O(1)$ changes in fuel and chain carrier concentration but only an exponentially small change in temperature during this stage, as is actually the case in chain-branching explosions.

Our complete equations (2.20)–(2.23) now become

$$
\begin{aligned}
\frac{d\hat{F}}{d\hat{\tau}} &= -\left(1+\hat{F}\right)\frac{e_I}{e_B}\exp\left[\frac{1}{\varepsilon_I}\left(1-\frac{1}{1+\frac{1}{e_B}\hat{\theta}}\right)\right] \\
&\quad -\left(1+\hat{F}\right)\hat{Y}\exp\left[\frac{1}{\varepsilon_B}\left(1-\frac{1}{1+\frac{1}{e_B}\hat{\theta}}\right)\right], \qquad (2.34)\\
\frac{d\hat{Y}}{d\hat{\tau}} &= \left(1+\hat{F}\right)\frac{e_I}{e_B}\exp\left[\frac{1}{\varepsilon_I}\left(1-\frac{1}{1+\frac{1}{e_B}\hat{\theta}}\right)\right] \\
&\quad +\left(1+\hat{F}\right)\hat{Y}\exp\left[\frac{1}{\varepsilon_B}\left(1-\frac{1}{1+\frac{1}{e_B}\hat{\theta}}\right)\right]-\frac{1}{e_B}\hat{Y}, \qquad (2.35)\\
\frac{d\hat{\theta}}{d\hat{\tau}} &= \beta\hat{Y}. \qquad (2.36)
\end{aligned}
$$

Matching conditions are

$$
\hat{F}\sim -e^{\hat{\tau}}, \qquad \hat{Y}\sim e^{\hat{\tau}}, \qquad \hat{\theta}\sim \beta e^{\hat{\tau}} \qquad (2.37)
$$

as $\hat{\tau}\to-\infty$ i.e. back into Region I.

To leading order, the exponential factors can be written as

$$
\begin{aligned}
\exp\left[\frac{1}{\varepsilon_I}\left(1-\frac{1}{1+\frac{1}{e_B}\hat{\theta}}\right)\right] &\sim \exp\left[\frac{1}{\varepsilon_I}\left(1-1+\frac{1}{e_B}\hat{\theta}\right)\right] \\
&= \exp\left(\frac{1}{\varepsilon_I e_B}\hat{\theta}\right)\sim 1+\frac{1}{\varepsilon_I e_B}\hat{\theta}\sim 1,
\end{aligned} \qquad (2.38)
$$

assuming $\hat{\theta}=o\left(e_B\right)$ and $\hat{\theta}=o\left(\varepsilon_I e_B\right)$, and

$$
\begin{aligned}
\exp\left[\frac{1}{\varepsilon_B}\left(1-\frac{1}{1+\frac{1}{e_B}\hat{\theta}}\right)\right] &\sim \exp\left[\frac{1}{\varepsilon_B}\left(1-1+\frac{1}{e_B}\hat{\theta}\right)\right] \\
&= \exp\left(\frac{1}{\varepsilon_B e_B}\hat{\theta}\right)\sim 1+\frac{1}{\varepsilon_B e_B}\hat{\theta}\sim 1,
\end{aligned} \qquad (2.39)
$$

assuming $\hat{\theta}=o\left(e_B\right)$ and $\hat{\theta}=o\left(\varepsilon_B e_B\right)$, which give rise to the following leading order

approximation to equations (2.34)–(2.36)

$$\frac{d\hat{F}}{d\hat{\tau}} = -\left(1+\hat{F}\right)\hat{Y}, \tag{2.40}$$

$$\frac{d\hat{Y}}{d\hat{\tau}} = \left(1+\hat{F}\right)\hat{Y}, \tag{2.41}$$

$$\frac{d\hat{\theta}}{d\hat{\tau}} = \beta\hat{Y}. \tag{2.42}$$

Equations (2.40) and (2.41) and the first two matching conditions in (2.37) give

$$\frac{d\hat{F}}{d\hat{Y}} = -1 \qquad \Rightarrow \hat{F} = -\hat{Y},$$

and so (2.40) becomes

$$\frac{d\hat{F}}{d\hat{\tau}} = (1+\hat{F})\hat{F} \qquad \Rightarrow \hat{F} = \frac{Ce^{\hat{\tau}}}{1-Ce^{\hat{\tau}}} \qquad (C \text{ constant})$$

but (2.37) gives $C = -1$.

Equation (2.42) then becomes $\frac{d\hat{\theta}}{d\hat{\tau}} = \beta\frac{e^{\hat{\tau}}}{1+e^{\hat{\tau}}}$, and so $\hat{\theta} = \beta\ln(1+e^{\hat{\tau}})$ after matching with Region I.

Our Region II leading order solutions are therefore

$$\boxed{\begin{aligned} \hat{F} &= \frac{-e^{\hat{\tau}}}{1+e^{\hat{\tau}}}, && (2.43)\\ \hat{Y} &= \frac{e^{\hat{\tau}}}{1+e^{\hat{\tau}}}, && (2.44)\\ \hat{\theta} &= \beta\ln(1+e^{\hat{\tau}}). && (2.45) \end{aligned}}$$

With respect to f, y and T, these solutions are

$$f = \frac{1}{1+e^{\hat{\tau}}}, \qquad y = \frac{e^{\hat{\tau}}}{1+e^{\hat{\tau}}}, \qquad T = 1 + \frac{1}{e_B}\beta\ln(1+e^{\hat{\tau}}), \tag{2.46}$$

meaning that by the end of this region (i.e. as $\hat{\tau} \to \infty$), $f \to 0$ and $y \to 1$. In other words, most of the fuel has been depleted and has been replaced with chain carriers in

a symmetric fashion (since $f + y = 1$ to leading order in this region), i.e. a decrease in f by an amount x is marked by an increase in y by x. This symmetry is very clear in the zoomed-in plots of figures 2.5 and 2.6 which show numerical solutions to the original governing equations. As evident in figures 2.3–2.6, the symmetry is stronger for values of T_B further away from the critical value of one, but this lack of symmetry for values of T_B close to one only exists if ε_B is not small enough - as in our numerics. The symmetry will of course be stronger for smaller values of ε_B, so that as $\varepsilon_B \to 0$ we get the above symmetric solution.

The non-uniformity that brought us to this region tells us that the chain-branching explosion begins (i.e. is ignited) at the time

$$\begin{aligned} t_{ign} &= \frac{1}{e_B} \ln\left(\frac{e_B}{e_I}\right) \\ &= \exp\left[\frac{1}{\varepsilon_B}\left(1 - \frac{1}{T_B}\right)\right] \left\{\frac{1}{\varepsilon_B}\left(\frac{1}{T_B} - 1\right) - \frac{1}{\varepsilon_I}\left(\frac{1}{T_I} - 1\right)\right\}. \end{aligned} \tag{2.47}$$

The exponential factor confirms that smaller ε_B or smaller T_B means a faster ignition time. The accuracy of t_{ign} is discussed in section 2.5.

Non-uniformities in our asymptotic solutions for Region II occur (or may seem to occur) when

1. $\hat{\theta} = O(e_B)$, i.e. when the temperature increases significantly. (2.45) tells us this occurs when $\hat{\tau} = O(e_B)$.

2. $\hat{\theta} = O(\varepsilon_B e_B)$, i.e. when the temperature increases significantly - but not as significantly as in number 1. (2.45) tells us this occurs when $\hat{\tau} = O(\varepsilon_B e_B)$.

3. $\hat{\theta} = O(\varepsilon_I e_B)$, i.e. when the temperature increases significantly - but not as significantly as in number 2. (2.45) tells us this occurs when $\hat{\tau} = O(\varepsilon_I e_B)$.

4. $\hat{Y} = O\left(\frac{e_I}{e_B}\right)$, i.e. the initiation reaction might reappear after losing it to leading order in (2.40) and (2.41). This, however, cannot happen since $\hat{Y} \to 1$ as $\hat{\tau} \to \infty$,

and so this is not a non-uniformity.

5. $1+\hat{F}=O\left(\frac{1}{e_B}\right)$, i.e. the termination reaction coming into play after losing it to leading order in (2.41). (2.43) tells us this occurs when $\hat{\tau}=O(\ln e_B)$.

It seems that non-uniformity 5 occurs first. This makes sense since the termination reaction must be dominant in the next region now that the initiation and branching reactions have been exhausted of fuel. However, as the following argument shows, we must be careful when rescaling for the next region.

If in Region II we had used the higher order expansion $\hat{Y}=\hat{Y}_0+\cdots+\frac{1}{e_B}\hat{Y}_n$, where $\frac{1}{e_B}\hat{Y}_n$ is included for a higher order balance, then (2.35) would become

$$\begin{aligned}\frac{d}{d\hat{\tau}}\left(\hat{Y}_0+\cdots+\frac{1}{e_B}\hat{Y}_n\right)&=\left(1+\hat{F}\right)\frac{e_I}{e_B}\exp\left[\frac{1}{\varepsilon_I}\left(1-\frac{1}{1+\frac{1}{e_B}\hat{\theta}}\right)\right]\\&+\left(1+\hat{F}\right)\left(\hat{Y}_0+\cdots+\frac{1}{e_B}\hat{Y}_n\right)\exp\left[\frac{1}{\varepsilon_B}\left(1-\frac{1}{1+\frac{1}{e_B}\hat{\theta}}\right)\right]\\&-\frac{1}{e_B}\left(\hat{Y}_0+\cdots+\frac{1}{e_B}\hat{Y}_n\right).\end{aligned}\tag{2.48}$$

The leading order solution $\hat{Y}_0$ is given by (2.44), and so $\hat{Y}_0\sim 1-e^{-\hat{\tau}}$ as $\hat{\tau}\to\infty$ i.e. as we move from Region II to Region III.

At $O\left(\frac{1}{e_B}\right)$, we have

$$\frac{d\hat{Y}_n}{d\hat{\tau}}=\left(1+\hat{F}\right)\hat{Y}_n-\hat{Y}_0\sim-\hat{Y}_0$$

as $\hat{\tau}\to\infty$ since $\hat{F}\to-1$, which can be integrated to give

$$\hat{Y}_n=-\hat{\tau}-e^{-\hat{\tau}}+E\sim-\hat{\tau}\tag{2.49}$$

as $\hat{\tau}\to\infty$ (E a constant). Hence, a higher order solution to (2.35) is

$$\hat{Y}=1-e^{-\hat{\tau}}-\frac{\hat{\tau}}{e_B}+\ldots,\tag{2.50}$$

where $-\frac{\hat{\tau}}{e_B}$ is the dominant term as $\hat{\tau} \to \infty$.

But if we then go on to rescale for Region III according to non-uniformity 5 (i.e. using $\hat{\tau} = \ln e_B + \tilde{\tau}$,...) then we would get the following solution to the resulting chain carrier equation

$$\tilde{Y} = -e^{-\tilde{\tau}} - \tilde{\tau} + G \qquad (G \text{ a constant}), \tag{2.51}$$

where $-e^{-\tilde{\tau}}$ is the dominant term as $\tilde{\tau} \to -\infty$ i.e. as we move back into Region II).

Hence the only real difference between the solutions of the chain carrier equations of Regions II and III is a switch in the dominant term. For this reason, we consider this non-uniformity weak.

There will be a non-uniformity in our Region II solutions when the initiation and branching terms balance[4] in equations (2.34) and (2.35):

$$\frac{e_I}{e_B} \exp\left[\frac{1}{\varepsilon_I}\left(1 - \frac{1}{1+\frac{1}{e_B}\hat{\theta}}\right)\right] = O\left(\exp\left[\frac{1}{\varepsilon_B}\left(1 - \frac{1}{1+\frac{1}{e_B}\hat{\theta}}\right)\right]\right).$$

After a bit of work, we find out that this non-uniformity occurs when $\hat{\theta} = O(e_B)$, and so at $\hat{\tau} = O(e_B)$ (see appendix A.2 for details). This actually corresponds to non-uniformity 1 in the above list. So in the next region, we expect to see a significant increase in temperature.

Region III - Chain carrier depletion

In this region, fuel is virtually non-existent, and hence the initiation and, most importantly, the branching reactions are no longer taking place. Thus according to (2.3) and (2.11)–(2.12), we expect to see a gradual ($O(1)$) decrease in chain carrier concentration and a proportional increase in temperature.

[4]Such balance does not mean that initiation still has a role to play, but rather that the branching rate has become so small that it is comparable with that of the initiation reaction.

We transform the variables as follows[5]:

$$\hat{F} = -1 + e^{-e_B \tilde{F}}, \qquad \hat{Y} = \tilde{Y}, \qquad \hat{\theta} = e_B \tilde{\theta}, \qquad \hat{\tau} = e_B \tilde{\tau}, \tag{2.52}$$

$$\tilde{F},\ \tilde{Y},\ \tilde{\theta},\ \tilde{\tau} = O(1).$$

With respect to our original variables, we get

$$f = e^{-e_B \tilde{F}}, \qquad y = \tilde{Y}, \qquad T = 1 + \tilde{\theta}, \qquad t = \frac{1}{e_B}\left[\ln\left(\frac{e_B}{e_I}\right) + e_B \tilde{\tau}\right], \tag{2.53}$$

and so fuel concentration is exponentially-exponentially small in this region, whereas $O(1)$ changes in chain carrier concentration and temperature can be expected.

Our complete equations (2.34)–(2.37) now become

$$-\frac{d\tilde{F}}{d\tilde{\tau}} = -\frac{e_I}{e_B}\exp\left[\frac{1}{\varepsilon_I}\left(1 - \frac{1}{1+\tilde{\theta}}\right)\right] - \tilde{Y}\exp\left[\frac{1}{\varepsilon_B}\left(1 - \frac{1}{1+\tilde{\theta}}\right)\right], \tag{2.54}$$

$$\frac{d\tilde{Y}}{d\tilde{\tau}} = e_B e^{-e_B \tilde{F}}\left\{\frac{e_I}{e_B}\exp\left[\frac{1}{\varepsilon_I}\left(1 - \frac{1}{1+\tilde{\theta}}\right)\right] + \tilde{Y}\exp\left[\frac{1}{\varepsilon_B}\left(1 - \frac{1}{1+\tilde{\theta}}\right)\right]\right\} - \tilde{Y}, \tag{2.55}$$

$$\frac{d\tilde{\theta}}{d\tilde{\tau}} = \beta\tilde{Y}, \tag{2.56}$$

with matching conditions

$$\tilde{F} \sim -1, \qquad \tilde{Y} \sim 1, \qquad \tilde{\theta} \sim \beta\tilde{\tau} \tag{2.57}$$

as $\tilde{\tau} \to 0$ back into Region II.

We are not really concerned with the fuel equation (2.54) since we can consider $f = 0$ to be true for all our intents and purposes. To leading order, (2.55) becomes $\frac{d\tilde{Y}}{d\tilde{\tau}} = -\tilde{Y}$

[5] At the end of Region II, $\hat{F} \to -1 + e^{-\hat{\tau}}$ and so we use a WKB rescaling for $\hat{F}$ in (2.52). However, it makes no sense to use a similar rescaling for $\hat{Y}$ (i.e. $\hat{Y} = 1 - e^{-e_B \tilde{Y}}$) since this will not yield the expected $O(1)$ change in chain carrier concentration, only an exponentially-exponentially small perturbation. Hence we leave $\hat{Y}$ unchanged.

(ignoring the negligible first term), and so $\tilde{Y} = He^{-\tilde{\tau}}$ (H constant). As $\tilde{\tau} \to 0$, $\tilde{Y} \sim H$ and so $H = 1$ from our matching condition (2.57). Equation (2.56) then gives that $\frac{d\tilde{\theta}}{d\tilde{\tau}} = \beta e^{-\tilde{\tau}} \Rightarrow \tilde{\theta} = -\beta e^{-\tilde{\tau}} + I$ (I constant). As $\tilde{\tau} \to 0$, $\tilde{\theta} \sim -\beta(1-\tilde{\tau}) + I = \beta\tilde{\tau} - \beta + I$ and so $I = \beta$ using (2.57).

Hence our solutions for this region are:

$$\boxed{\begin{aligned} f &= 0, && (2.58)\\ \tilde{Y} &= e^{-\tilde{\tau}}, && (2.59)\\ \tilde{\theta} &= \beta(1-e^{-\tilde{\tau}}). && (2.60) \end{aligned}}$$

This is the final region since as $\tilde{\tau} \to \infty$, we reach the stable chemical equilibrium

$$f = 0, \qquad y = 0, \qquad z = 1, \qquad T = 1 + \beta = T_M.$$

2.3.3 Comparing the asymptotic and numerical solutions

This can be accomplished by plotting the numerical solution against either a composite asymptotic solution or the individual asymptotic solutions. A composite solution, which is uniformly valid throughout the whole chemical process, can be constructed by adding the asymptotic solutions for each region and subtracting the matched parts. Table 2.1 provides a summary of all that is required to create such a composite solution.

Unfortunately, owing to our solutions being to leading order only, coupled with the fact that the values of ε_I and more crucially ε_B used in the numerics are not actually very small, the composite asymptotic solution becomes poor for the larger values of T_B. With our current values of ε_I and ε_B, the composite solution for y is highly erroneous in the first region (induction zone) for $T_B = 0.6$ (see figure 2.7(a)). For larger values of T_B, say for $T_B = 0.8$, the solution becomes very deteriorated and one then has to either decrease ε_B or determine the next order terms. Figure 2.7 shows the $T_B = 0.6$ species and temperature history using the composite solution plotted against the numerical solution for three decreasing values of ε_B starting at our original value of $\frac{1}{5}$. The errors in y, T

Table 2.1: The asymptotic solution for each region, together with the behaviour of each solution in the previous region (i.e. the matched part). All with respect to the original variables.

	f	y	T
Region I	$1+\frac{e_I}{e_B}\left(1-e^{e_B t}\right)$	$\frac{e_I}{e_B}\left(e^{e_B t}-1\right)$	$1+\beta\frac{e_I}{{e_B}^2}\left(e^{e_B t}-e_B t-1\right)$
Region II	$\frac{1}{1+\frac{e_I}{e_B}e^{e_B t}}$	$\frac{\frac{e_I}{e_B}e^{e_B t}}{1+\frac{e_I}{e_B}e^{e_B t}}$	$1+\frac{\beta}{e_B}\ln\left(1+\frac{e_I}{e_B}e^{e_B t}\right)$
Behaviour of Reg II in Reg I	$1-\frac{e_I}{e_B}e^{e_B t}$	$\frac{e_I}{e_B}e^{e_B t}$	$1+\beta\frac{e_I}{{e_B}^2}e^{e_B t}$
Region III	super-exponentially small	$\left(\frac{e_B}{e_I}\right)^{\frac{1}{e_B}}e^{-t}$	$1+\beta\left(1-\left(\frac{e_B}{e_I}\right)^{\frac{1}{e_B}}e^{-t}\right)$
Behaviour of Reg III in Reg II	0	1	$1+\frac{\beta}{e_B}\left(e_B t-\ln\left(\frac{e_B}{e_I}\right)\right)$

and z in the induction zone decrease rapidly as we decrease ε_B to more asymptotically suitable values.

For comparative reasons, it is however adequate to just plot the numerical solution against the individual asymptotic solutions as opposed to the composite solution. This has been done for values of $T_B = 0.6$ and beyond in figure 2.8. Figure 2.8(a) shows that for $T_B = 0.6$ the asymptotics and numerics are very much in agreement in every aspect. However, for $T_B = 0.8$ in figure 2.8(b), we see that although qualitatively correct, even the individual asymptotic solutions are struggling to produce accurate plots when compared with the numerics - the most obvious discrepancy is the premature branching explosion. This of course is because we are now much closer to $T_B = 1$, and so to achieve high asymptotic accuracy we must either determine higher order terms or decrease ε_B.

Figure 2.7: Comparing the composite asymptotic solution (- - -) with the numerical solution (—) for $T_B = 0.6$ using three values of ε_B.

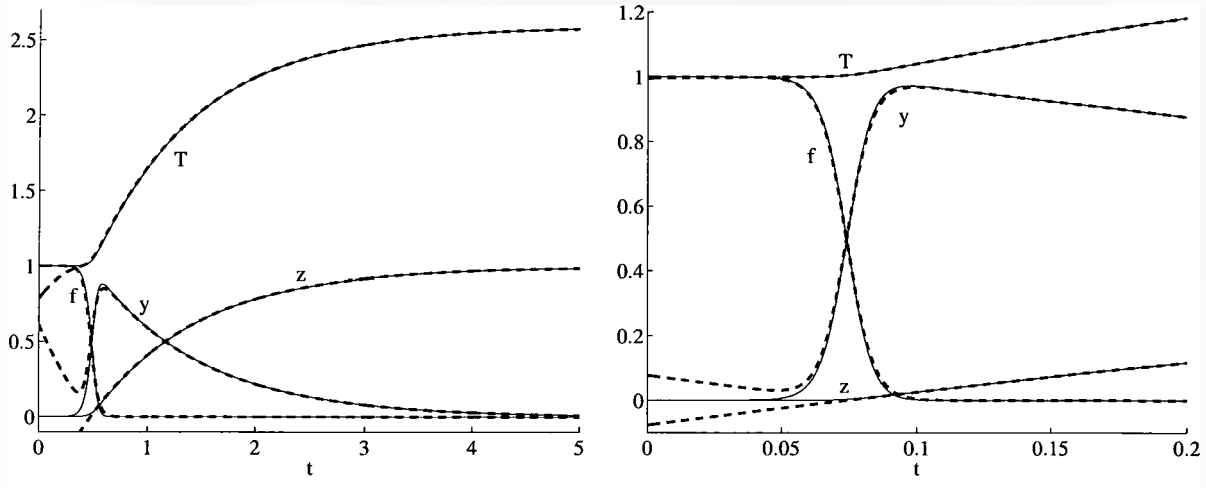

(a) $\varepsilon_B = 1/5$ (b) $\varepsilon_B = 1/8$

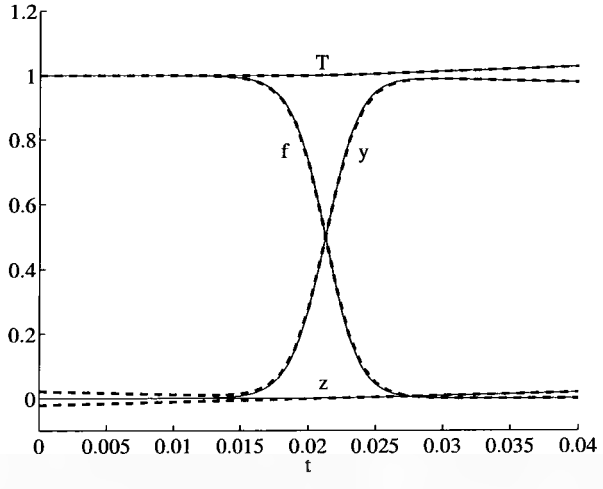

(c) $\varepsilon_B = 1/10$

For values of T_B further away from the critical value of unity, our leading order composite solution is actually rather accurate. Figure 2.9 shows our composite solution for $T_B = 0.3$ to be virtually the same as the numerical solution.

It is the appearance of ε_B and T_B in $e_B \stackrel{def}{=} \exp\left[\frac{1}{\varepsilon_B}\left(\frac{1}{T_B} - 1\right)\right]$ that makes e_B so sensitive to changes in ε_B or T_B. A small change in either produces an exponential

Figure 2.8: Comparing the asymptotic solution (- - -) from each region individually with the numerical solution (—).

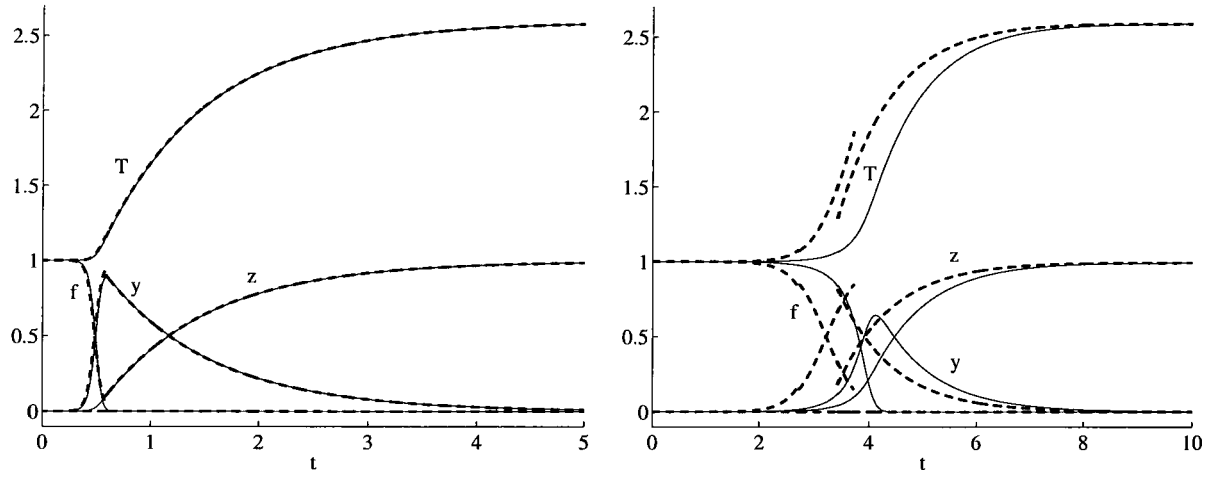

(a) $T_B = 0.6$ (b) $T_B = 0.8$

Figure 2.9: Comparing the composite asymptotic solution (- - -) with the numerical solution (—) for $T_B = 0.3$ (left: full display, right: zoomed in at explosion).

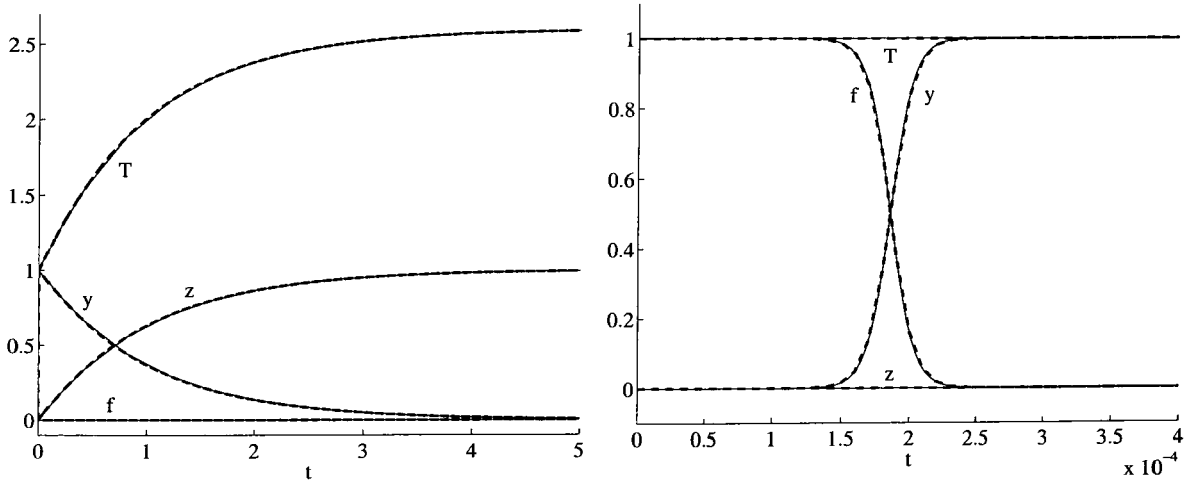

change in e_B and so it is really the value of e_B that determines how good the asymptotics are, rather than ε_B or T_B individually.

2.4 Suppressed branching factor ($T_B > 1$)

We have so far tackled the case where the branching factor $\exp\left[\frac{1}{\varepsilon_B}\left(\frac{1}{T_B}-\frac{1}{T}\right)\right]$ is exponentially large from the start through till the end of the reaction owing to the initial temperature being already above the branching crossover temperature i.e. $T_B < 1$. The result was that the reactions proceed in a chain-branching manner. Here, we consider the case where $T_B > 1$, i.e. this exponential factor is now exponentially small initially. The values of T_B we shall use will ensure that this factor does not remain exponentially small throughout the entire reaction, but that it becomes exponentially large when T exceeds T_B. This condition will be applied by choosing values of T_B that are less than T_M, otherwise chain-branching will never come into play. But such a condition does not necessarily mean that R_B also becomes exponentially large, since the chain carrier concentration may still be too small or the fuel may have been depleted to such an extent that the magnitude of $\exp\left[\frac{1}{\varepsilon_B}\left(\frac{1}{T_B}-\frac{1}{T}\right)\right]$ becomes physically irrelevant.

2.4.1 Numerical results

Figures 2.10 and 2.11 show the species and temperature histories for $T_B = 1.1$ and 1.5 respectively. What we immediately notice in both figures, in contrast with the $T_B < 1$ case, is a very long induction zone characterized by a slow but noticeable consumption of fuel. The induction zone is long because there is no chain-branching to accelerate the conversion of fuel into chain carriers. The dormancy of the branching reaction results primarily from the small branching exponential factor and also, but much less importantly, from losing out to the termination reaction in competing for chain carriers which are consequently converted directly into stable products. The formation of products means that heat is emitted and so the induction zone is moderately thermal. When the temperature

Figure 2.10: Histories of species for $T_B = 1.1$ (left: full display, right: zoomed in at explosion).

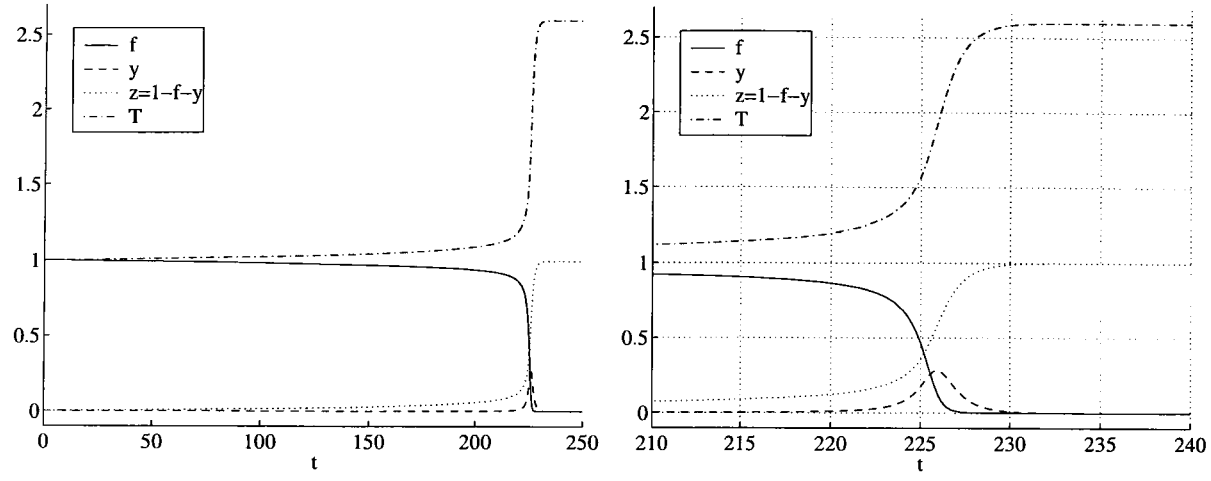

approaches T_B, the branching reaction gathers pace and competes more successfully for chain carriers. For $T_B = 1.1$, we get branching-crossover very early on when the chemical mixture is still about 95% fuel and hence the branching rate R_B is actually sufficiently large to start a small chain branching explosion in which the remaining fuel is depleted and in which chain carrier concentration is boosted to nearly 30%. The zoomed in diagram of figure 2.10 is in fact very similar, apart from the induction times of course, to the $T_B = 0.9$ diagram in figure 2.3. Both values of T_B are very close to the critical value of unity but crucially one is smaller than unity and the other is bigger. For $T_B = 1.5$, the induction zone is much longer than for $T_B = 1.1$. Branching crossover occurs much later and by then the fuel mass is only at 65%. The smaller branching exponential factor coupled with a smaller fuel fraction means that R_B is much smaller than it was with the $T_B = 1.1$ case and hence this time chain carriers struggle to reach even 5% of the total chemical mass. This reaction can only really be described as a thermal explosion since it does not consist of the three distinct zones typical of chain-branching explosions but duplicates the behaviour of typical thermal explosions as was shown in figure 1.2.

Will the induction zones continue to grow rapidly as we increase T_B? We have already seen that for $T_B = 1.5$, the branching reaction (with rate $R_B = fy \exp\left[\frac{1}{\varepsilon_B}\left(\frac{1}{T_B} - \frac{1}{T}\right)\right]$)

Figure 2.11: Histories of species for $T_B = 1.5$ (left: full display, right: zoomed in at explosion).

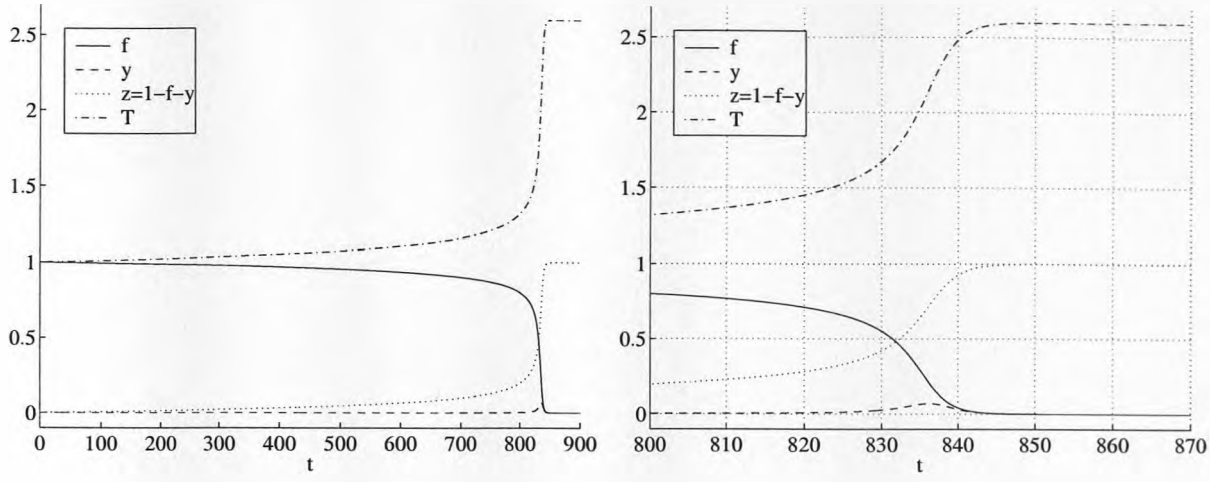

is having very little impact on chain carrier growth even though the branching factor $\exp\left[\frac{1}{\varepsilon_B}\left(\frac{1}{T_B}-\frac{1}{T}\right)\right]$ becomes exponentially large when fuel is still as high as 65% of the total chemical mass. The fact though is that R_B is now much smaller than it was, and it rapidly tends to zero for larger values of T_B. If we then go further and take values of $T_B > T_M$, and hence the branching factor can never be exponentially large, we realise that the induction zones are no longer growing at substantial rates. In fact, we notice that there is very little difference in the species and temperature histories between $T_B = 3.0$ in figure 2.12 and $T_B = 5.0$ in figure 2.13(a). Plotting the ignition time of fuel (as an indicator of the induction time) against T_B in figure 2.13(b) (as in figure 2.2 but this time including large T_B values), we see that the ignition times begin to grow quite spectacularly but then this growth gradually decays. Beyond $T_B = T_M$ (2.6 with our current set of parameters), the induction zone grows at a very slow, seemingly logarithmic, pace[6]. Increasing T_B to even larger values has very little impact on our system since R_B becomes so small that it no longer plays any role in our governing equations. It is only the initiation and termination reactions that are governing how the reactants react, and since neither

[6]The growth for $T_B < 1$ was already proven to be exponential in equation (2.47) for the asymptotic domain.

Figure 2.12: Histories of species for $T_B = 3.0$ (left: full display, right: zoomed in at explosion).

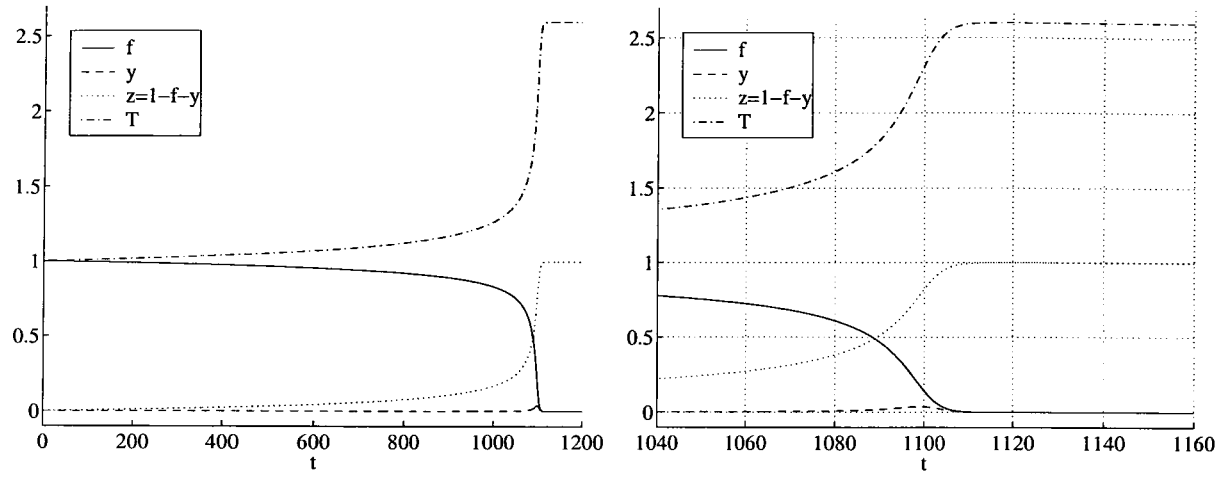

reaction involves T_B, increasing T_B will not make a difference. The thermal explosion zone, which incidentally is actually much slower than the branching explosions witnessed in the $T_B < 1$ case, occurs solely because the heat released in the thermal induction zone speeds up the rate R_I of the initiation reaction. Such behaviour is synonymous with that observed in one-step Arrhenius chemical reactions.

2.4.2 Asymptotic analysis

As already mentioned in the introduction, Blythe, Kapila and Short [14] produced asymptotic solutions to our governing equations (2.10)–(2.13) for various values of T_B. Although they considered the case $T_B > 1$, I shall still present the first two regions here as they were resolved independently before their paper was submitted. Plus, our solutions are derived in a different manner: whereas we derive the asymptotic solutions in each region directly from the governing equations (2.10)–(2.13), Blythe et al. rewrite these equations by viewing time as a dependent variable and considering some function of temperature as the new independent variable. The following two regions will be more than sufficient to allow for the derivation of an expression for the ignition time, and also for parameter matching between the one-step model and our three-step model.

Figure 2.13: Showing the insignificance of large T_B.

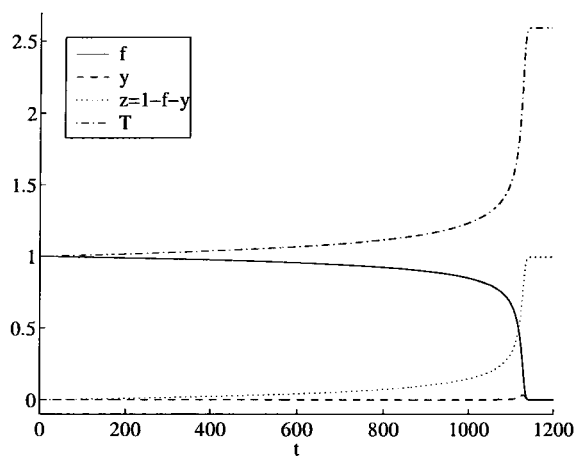

(a) Histories of species for $T_B = 5.0$.

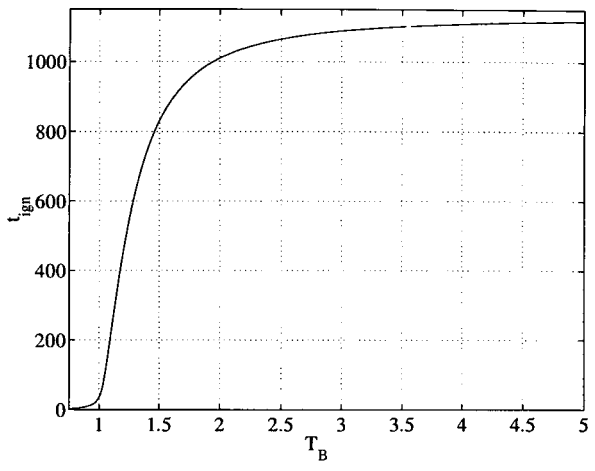

(b) Ignition time of fuel for various values, including large values, of T_B.

We already have that e_I is exponentially small, but because $T_B > 1$ here, e_B becomes exponentially small too (reflecting the smallness of the branching reaction in the initial phase at least).

Region I - Induction

The induction zone expansions are

$$f = 1 + \varepsilon_I F, \qquad y = 0 + e_I Y, \qquad T = 1 + \varepsilon_I \theta, \qquad t = \frac{\varepsilon_I}{e_I}\tau, \tag{2.61}$$

$$F,\ Y,\ \theta,\ \tau = O(1).$$

Hence we expect to see a small reduction in fuel mass, coupled with a small increase in temperature (as is the case with one-step thermal systems). Chain carrier growth is expected to be exponentially small.

Substituting into our governing equations (2.10)–(2.13) gives

$$
\begin{aligned}
e_I \frac{dF}{d\tau} &= -(1+\varepsilon_I F)\exp\left[\frac{1}{\varepsilon_I}\left(\frac{1}{T_I}-\frac{1}{1+\varepsilon_I\theta}\right)\right] \\
&- (1+\varepsilon_I F)\, e_I Y \exp\left[\frac{1}{\varepsilon_B}\left(\frac{1}{T_B}-\frac{1}{1+\varepsilon_I\theta}\right)\right], \qquad (2.62)\\
\frac{{e_I}^2}{\varepsilon_I}\frac{dY}{d\tau} &= (1+\varepsilon_I F)\exp\left[\frac{1}{\varepsilon_I}\left(\frac{1}{T_I}-\frac{1}{1+\varepsilon_I\theta}\right)\right] \\
&+ (1+\varepsilon_I F)\, e_I Y \exp\left[\frac{1}{\varepsilon_B}\left(\frac{1}{T_B}-\frac{1}{1+\varepsilon_I\theta}\right)\right] - e_I Y, \qquad (2.63)\\
\frac{d\theta}{d\tau} &= \beta Y. \qquad (2.64)
\end{aligned}
$$

Initial conditions are

$$F(0) = Y(0) = \theta(0) = 0. \tag{2.65}$$

To leading order, the exponential factors can be written as

$$
\begin{aligned}
\exp\left[\frac{1}{\varepsilon_I}\left(\frac{1}{T_I}-\frac{1}{1+\varepsilon_I\theta}\right)\right] &\sim \exp\left[\frac{1}{\varepsilon_I}\left(\frac{1}{T_I}-1+\varepsilon_I\theta\right)\right] \\
&= e_I e^{\theta},
\end{aligned} \tag{2.66}
$$

assuming $\theta = o\left(\frac{1}{\varepsilon_I}\right)$, and

$$
\begin{aligned}
\exp\left[\frac{1}{\varepsilon_B}\left(\frac{1}{T_B}-\frac{1}{1+\varepsilon_I\theta}\right)\right] &\sim \exp\left[\frac{1}{\varepsilon_B}\left(\frac{1}{T_B}-1+\varepsilon_I\theta\right)\right] \\
&= e_B \exp\left(\frac{\varepsilon_I}{\varepsilon_B}\theta\right) \sim e_B,
\end{aligned} \tag{2.67}
$$

assuming $\theta = o\left(\frac{1}{\varepsilon_I}\right)$ and $\theta = o\left(\frac{\varepsilon_B}{\varepsilon_I}\right)$.

Hence we arrive at the following leading order approximation to equations (2.62)–(2.64)

$$\frac{dF}{d\tau} = -e^{\theta}, \tag{2.68}$$

$$Y = e^{\theta}, \tag{2.69}$$

$$\frac{d\theta}{d\tau} = \beta Y. \tag{2.70}$$

Figure 2.14: Finite time singularity in Region I solutions at $\tau = \frac{1}{\beta}$

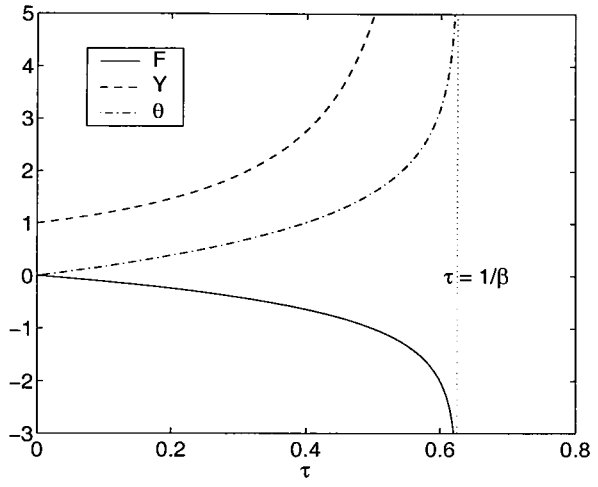

Solving and applying the initial conditions (2.65) give the leading order solutions

$$\boxed{\begin{aligned} F &= \frac{1}{\beta}\ln(1-\beta\tau), \quad (2.71) \\ Y &= \frac{1}{1-\beta\tau}, \quad (2.72) \\ \theta &= -\ln(1-\beta\tau). \quad (2.73) \end{aligned}}$$

What we immediately notice is that a singularity develops in all three induction zone solutions at the finite time $\tau = \frac{1}{\beta}$ (see figure 2.14). This blow-up of solutions characterizes a rapid reaction or explosion in which fuel is quickly consumed and heat is rapidly released i.e. a thermal explosion. In terms of our original time variable, the ignition time for this explosion is

$$t_{ign} = \frac{\varepsilon_I}{\beta e_I} = \frac{\varepsilon_I}{\beta}\exp\left[\frac{1}{\varepsilon_I}\left(1-\frac{1}{T_I}\right)\right]. \quad (2.74)$$

The exponential factor tells us that smaller ε_I (i.e. larger activation energy for the initiation reaction) means a much longer ignition time. We also note the absence of T_B, a fact that tells us branching plays no part in our leading order asymptotic expression in determining the time to ignition. The expression thus seems to model behaviour characteristic of one-step thermal reactions, and indeed we shall see later in section 2.6.1 that,

with the correct identification of the various parameters, the expression matches exactly that which is deduced from one-step systems (such as that in [29]). The accuracy of our expression for t_{ign} is discussed in section 2.5.

The singular behaviour of the induction zone's solutions (2.71)–(2.73) means we require new asymptotics near time t_{ign}. The following possible non-uniformities should point us in the right direction:

1. $F = O\left(-\frac{1}{\varepsilon_I}\right)$, i.e. when there is significant fuel consumption. (2.71) tells us this occurs when $\tau = O\left(\frac{1-\frac{1}{\varepsilon_I}}{\beta}\right)$.

2. $\theta = O\left(\frac{1}{\varepsilon_I}\right)$, i.e. when the temperature is high enough. (2.73) tells us that this occurs when $\tau = O\left(\frac{1-\frac{1}{\varepsilon_I}}{\beta}\right)$.

3. $\theta = O\left(\frac{\varepsilon_B}{\varepsilon_I}\right)$, i.e. when the temperature is high, but not as high as in number 2. (2.73) tells us that this occurs when $\tau = O\left(\frac{1-\frac{\varepsilon_B}{\varepsilon_I}}{\beta}\right)$.

4. $Y = O\left(\frac{1}{e_B}\right)$, i.e. when the branching rate becomes important (as it was dropped when determining the leading order equation (2.68)). (2.72) tells us that this occurs when $\tau = O\left(\frac{1-e_B}{\beta}\right)$.

Although the earliest of the above times is that in number 4, rescaling according to it leads us to the same set of leading order differential equations as (2.68)–(2.70). We can also disregard possible non-uniformity number 3 as it occurs in the exponential branching factor which we do not expect to be vital just yet. We are left with non-uniformities numbers 1 and 2, both of which unsurprisingly lead to the same rescalings since F and θ are proportional in magnitude, which again is typical of the behaviour of one-step systems.

Region II - Thermal Explosion

Non-uniformities 1 or 2 together with equation (2.69) suggest we rescale our variables as follows:

$$F = \frac{1}{\varepsilon_I}\hat{F}, \qquad Y = e^{\frac{\hat{Y}}{e_I}}, \qquad \theta = \frac{1}{\varepsilon_I}\hat{\theta}, \qquad \tau = \frac{1 - e^{-\frac{\hat{\tau}}{e_I}}}{\beta}, \tag{2.75}$$

$$\hat{F},\ \hat{Y},\ \hat{\theta},\ \hat{\tau} = O(1).$$

Note that we can only have $\tau < \frac{1}{\beta}$ with time rescaled in this way, and hence at least another asymptotic region would be required if we were to consider the complete time history of the variables.

With respect to our original variables f, y, T and t, we have

$$f = 1 + \hat{F}, \qquad y = e_I e^{\frac{\hat{Y}}{e_I}}, \qquad T = 1 + \hat{\theta}, \qquad t = \frac{\varepsilon_I}{e_I}\left(\frac{1 - e^{-\frac{\hat{\tau}}{e_I}}}{\beta}\right), \tag{2.76}$$

hence we envisage $O(1)$ changes in fuel concentration and temperature as expected with thermal explosions. This is in contrast with the chain-branching explosion witnessed with the $T_B < 1$ case where an $O(1)$ change in fuel concentration occurs but with only an exponentially small change in temperature (see the scalings in (2.33)).

Our complete equations (2.62)–(2.65) now become

$$\begin{aligned}
\beta e_I \frac{d\hat{F}}{d\hat{\tau}} &= -\left(1+\hat{F}\right)\exp\left[\frac{1}{\varepsilon_I}\left(\frac{1}{T_I} - \frac{1}{1+\hat{\theta}} - \hat{\tau}\right)\right] \\
&\quad - \left(1+\hat{F}\right) e_I e^{\frac{\hat{Y}-\hat{\tau}}{e_I}} \exp\left[\frac{1}{\varepsilon_B}\left(\frac{1}{T_B} - \frac{1}{1+\hat{\theta}}\right)\right], \qquad (2.77) \\
\frac{{e_I}^2}{\varepsilon_I} e^{\frac{\hat{Y}}{e_I}} \frac{d\hat{Y}}{d\hat{\tau}} &= \left(1+\hat{F}\right)\exp\left[\frac{1}{\varepsilon_I}\left(\frac{1}{T_I} - \frac{1}{1+\hat{\theta}} - \hat{\tau}\right)\right] \\
&\quad + \left(1+\hat{F}\right) e_I e^{\frac{\hat{Y}-\hat{\tau}}{e_I}} \exp\left[\frac{1}{\varepsilon_B}\left(\frac{1}{T_B} - \frac{1}{1+\hat{\theta}}\right)\right] - e_I e^{\frac{\hat{Y}-\hat{\tau}}{e_I}}, \qquad (2.78) \\
\frac{d\hat{\theta}}{d\hat{\tau}} &= e^{\frac{\hat{Y}-\hat{\tau}}{e_I}}. \qquad (2.79)
\end{aligned}$$

Matching conditions are

$$\hat{F} \sim -\frac{\hat{\tau}}{\beta}, \qquad \hat{Y} \sim \hat{\tau}, \qquad \hat{\theta} \sim \hat{\tau} \tag{2.80}$$

as $\hat{\tau} \to 0$ i.e. back into Region I.

For a leading order balance, we require that

$$\hat{Y} = \hat{\tau} \tag{2.81}$$

from the temperature equation (2.79). The fuel equation (2.77) requires that

$$\exp\left[\frac{1}{\varepsilon_I}\left(\frac{1}{T_I} - \frac{1}{1+\hat{\theta}} - \hat{\tau}\right)\right] = O(e_I), \tag{2.82}$$

provided that we have not reached the branching crossover temperature, i.e. $T = 1 + \hat{\theta} < T_B$, which then gives

$$\hat{\theta} = \frac{\hat{\tau}}{1-\hat{\tau}}. \tag{2.83}$$

In order to arrive at the leading order terms for $\hat{Y}$ and $\hat{\theta}$ we require the two term expansions

$$\hat{Y} = \hat{\tau} + \varepsilon_I \hat{Y}_1 \text{ and} \tag{2.84}$$

$$\hat{\theta} = \frac{\hat{\tau}}{1-\hat{\tau}} + \varepsilon_I \hat{\theta}_1. \tag{2.85}$$

To leading order, the exponential factors in our equations (2.77)–(2.80) can then be written as

$$\exp\left[\frac{1}{\varepsilon_I}\left(\frac{1}{T_I} - \frac{1}{1+\hat{\theta}} - \hat{\tau}\right)\right] \sim e_I e^{(1-\hat{\tau})^2\hat{\theta}_1}, \tag{2.86}$$

$$\exp\left[\frac{1}{\varepsilon_B}\left(\frac{1}{T_B} - \frac{1}{1+\hat{\theta}}\right)\right] \sim \exp\left[\frac{1}{\varepsilon_B}\left(\frac{1}{T_B} - (1-\hat{\tau})\right)\right] \exp\left[\frac{\varepsilon_I}{\varepsilon_B}(1-\hat{\tau})^2\hat{\theta}_1\right] \text{ and} \tag{2.87}$$

$$e^{\frac{\hat{Y}-\hat{\tau}}{\varepsilon_I}} \sim e^{\hat{Y}_1}. \tag{2.88}$$

The $\exp\left[\frac{1}{\varepsilon_B}\left(\frac{1}{T_B} - (1-\hat{\tau})\right)\right]$ factor in (2.87) is exponentially small while $\hat{\tau} < 1 - \frac{1}{T_B}$, or

using (2.83), while $T < T_B$. Hence, treating this factor as zero in our approximations below would, as expected, cause a non-uniformity when branching crossover occurs.

To leading order then, and while the branching reaction is negligible, the fuel equation (2.77) becomes

$$\beta \frac{d\hat{F}}{d\hat{\tau}} = -(1+\hat{F})e^{(1-\hat{\tau})^2\hat{\theta}_1}. \tag{2.89}$$

The chain carrier equation (2.78) can be reduced to

$$\frac{e_I}{\varepsilon_I} e^{\frac{\hat{Y}}{\varepsilon_I}} \frac{d\hat{Y}}{d\hat{\tau}} = (1+\hat{F})e^{(1-\hat{\tau})^2\hat{\theta}_1} - e^{\hat{Y}_1}, \tag{2.90}$$

but

$$e_I e^{\frac{\hat{Y}}{\varepsilon_I}} = \exp\left[\frac{1}{\varepsilon_I}\left(\frac{1}{T_I}-1\right) + \frac{\hat{\tau}+\varepsilon_I\hat{Y}_1}{\varepsilon_I}\right] \sim \exp\left[\frac{1}{\varepsilon_I}\left(\frac{1}{T_I}-1+\hat{\tau}\right)\right], \tag{2.91}$$

which is exponentially small while $\hat{\tau} < 1 - \frac{1}{T_I}$, i.e. while $T < T_I$. Treating this factor as zero in our leading order analysis would lead to a non-uniformity when (and if) the temperature reaches T_I, however, assumption (2.9) tells us that the temperature must reach T_B before it can reach T_I. Moreover, we have already assumed in our model that, for physical reasons, the temperature cannot ever reach T_I. Hence this non-uniformity is ignored, and our leading order chain carrier equation can now be written as

$$(1+\hat{F})e^{(1-\hat{\tau})^2\hat{\theta}_1} - e^{\hat{Y}_1} = 0. \tag{2.92}$$

The temperature equation (2.79) can be written as

$$\frac{d\hat{\theta}}{d\hat{\tau}} = e^{\hat{Y}_1}, \tag{2.93}$$

and also as

$$\frac{d\hat{\theta}}{d\hat{\tau}} = \frac{1}{(1-\hat{\tau})^2} + \varepsilon_I \frac{d\hat{\theta}_1}{d\hat{\tau}} \tag{2.94}$$

by differentiating (2.85). Comparing (2.93) with (2.94), and then integrating gives

$$\hat{Y}_1 = -2\ln(1-\hat{\tau}), \tag{2.95}$$

which becomes non-uniform when $\hat{\tau} = 1$.

The chain carrier equation (2.92) becomes

$$(1+\hat{F})e^{(1-\hat{\tau})^2\hat{\theta}_1} = \frac{1}{(1-\hat{\tau})^2}, \tag{2.96}$$

and hence the fuel equation (2.89) becomes

$$\beta\frac{d\hat{F}}{d\hat{\tau}} = -\frac{1}{(1-\hat{\tau})^2}, \tag{2.97}$$

which can be integrated to give

$$\hat{F} = \frac{\tau}{\beta(\hat{\tau}-1)}. \tag{2.98}$$

Finally, substituting this solution into (2.96) gives

$$\hat{\theta}_1 = \frac{1}{(1-\hat{\tau})^2}\ln\left[\frac{1}{(\hat{\tau}-1)\left(\frac{\beta+1}{\beta}\hat{\tau}-1\right)}\right], \tag{2.99}$$

So our Region II leading order solutions are

$$\begin{aligned}
\hat{F} &= \frac{\hat{\tau}}{\beta(\hat{\tau}-1)}, && (2.100)\\
\hat{Y} &= \hat{\tau} - 2\varepsilon_I\ln(1-\hat{\tau}), && (2.101)\\
\hat{\theta} &= \frac{\hat{\tau}}{1-\hat{\tau}} + \frac{\varepsilon_I}{(1-\hat{\tau})^2}\ln\left[\frac{1}{(\hat{\tau}-1)\left(\frac{\beta+1}{\beta}\hat{\tau}-1\right)}\right]. && (2.102)
\end{aligned}$$

The next region can be resolved by considering the non-uniformities arising from the above analysis. For instance, (2.99) becomes non-uniform when $\hat{\tau} = 1$ or when $\hat{\tau} = \frac{\beta}{\beta+1}$. The latter occurs first, and (2.102) tells us that the temperature is then an $O(\varepsilon_I)$ amount

away from the maximum temperature $T_M = 1 + \beta$, i.e. near the end of the complete reaction. Another non-uniformity, which may occur before or after the latter depending on T_B, is when branching crossover occurs (i.e. when $T = T_B$). As we have already seen in the numerics, if branching crossover occurs very late in the reaction, then the effect of the branching reaction may be too small to have any impact. Indeed, the effect quickly diminishes for values of $T_B > 2$ (see figure 2.13(b)). Blythe et al. [14] consider the entire time history of the reactants and temperature, albeit in a different way, and hence we shall move on to compare our asymptotic results with our numerical work from section 2.4.1. Importantly, we have the asymptotic ignition time for this case.

2.4.3 Comparing the asymptotic and numerical solutions

As in section 2.3.3, we can construct a composite asymptotic solution for our two regions by adding the individual solutions for each region and subtracting the matched parts. Table 2.2 contains all the expressions required to set up such a solution.

A crucial point to make in this $T_B > 1$ case is that none of our asymptotic solutions involve the T_B parameter. This was noticed too in the asymptotic expression for the time to ignition, t_{ign}, in (2.74). This absence implies that our asymptotic solutions for the $T_B > 1$ case are only really valid for values of T_B that do not produce a large variance in resulting values of the governing equations (2.10)–(2.13). A logical conclusion from this is that our asymptotics are valid for values of $T_B > 1$ that are not close to unity, i.e. where

$$T_B - 1 = O(1),$$

since it is only then that the branching factors in the governing equations (2.10)–(2.13) become negligible. Our asymptotic solutions thus get better if we apply the double limiting process:

$$\varepsilon_I \to 0 \text{ and } T_B \to \infty.^7 \tag{2.103}$$

[7] The conditions on T_B, namely that $T_B < T_I$ and $T_B < T_M$, must still be satisfied. Hence, the limiting

Table 2.2: The asymptotic solution for each region, together with the behaviour of the Region II solution in Region I (i.e. the matched part, M.P.). All with respect to the original variables.

	f	y	T
R. I	$1+\frac{\varepsilon_I}{\beta}\ln\left(1-\beta\frac{e_I}{\varepsilon_I}t\right)$	$\frac{e_I}{1-\beta\frac{e_I}{\varepsilon_I}t}$	$1-\varepsilon_I\ln\left(1-\beta\frac{e_I}{\varepsilon_I}t\right)$
R. II	$1+\frac{\varepsilon_I\ln\left(1-\beta\frac{e_I}{\varepsilon_I}t\right)}{\beta\left[1+\varepsilon_I\ln\left(1-\beta\frac{e_I}{\varepsilon_I}t\right)\right]}$	$\frac{e_I}{\left(1-\beta\frac{e_I}{\varepsilon_I}t\right)\left[1+\varepsilon_I\ln\left(1-\beta\frac{e_I}{\varepsilon_I}t\right)\right]^2}$	$1-\frac{\varepsilon_I\ln\left(1-\beta\frac{e_I}{\varepsilon_I}t\right)}{1+\varepsilon_I\ln\left(1-\beta\frac{e_I}{\varepsilon_I}t\right)}$ $+\frac{\varepsilon_I}{\left[1+\varepsilon_I\ln\left(1-\beta\frac{e_I}{\varepsilon_I}t\right)\right]^2}\cdots$ $\times\ln\left\{\frac{1}{\left[1+\varepsilon_I\ln\left(1-\beta\frac{e_I}{\varepsilon_I}t\right)\right]\left[1+\frac{\beta+1}{\beta}\varepsilon_I\ln\left(1-\beta\frac{e_I}{\varepsilon_I}t\right)\right]}\right\}$
M.P.	$1+\frac{\varepsilon_I}{\beta}\ln\left(1-\beta\frac{e_I}{\varepsilon_I}t\right)$	$\frac{e_I}{1-\beta\frac{e_I}{\varepsilon_I}t}$	$1-\varepsilon_I\ln\left(1-\beta\frac{e_I}{\varepsilon_I}t\right)$

Employing this double limiting process removes the effect of branching, and our governing equations would thus effectively be modelling one-step thermal reactions as opposed to chain-branching reactions.

Figure 2.15 shows the asymptotic solution[8] plotted against the numerical solution for $T_B = 1.5$ and for four decreasing values of ε_I. We notice in all four sub-figures that although the asymptotic solution is qualitatively accurate (especially in the latter three where ϵ_I is very small), the thermal explosion time is delayed. The relative error in the asymptotic time to ignition does not improve from the figure with the largest value of ε_I to the figure with the smallest value of ε_I. This is because the value of T_B used is not

process, $T_B \to \infty$, is only meant to signify the tending of T_B away from unity.

[8]The asymptotic solutions (- - -) in figures 2.15 and 2.16 have only been plotted for the two regions that have been resolved (Region I: Induction, and Region II: Thermal Explosion). We thus notice that at the end of the thermal explosion, the asymptotic solutions veer away from the profiles of the numerical solutions.

sufficiently distant from unity.

Figure 2.15: Comparing the composite asymptotic solution (- - -) with the numerical solution (—) for $T_B = 1.5$ using four decreasing values of ε_I.

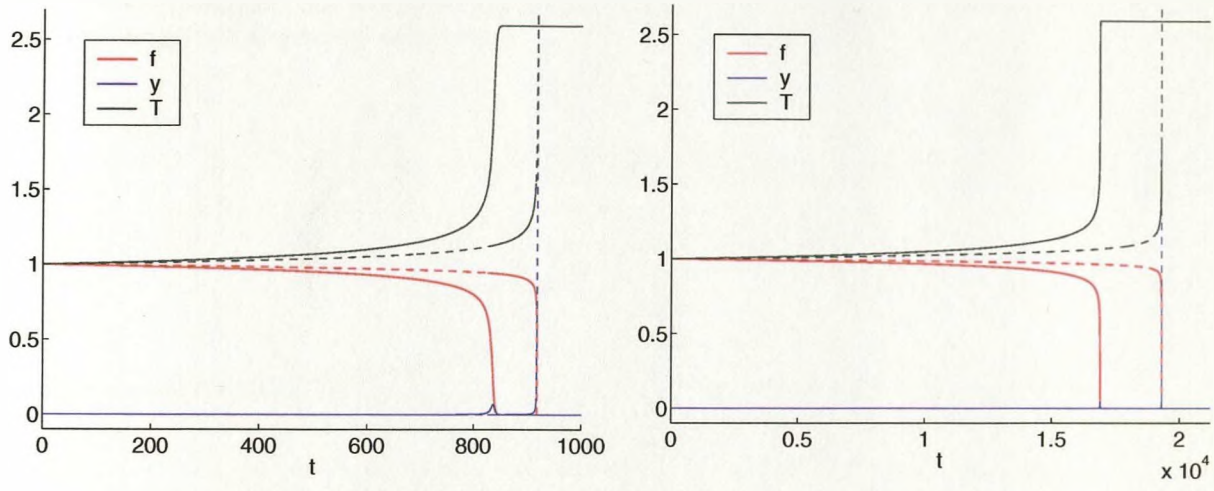

(a) $\varepsilon_I = 1/15$ (b) $\varepsilon_I = 1/20$

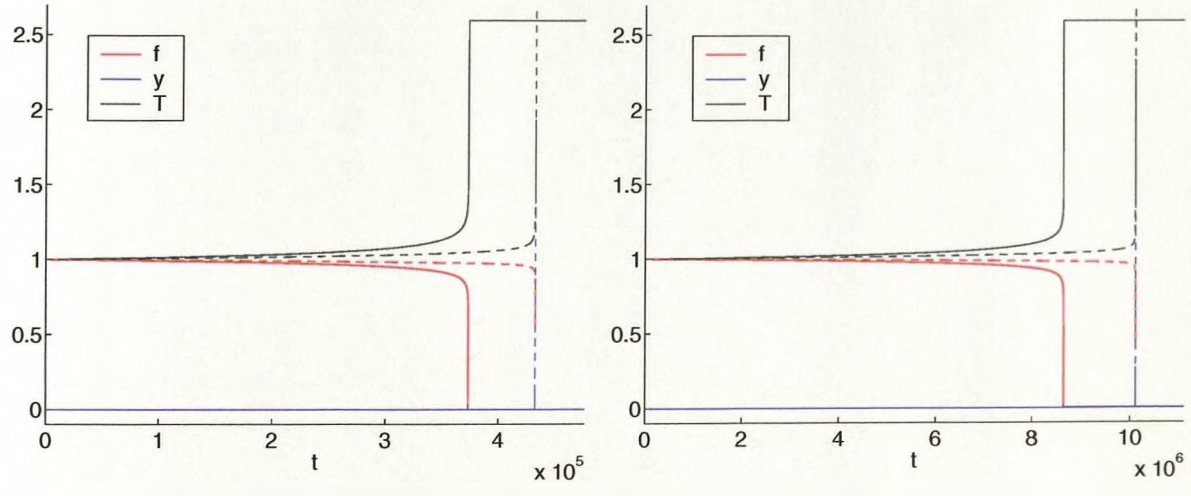

(c) $\varepsilon_I = 1/25$ (d) $\varepsilon_I = 1/30$

Figure 2.16 shows the same comparison but for $T_B = 2.5$ (which is just below the maximum possible temperature for the set of parameters used), and hence we should be more in conformity with our double limiting process (2.103). We immediately notice

that the asymptotic time to ignition is now improving with decreasing ε_I. Decreasing ε_I further should produce an even better agreement between our solutions, although doing so would become increasingly difficult computationally.

Figure 2.16: Comparing the composite asymptotic solution (- - -) with the numerical solution (—) for $T_B = 2.5$ using four decreasing values of ε_I.

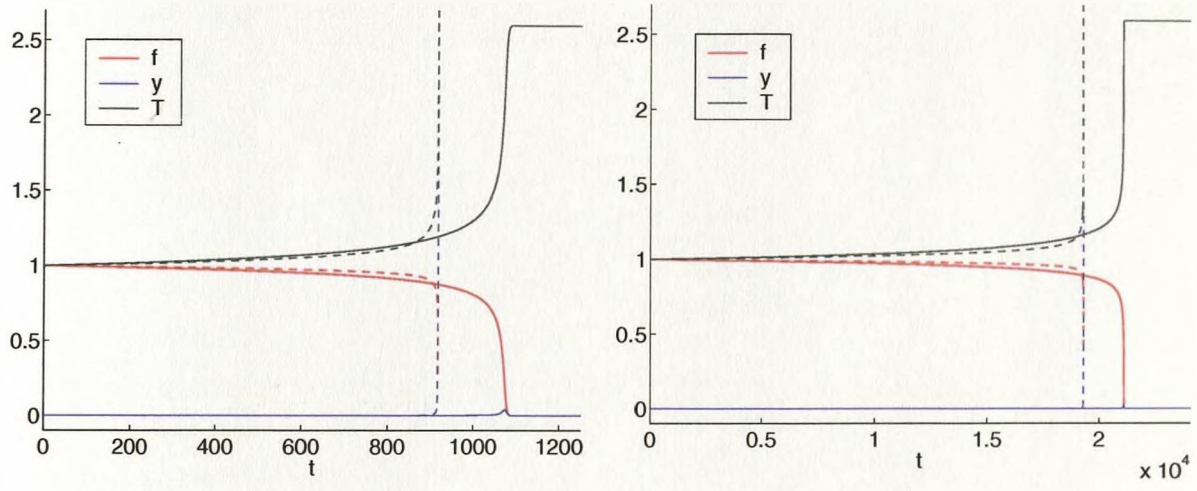

(a) $\varepsilon_I = 1/15$ (b) $\varepsilon_I = 1/20$

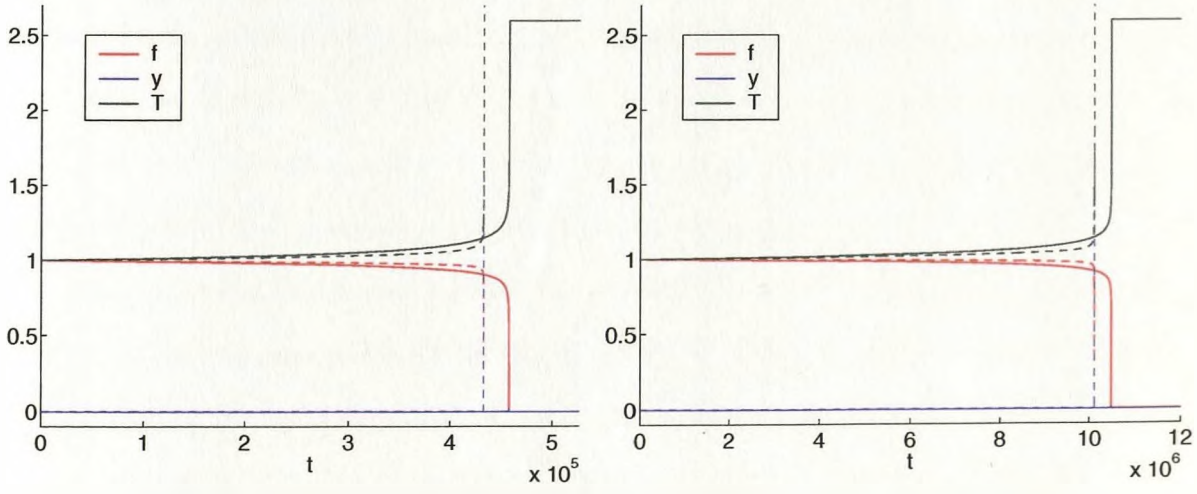

(c) $\varepsilon_I = 1/25$ (d) $\varepsilon_I = 1/30$

Figure 2.17: Comparing the asymptotic expressions for t_{ign} with the numerical t_{ign} for various T_B while keeping $\varepsilon_I = 1/15$ and $\varepsilon_B = 1/5$.

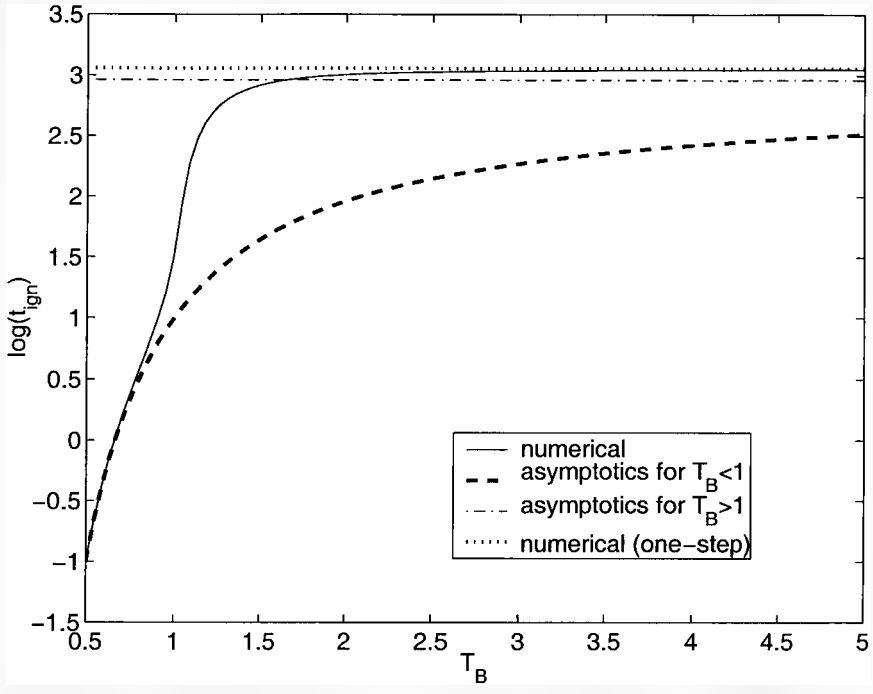

2.5 Validity of the asymptotics around $T_B = 1$

We have produced asymptotic solutions to our governing equations (2.10)–(2.13) for the two cases $T_B < 1$ and $T_B > 1$. Naturally, we have seen that these solutions agree more and more with the numerical solution the closer we get to the limiting values of the asymptotic parameters. For $T_B < 1$, we saw that the closer ε_B was to zero and the further away T_B was from unity, then the better the agreement was between the asymptotics and the numerics. In other words, the more these parameters reflected a higher degree of chain-branching then the better the agreement was. For $T_B > 1$, the absence of the T_B parameter in the asymptotics means that the asymptotic solutions do not accommodate or permit any level of chain-branching as they are actually representing thermal explosions. The agreement between the asymptotics and numerics was thus better for smaller ε_I and larger T_B.

Figure 2.17 shows the two asymptotic t_{ign} expressions[9], (2.47) and (2.74), plotted

[9]The logarithm of t_{ign} is plotted for clarity.

against the numerical t_{ign} for various T_B.[10] A clear discrepancy exists in the region around $T_B = 1$, where the asymptotic t_{ign}'s from both regions quickly diverge from the numerical t_{ign} as they move out of their domain of validity. The asymptotic t_{ign} for $T_B < 1$ shows excellent agreement for T_B less than about 0.6 (for our particular choice of parameter values). The $T_B > 1$ asymptotic t_{ign} agrees reasonably well for T_B greater than about 1.5, although the two plots do not coalesce exactly owing to our constant and not so small value of $\varepsilon_I = 1/15$. If we plot similar figures, decreasing ε_I from one to the next and hence employing the double limiting process (2.103), then the two plots should eventually converge (as observed earlier in figure 2.16). One-step studies [22, 30] show that the time to ignition is actually

$$t_{ign} = t_{ign}^{le}(1 + O(\varepsilon_I)),$$

where t_{ign}^{le} is our leading order asymptotic t_{ign} (2.74).

The general conclusion is that all the asymptotic expressions generated in both the $T_B < 1$ and $T_B > 1$ cases are only valid when $T_B - 1 = O(1)$. In order to improve the accuracy of our asymptotic solutions around the critical point $T_B = 1$, we can either use more asymptotically effective values of our parameters (ε_I, ε_B, T_B) in which case we risk rendering the problem inapplicable to the physical world and probably making it computationally too expensive, or we can determine higher order terms. It could be more fruitful to examine new cases in which we would consider values of T_B that are a small but fixed distance from 1 (such as $T_B = 1 \pm \varepsilon_B$ or $T_B = 1 \pm \varepsilon_B \ln(\varepsilon_B)$). This is similar to what Blythe et al. [14] have done, though their work is still in review.

[10] Asymptotic t_{ign} for $T_B > 1$ is a straight line since it does not vary with T_B. The dotted line is the numerical t_{ign} for the *one-step* case and is plotted here for discussion in section 2.6.1.

2.6 Parameter matching our three-step model with other models

As we have seen, the three-step model used here allows one to model scenarios ranging from the nearly purely thermal to the nearly purely chain-branching. Purely thermal reactions are typically modelled using the standard one-step scheme (1.9) such as that used in [29], whose dimensional equations can be written as

$$\frac{d\tilde{f}}{d\tilde{t}} = -\tilde{k}\tilde{f}\exp\left(-\frac{1}{\tilde{\varepsilon}\tilde{T}}\right) \text{ and} \tag{2.104}$$

$$\frac{d\tilde{T}}{d\tilde{t}} = -\frac{\tilde{Q}}{\tilde{c}_v}\tilde{k}\tilde{f}\exp\left(-\frac{1}{\tilde{\varepsilon}\tilde{T}}\right), \tag{2.105}$$

where $\tilde{k}$ is the rate constant, $\tilde{\varepsilon}$ is the inverse activation energy of the reaction, $\tilde{c}_v$ is the specific heat at constant volume, and all other parameters are as in the three-step model.

Purely chain-branching reactions can be modelled using a two-step scheme such as that used in [21], the homogeneous version of which can be written in dimensional form as

$$\frac{d\xi}{d\tilde{t}} = \tilde{k}_1\exp\left(-\frac{1}{\tilde{\varepsilon}\tilde{T}}\right), \tag{2.106}$$

$$\frac{d\lambda}{d\tilde{t}} = H(\xi)\tilde{k}_2(1-\lambda) \text{ and} \tag{2.107}$$

$$\tilde{c}_v\frac{d\tilde{T}}{d\tilde{t}} = \tilde{Q}H(\xi)\tilde{k}_2(1-\lambda), \tag{2.108}$$

where $\tilde{k}_1$ is the rate constant for the first step that represents an isothermal initiation and branching stage (the induction zone), $\tilde{\varepsilon}$ is the inverse activation energy, and $\tilde{k}_2$ is the rate constant for the second step that represents the exothermic termination stage. Instead of fuel mass fractions, this model uses two reaction progress variables: ξ for the induction zone and λ for the termination zone. The start of the induction zone is given by $\xi = 0$ and the end is signalled by $\xi = 1$, at which point the second step begins with $\lambda = 0$ and ends with $\lambda = 1$ when all the fuel has been burnt into products. The Heaviside function

$H(\xi)$ is defined as

$$H(\xi) = \begin{cases} 0 & \text{if } \xi < 1, \\ 1 & \text{if } \xi \geq 1, \end{cases} \tag{2.109}$$

and hence allows the second step to be switched on for a particle as soon as the induction time elapses for it.

This two-step scheme, as opposed to a three-step scheme, is possible since it assumes that the induction zone ends (at $\xi = 1$) with a complete and instantaneous transformation from an all-fuel state to an all-chain carrier state. The downside is that this simplification does not allow for fuel or chain carrier mass fraction profiles to be determined.

The purpose of this section is to make parameter identifications, where possible, between our three-step model and the one-step and two-step models described above, by comparing the asymptotic and/or analytical expressions, where they exist.

2.6.1 One-step model parameter matching

Having already seen that for $T_B > 1$ (where $T_B - 1 = O(1)$) our three-step model is actually modelling thermal reactions, we shall in this case attempt to match the parameters from our three-step model to those from the one-step model.

Time to ignition

From Kapila's one-step analysis [29], the asymptotic time to ignition for the one-step model (2.104)–(2.105) can be written in dimensional form as

$$\tilde{t}_{ign}^{1step} = \frac{\tilde{\varepsilon}\tilde{T}_0^2\tilde{c}_v}{\tilde{Q}\tilde{k}} \exp\left(\frac{1}{\tilde{\varepsilon}\tilde{T}_0}\right). \tag{2.110}$$

Rewriting our ($T_B > 1$) three-step asymptotic time to ignition (2.74) in terms of k_I, Q and γ, we get

$$t_{ign}^{3step} = \frac{\varepsilon_I}{Q(\gamma-1)k_I} \exp\left(\frac{1}{\varepsilon_I}\right). \tag{2.111}$$

Dimensionalizing and then using the definition $\tilde{c}_v = \frac{\tilde{R}}{\tilde{\mu}(\gamma-1)}$ gives

$$\tilde{t}_{ign}^{3step} = \frac{\tilde{\varepsilon}_I \tilde{T}_0^2 \tilde{c}_v}{\tilde{Q}\tilde{k}_I} \exp\left(\frac{1}{\tilde{\varepsilon}_I \tilde{T}_0}\right). \tag{2.112}$$

Comparing $\tilde{t}_{ign}^{1step}$ with $\tilde{t}_{ign}^{3step}$ we see that we have equivalence between the three-step model (when $T_B > 1$) and the one-step model, if we make the following parameter matches:

$$\tilde{\varepsilon}_I^{3step} = \tilde{\varepsilon}^{1step}, \quad \tilde{Q}^{3step} = \tilde{Q}^{1step}, \quad \tilde{k}_I^{3step} = \tilde{k}^{1step}. \tag{2.113}$$

This simple and straightforward match is further confirmation that our three-step model is capable of modelling thermal reactions, and also shows that the one-step reaction actually represents the three-step initiation reaction.

Region I: Fuel and temperature

Given our parameter identifications (2.113), we can now check if our three-step asymptotic solutions for f and T are the same as those of the one-step model (the three-step y solution - which is nearly zero in the $T_B > 1$ case - cannot be compared because the one-step model, by definition, does not involve chain carriers).

In Region I, the ($T_B > 1$) three-step fuel solution (2.71) can be written in dimensional form as

$$f^{3step} = 1 + \frac{\tilde{\varepsilon}_I \tilde{T}_0^2 \tilde{c}_v}{\tilde{Q}} \ln\left[1 - \frac{\tilde{Q}\tilde{k}_I}{\tilde{\varepsilon}_I \tilde{T}_0^2 \tilde{c}_v} \exp\left(-\frac{1}{\tilde{\varepsilon}_I \tilde{T}_0}\right)\tilde{t}\right], \tag{2.114}$$

and the ($T_B > 1$) three-step temperature (2.73) can be written in dimensional form as

$$\tilde{T}^{3step} = \tilde{T}_0 \left\{1 - \tilde{\varepsilon}_I \tilde{T}_0 \ln\left[1 - \frac{\tilde{Q}\tilde{k}_I}{\tilde{\varepsilon}_I \tilde{T}_0^2 \tilde{c}_v} \exp\left(-\frac{1}{\tilde{\varepsilon}_I \tilde{T}_0}\right)\tilde{t}\right]\right\}. \tag{2.115}$$

Writing Kapila's one-step temperature profile [29] for Region I in dimensional form gives

$$\tilde{T}^{1step} = \tilde{T}_0 \left\{ 1 - \tilde{\varepsilon}\tilde{T}_0 \ln \left[1 - \frac{\tilde{Q}\tilde{k}}{\tilde{\varepsilon}\tilde{T}_0^2 \tilde{c}_v} \exp\left(-\frac{1}{\tilde{\varepsilon}\tilde{T}_0} \right) \tilde{t} \right] \right\}, \tag{2.116}$$

while using his relation,

$$f = 1 - \frac{\tilde{c}_v}{\tilde{Q}}(\tilde{T} - \tilde{T}_0), \tag{2.117}$$

between fuel and temperature, gives the one-step fuel profile as

$$f^{1step} = 1 + \frac{\tilde{\varepsilon}\tilde{T}_0^2 \tilde{c}_v}{\tilde{Q}} \ln \left[1 - \frac{\tilde{Q}\tilde{k}}{\tilde{\varepsilon}\tilde{T}_0^2 \tilde{c}_v} \exp\left(-\frac{1}{\tilde{\varepsilon}\tilde{T}_0} \right) \tilde{t} \right]. \tag{2.118}$$

Comparing f^{3step} with f^{1step}, and $\tilde{T}^{3step}$ with $\tilde{T}^{1step}$, we can see that these solutions are exactly equivalent given our parameter matches (2.113).

Region II: Fuel and temperature

In this thermal explosion zone, the ($T_B > 1$) three-step temperature (2.102) can be written in dimensional form as

$$\tilde{T}^{3step} = \tilde{T}_0 \left\{ \frac{1}{1 + J(\tilde{t})} - \frac{\tilde{\varepsilon}_I \tilde{T}_0}{\left[1 + J(\tilde{t})\right]^2} \ln \left[\left[1 + J(\tilde{t})\right] \left(1 + \frac{\tilde{\mu}\tilde{Q}(\gamma - 1) + \tilde{R}\tilde{T}_0}{\tilde{\mu}\tilde{Q}(\gamma - 1)} J(\tilde{t}) \right) \right] \right\}, \tag{2.119}$$

where

$$J(\tilde{t}) = \tilde{\varepsilon}_I \tilde{T}_0 \ln \left[1 - \frac{\tilde{Q}\tilde{k}_I}{\tilde{\varepsilon}_I \tilde{T}_0^2 \tilde{c}_v} \exp\left(-\frac{1}{\tilde{\varepsilon}_I \tilde{T}_0} \right) \tilde{t} \right]. \tag{2.120}$$

Kapila's one-step temperature profile [29] can be written dimensionally as

$$\tilde{T}^{1step} = \tilde{T}_0 \left\{ \frac{1}{1 + K(\tilde{t})} - \frac{\tilde{\varepsilon}\tilde{T}_0}{\left[1 + K(\tilde{t})\right]^2} \ln \left[\left[1 + K(\tilde{t})\right] \left(1 + \frac{\tilde{\mu}\tilde{Q}(\gamma - 1) + \tilde{R}\tilde{T}_0}{\tilde{\mu}\tilde{Q}(\gamma - 1)} K(\tilde{t}) \right) \right] \right\}, \tag{2.121}$$

where

$$K(\tilde{t}) = \tilde{\varepsilon}\tilde{T}_0 \ln \left[1 - \frac{\tilde{Q}\tilde{k}}{\tilde{\varepsilon}\tilde{T}_0^2 \tilde{c}_v} \exp\left(-\frac{1}{\tilde{\varepsilon}\tilde{T}_0} \right) \tilde{t} \right]. \tag{2.122}$$

Hence, we have equivalence between $\tilde{T}^{3step}$ and $\tilde{T}^{1step}$ given our parameter matches (2.113).

Using (2.117), the one-step fuel solution can be written in terms of $\tilde{T}^{1step}$ as

$$f^{1step} = 1 - \frac{\tilde{c}_v}{\tilde{Q}}(\tilde{T^{1step}} - \tilde{T}_0). \tag{2.123}$$

Writing our three-step relation between fuel and temperature (2.16) in dimensional form gives

$$f = 1 - y - \frac{\tilde{c}_v}{\tilde{Q}}(\tilde{T} - \tilde{T}_0), \tag{2.124}$$

and hence if $y = o(f, T)$ in this region, then at leading order our three-step fuel solution would be

$$f^{3step} = 1 - \frac{\tilde{c}_v}{\tilde{Q}}(\tilde{T} - \tilde{T}_0), \tag{2.125}$$

which is equivalent to f^{1step} assuming our parameter matches (2.113). Now, in this region,

$$y = e_I e^{\frac{\hat{Y}}{\varepsilon_I}} = \frac{1}{(1-\hat{\tau})^2} \exp\left[\frac{1}{\varepsilon_I}\left(\frac{1}{T_I} - 1 + \hat{\tau}\right)\right], \tag{2.126}$$

and we have already seen that $\exp\left[\frac{1}{\varepsilon_I}\left(\frac{1}{T_I} - 1 + \hat{\tau}\right)\right]$ is exponentially small throughout this region. Hence, since τ, f and T are all $O(1)$ in this region, then we can safely ignore y here, and so f^{3step} is indeed equivalent to f^{1step} given our parameter matches (2.113).

Verifying the one-step to three-step parameter matches

Having identified which parameters in the one-step model correspond to which parameters in our three-step model, and consequently verified the equivalence of the asymptotic solutions, it would be beneficial to compare the numerical solutions of the full equations of both models for the same set of matched parameters. Figure 2.18 does this for two values of ε_I^{3step} ($\equiv \varepsilon^{1step}$), where for each one we plot the solution for three increasing values of T_B. As expected, for both values of ε_I, we see that larger T_B leads to a better agreement between the one-step and three-step models. Indeed, figure 2.17 shows that,

for finite ε_I, the three-step numerical t_{ign} asymptotes to the one-step numerical t_{ign} as $T_B \to \infty$. The smaller value of ε_I should, in accordance with our double limit (2.103), produce a faster convergence of the solutions. Figure 2.18(b) shows that although the solutions are relatively better, they are not drastically improved. Nevertheless, the figures do illustrate the qualitative equivalence of the one-step and three-step models via our parameter matches.

Figure 2.18: Comparing the one-step numerical solution (—) with the three-step numerical solution for $T_B = 1.5$ (- - -), $T_B = 2.0$ (— · —·) and $T_B = 2.5$ (· · ·).

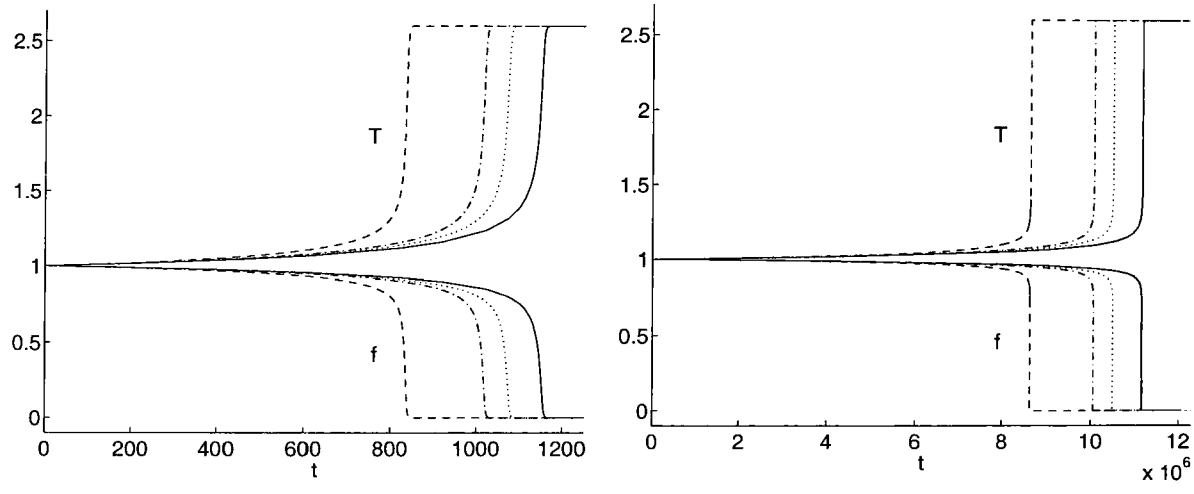

(a) $\varepsilon_I = 1/15$ (b) $\varepsilon_I = 1/30$

2.6.2 Two-step model parameter matching

The two-step scheme models purely chain-branching scenarios, and hence we can seek to match its parameters with those of our $T_B < 1$ three-step model (where $T_B - 1 = O(1)$).

Time to ignition

In the two-step model, the induction zone is completely isothermal (with $T = T_0$), and so the reciprocal of (2.106) becomes

$$\frac{d\tilde{t}}{d\xi} = \frac{1}{\tilde{k}_1} \exp\left(\frac{1}{\tilde{\varepsilon}\tilde{T}_0}\right). \tag{2.127}$$

Integrating through the induction zone gives

$$\int_{\tilde{t}=0}^{\tilde{t}=\tilde{t}_{ign}^{2step}} d\tilde{t} = \int_{\xi=0}^{\xi=1} \frac{1}{\tilde{k}_1} \exp\left(\frac{1}{\tilde{\varepsilon}\tilde{T}_0}\right) d\xi, \tag{2.128}$$

and so the exact analytical expression for the two-step ignition time is

$$\tilde{t}_{ign}^{2step} = \frac{1}{\tilde{k}_1} \exp\left(\frac{1}{\tilde{\varepsilon}\tilde{T}_0}\right). \tag{2.129}$$

If we now dimensionalize the ($T_B < 1$) three-step asymptotic ignition time (2.47) we get

$$\tilde{t}_{ign}^{3step} = \frac{1}{\tilde{k}_C} \exp\left(\frac{1}{\tilde{\varepsilon}_B\tilde{T}_0} - \frac{1}{\tilde{\varepsilon}_B\tilde{T}_B}\right)\left(\frac{1}{\tilde{\varepsilon}_B\tilde{T}_B} - \frac{1}{\tilde{\varepsilon}_B\tilde{T}_0} - \frac{1}{\tilde{\varepsilon}_I\tilde{T}_I} + \frac{1}{\tilde{\varepsilon}_I\tilde{T}_0}\right). \tag{2.130}$$

Dimensionalizing (2.6) gives $\frac{\tilde{k}_B}{\tilde{k}_C} = \exp\left(\frac{1}{\tilde{\varepsilon}_B\tilde{T}_B}\right)$, and hence

$$\tilde{t}_{ign}^{3step} = \frac{1}{\tilde{k}_B} \exp\left(\frac{1}{\tilde{\varepsilon}_B\tilde{T}_0}\right)\left(\frac{1}{\tilde{\varepsilon}_B\tilde{T}_B} - \frac{1}{\tilde{\varepsilon}_B\tilde{T}_0} - \frac{1}{\tilde{\varepsilon}_I\tilde{T}_I} + \frac{1}{\tilde{\varepsilon}_I\tilde{T}_0}\right). \tag{2.131}$$

Comparing $\tilde{t}_{ign}^{3step}$ with $\tilde{t}_{ign}^{2step}$ we see that they are equivalent if we apply the following parameter matches

$$\tilde{\varepsilon}_B^{3step} = \tilde{\varepsilon}^{2step}, \quad \tilde{k}_B^{3step} = \tilde{k}_1^{2step}\left(\frac{1}{\tilde{\varepsilon}_B\tilde{T}_B} - \frac{1}{\tilde{\varepsilon}_B\tilde{T}_0} - \frac{1}{\tilde{\varepsilon}_I\tilde{T}_I} + \frac{1}{\tilde{\varepsilon}_I\tilde{T}_0}\right). \tag{2.132}$$

So although the inverse activation temperatures of the first step in the two-step model is shown to be equivalent to the inverse activation energy of the branching step in the three-

step model, the rate constants involve a factor (which is a function of other parameters) in their relation. Indeed, this result shows that the two-step induction step actually represents a combination of initiation and branching effects.

Termination zone temperature

Owing to the simplifications made in the two-step model, we cannot identify f or y with anything from it. Nor can we compare the three-step branching region solutions with two-step equivalents since the branching step has been replaced with a discontinuity in the two-step model. We can however compare the temperatures in the termination region since the termination step is explicitly defined in both models.

The simplicity of the two-step model already allowed us to determine the exact analytical ignition time, but we can also determine the exact analytical solution for the temperature in this region. We first note that $H(\xi) = 1$ since $\xi \geq 1$ here. Hence, (2.108) becomes

$$\frac{d\tilde{T}}{d\tilde{t}} = \frac{\tilde{Q}\tilde{k}_2}{\tilde{c}_v}(1-\lambda), \tag{2.133}$$

with boundary condition $\tilde{T}(\tilde{t} = \tilde{t}_{ign}^{2step}) = \tilde{T}_0$ since no heat is released up until ignition. To determine the required λ, we can write (2.107) as

$$\frac{d\lambda}{d\tilde{t}} = \tilde{k}_2(1-\lambda), \tag{2.134}$$

with boundary condition $\lambda(\tilde{t} = \tilde{t}_{ign}^{2step}) = 0$ since the termination reaction begins at ignition. Integrating gives

$$\lambda = 1 - \exp\left[\frac{\tilde{k}_2}{\tilde{k}_1}\exp\left(\frac{1}{\tilde{\varepsilon}\tilde{T}_0}\right) - \tilde{k}_2\tilde{t}\right], \tag{2.135}$$

and hence (2.133) becomes

$$\frac{d\tilde{T}}{d\tilde{t}} = \frac{\tilde{Q}\tilde{k}_2}{\tilde{c}_v}\exp\left[\frac{\tilde{k}_2}{\tilde{k}_1}\exp\left(\frac{1}{\tilde{\varepsilon}\tilde{T}_0}\right) - \tilde{k}_2\tilde{t}\right], \tag{2.136}$$

which after integration gives

$$\tilde{T}^{2step} = \tilde{T}_0 + \frac{\tilde{Q}}{\tilde{c}_v}\left\{1 - \exp\left[\frac{\tilde{k}_2}{\tilde{k}_1}\exp\left(\frac{1}{\tilde{\varepsilon}\tilde{T}_0}\right) - \tilde{k}_2\tilde{t}\right]\right\}. \tag{2.137}$$

The ($T_B < 1$) three-step asymptotic temperature (2.60) can be written in dimensional form as

$$\tilde{T}^{3step} = \tilde{T}_0 + \frac{\tilde{Q}}{\tilde{c}_v}\left\{1 - \exp\left[\left(\frac{1}{\tilde{\varepsilon}_B\tilde{T}_B} - \frac{1}{\tilde{\varepsilon}_B\tilde{T}_0} - \frac{1}{\tilde{\varepsilon}_I\tilde{T}_I} + \frac{1}{\tilde{\varepsilon}_I\tilde{T}_0}\right)\frac{\tilde{k}_C}{\tilde{k}_B}\exp\left(\frac{1}{\tilde{\varepsilon}_B\tilde{T}_0}\right) - \tilde{k}_C\tilde{t}\right]\right\}. \tag{2.138}$$

Hence, $\tilde{T}^{3step}$ is the same as $\tilde{T}^{2step}$ if we apply both the parameter identifications already made in (2.132) and the following remaining parameter match

$$\tilde{k}_C^{3step} = \tilde{k}_2^{2step}. \tag{2.139}$$

This is as expected since the two-step termination reaction (which has rate constant $\tilde{k}_2$) corresponds exactly to the three-step termination reaction (which has rate constant $\tilde{k}_C$).

Verifying the two-step to three-step parameter matches

We can now attempt a verification of our matched parameters by comparing (in the termination zone) the numerical temperature solution of the three-step model with the exact analytical temperature solution of the two-step model (2.137). Figure 2.19 shows such a comparison for ε_B^{3step} ($\equiv \varepsilon^{2step}$) $= 1/5$ and for three decreasing values of T_B, and figure 2.20 shows a similar comparison but for a slightly smaller ε_B value of $1/6$. We notice that the temperature solutions converge very well with decreasing T_B, but that they converge much quicker for smaller ε_B, as expected. The exponential factors involving ε_B ($\equiv \varepsilon$) that appear in the asymptotic (2.138) and analytical (2.137) temperature solutions for this termination zone do suggest a rapid convergence of the two models.

Figure 2.19: Comparing the two-step exact analytical temperature (—) with the three-step numerical temperature (- - -) for $\varepsilon_B = 1/5$.

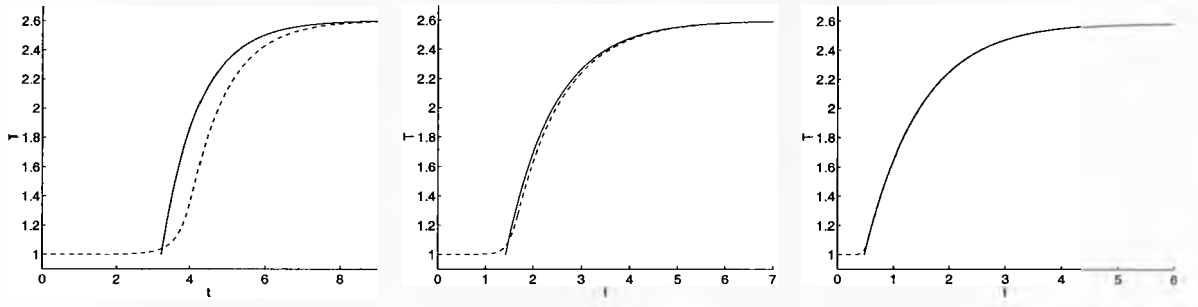

(a) $T_B = 0.8$ (b) $T_B = 0.7$ (c) $T_B = 0.6$

Figure 2.20: Comparing the two-step exact analytical temperature (—) with the three-step numerical temperature (- - -) for $\varepsilon_B = 1/6$.

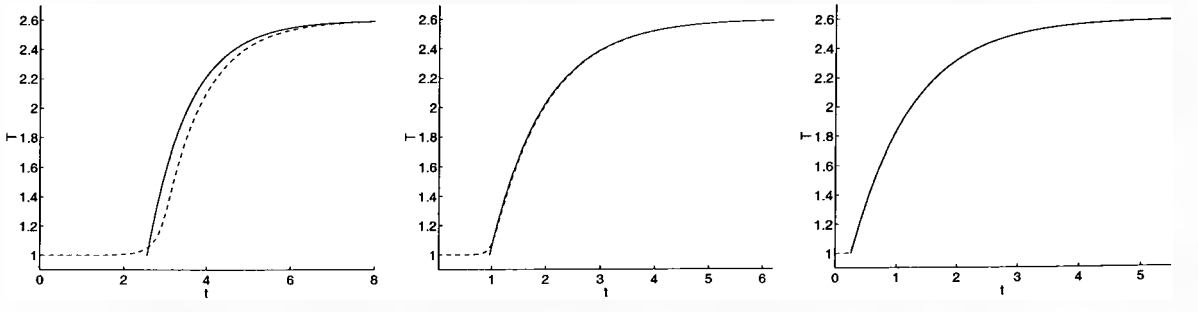

(a) $T_B = 0.8$ (b) $T_B = 0.7$ (c) $T_B = 0.6$

Chapter 3

PISTON-DRIVEN SHOCK-INDUCED INITIATION OF DETONATION WAVES

3.1 The mathematical model

Consider a solid piston moving at a constant velocity u_p through a long channel full of reactive gas that is initially motionless and homogeneous. In a conventional shock tube system as used in experiments, the tube is a round or rectangular rigid pipe and the piston is substituted with a rapidly expanding driver gas which is initially separated from the reactive gas by a diaphragm. The sudden rupture of this diaphragm causes the high pressure in the driver gas to expand rapidly into the reactive gas forming a weak shock wave [15]. This weak shock wave eventually reflects off the end wall of the tube to produce a stronger shock capable of igniting the gas in its wake[1]. Assuming diaphragm rupture is instantaneous and does not disturb the subsequent flow, this shock reflection from a wall setup would be equivalent to our solid piston system.

The shock is formed immediately at the piston and travels into the gas at an initial velocity u_s relative to the tube. Ahead of the shock we have the upstream "undisturbed" gas (whose state is denoted by the subscript '0'), and behind the shock we have the

[1]If diaphragm rupture results in a sufficiently strong shock wave and a driving contact surface, then this can lead to ignition without the need for reflection off a wall. This is the subject of chapter 4.

Figure 3.1: Piston-tube system.

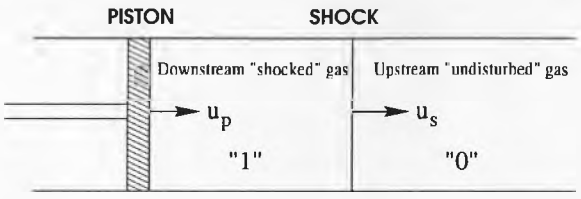

downstream "shocked" gas (whose state is denoted by the subscript '1') (figure 3.1). The dependent variables involved are those of the homogeneous case (f, y, z and T), as well as gas velocity u, pressure p, density ρ and internal energy e, whereas the independent variables are those of time t and distance x from the piston's starting position.

Piston-tube systems usually entail one-dimensional modelling, and this assumption is nearly always made in this kind of work. However, careful observations in the late 1950s and early 1960s revealed that detonations typically have an unsteady three-dimensional cellular structure [28]. The cell boundaries are transverse waves which collide with one another and with the leading shock wave making it wrinkled. However, one-dimensional modelling of the detonation front is still a very good approximation and is commonly used today, and needless to say it is important to theoretical development because it can provide a firm platform for understanding and tackling the problem in higher dimensions. Also, tube experiments of shock ignition [38] have shown that the evolution before a full detonation is achieved is actually highly one-dimensional.

Transport effects (such as heat conduction and diffusion) were bypassed in the homogeneous study by assuming a well-stirred chemical mixture. In detonation studies, transport effects can be ignored because velocities and changes of velocities in detonations are typically of the order of the sound speed or greater. Any role played by transport effects is thus negligibly small.

3.1.1 Governing equations

The gas dynamics in our system are described by the one-dimensional Euler equations

$$\frac{\partial \rho}{\partial t} + u\frac{\partial \rho}{\partial x} + \rho\frac{\partial u}{\partial x} = 0, \tag{3.1}$$

$$\frac{\partial u}{\partial t} + u\frac{\partial u}{\partial x} + \frac{1}{\rho}\frac{\partial p}{\partial x} = 0, \tag{3.2}$$

$$\frac{\partial e}{\partial t} + u\frac{\partial e}{\partial x} - \frac{p}{\rho^2}\left(\frac{\partial \rho}{\partial t} + u\frac{\partial \rho}{\partial x}\right) = 0,$$

which represent the conservation of mass, momentum and energy, respectively. Using a polytropic equation of state, we can write the internal energy e of the gas as

$$e = \frac{p}{(\gamma - 1)\,\rho} - Q\,(1 - f - y)\,, \tag{3.3}$$

where the second term represents the internal energy liberated as a result of the exothermic termination reaction (note that, as in the homogeneous case, chemical heat release is proportional to the buildup of products). The ideal thermal equation of state,

$$T = \frac{p}{\rho}, \tag{3.4}$$

then allows us to write e as

$$e = \frac{T}{(\gamma - 1)} - Q\,(1 - f - y)\,. \tag{3.5}$$

Hence, we can replace the conservation of energy equation with the following temperature equation:

$$\frac{DT}{Dt} + Q\,(\gamma - 1)\left(\frac{Df}{Dt} + \frac{Dy}{Dt}\right) - (\gamma - 1)\,\frac{p}{\rho^2}\frac{D\rho}{Dt} = 0, \tag{3.6}$$

where $\frac{D\square}{Dt}$ is shorthand for the total (particle following) derivative $\frac{\partial \square}{\partial t} + u\frac{\partial \square}{\partial x}$.

These are coupled to equations representing the conservation of chemical species that

are derived by considering the conserved quantities (ρf and ρy), their fluxes ($\rho u f$ and $\rho u y$) and their reaction rates:

$$\frac{1}{t_{ign}}\frac{Df}{Dt} = -f\exp\left[\frac{1}{\varepsilon_I}\left(\frac{1}{T_I}-\frac{1}{T}\right)\right] - \rho f y \exp\left[\frac{1}{\varepsilon_B}\left(\frac{1}{T_B}-\frac{1}{T}\right)\right], \tag{3.7}$$

$$\frac{1}{t_{ign}}\frac{Dy}{Dt} = f\exp\left[\frac{1}{\varepsilon_I}\left(\frac{1}{T_I}-\frac{1}{T}\right)\right] + \rho f y \exp\left[\frac{1}{\varepsilon_B}\left(\frac{1}{T_B}-\frac{1}{T}\right)\right] - y. \tag{3.8}$$

Equations (3.1), (3.2), (3.4), (3.6), (3.7) and (3.8) form a closed system of six equations in six unknowns (u, p, ρ, T, f, y). Variables and constants have been non-dimensionalized with respect to the initial shocked state as follows:

$$\begin{gathered}\rho = \frac{\tilde{\rho}}{\tilde{\rho}_\star}, \quad p = \frac{\tilde{p}}{\tilde{p}_\star}, \quad T = \frac{\tilde{R}\tilde{\rho}_\star}{\tilde{\mu}\tilde{p}_\star}\tilde{T}, \quad u = \left(\frac{\tilde{\rho}_\star}{\tilde{p}_\star}\right)^{\frac{1}{2}}\tilde{u}, \quad c = \left(\frac{\tilde{\rho}_\star}{\tilde{p}_\star}\right)^{\frac{1}{2}}\tilde{c}, \\ t = \frac{\tilde{k}_C}{t_{ign}}\tilde{t}, \quad x = \left(\frac{\tilde{\rho}_\star}{\tilde{p}_\star}\right)^{\frac{1}{2}}\frac{\tilde{k}_C}{t_{ign}}\tilde{x}, \quad Q = \frac{\tilde{\rho}_\star}{\tilde{p}_\star}\tilde{Q}, \quad \varepsilon_I = \tilde{T}_\star\tilde{\varepsilon}_I, \quad \varepsilon_B = \tilde{T}_\star\tilde{\varepsilon}_B,\end{gathered} \tag{3.9}$$

where symbols with a tilde denote dimensional quantities, a '$\star$' subscript denotes values in the initial shocked state, R is the universal gas constant, μ is the mean molecular weight and c is the sound speed as given by

$$c^2 = \frac{\gamma p}{\rho}. \tag{3.10}$$

The value t_{ign} denotes the non-dimensional time-to-ignition as calculated in our homogeneous study. Here, it is determined numerically and defined as the half-reaction time, i.e. the time it takes to reach $f = 0.5$ for the corresponding homogeneous case.

Non-dimensionalizing in this way gives the initial shocked state as

$$\rho = 1, \quad p = 1, \quad T = 1, \quad u = u_p, \tag{3.11}$$

which, apart from u, is precisely the initial state of the gas in our homogeneous vessel study. Although we now consider the gas dynamics of our system, the fact that for $T_B < 1$

we expect a virtually isothermal induction zone means that our conservation of chemical species PDEs (3.7) and (3.8) reduce to our homogeneous chemical species ODEs (2.10) and (2.11). Therefore, we should expect to see the shocked gas at the piston ignite after an induction time that is the same as in the homogeneous case (and hence at $t = 1$ owing to our scaling of time in (3.9)). This is not so for $T_B > 1$ though, since now the induction zone is thermal and hence gas dynamics is important from the outset. The result is that the shocked gas ignites at a time that is not exactly the same as in the homogeneous case [19]. This is a trivial matter however, since the reason why we scale time with t_{ign} is so to cut short the otherwise very long evolution time-scale for the $T_B > 1$ cases, and we do not require an accurate induction time for this purpose.

3.1.2 Shock jump conditions

Our variable and parameter scalings (3.9) give us the initial shocked state (3.11), and hence we need to be able to determine the state of the upstream unshocked gas, given the shock velocity.

If we look at the inert case (i.e. with a non-reactive gas) then the first thing to note is that the shock velocity u_s remains constant, and hence the downstream gas (i.e. the gas between the piston and the shock) also remains at its constant shocked state. The downstream gas travels at the piston velocity u_p. For convenience we shall be using different inertial frames of reference appropriate to the task at hand, namely the tube frame (where the tube is stationary), the piston frame and the shock frame. Shock, piston and gas velocities in this inert case are shown in figure 3.2.

By considering the gas flow in the shock rest frame, we can arrive at shock jump conditions from the basic conservation equations. Conservation of mass requires that

$$\rho_1 v_1 = \rho_0 v_0 \stackrel{def}{=} m, \tag{3.12}$$

Figure 3.2: Shock, piston and gas velocities in the inert case in three frames of reference.

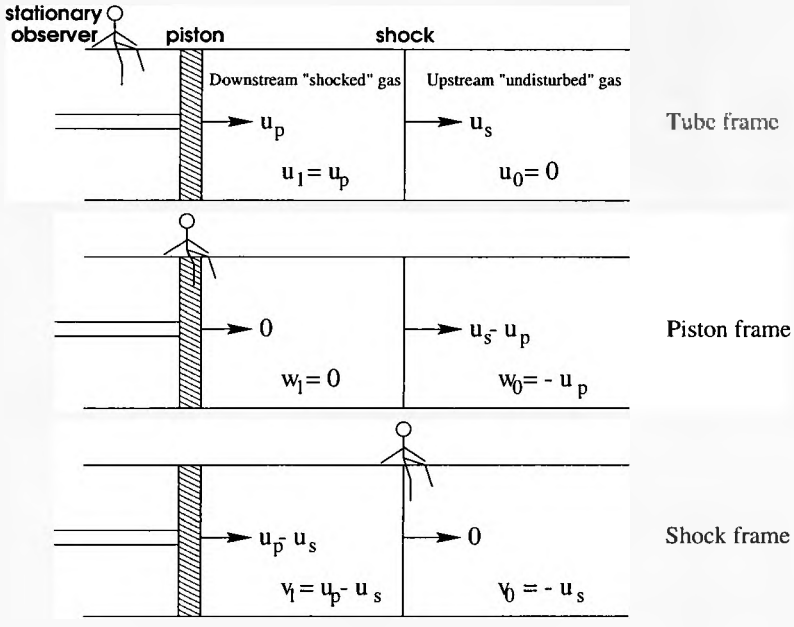

that is the mass flux m is the same on both sides of the shock. Conservation of momentum is expressed by

$$p_1 + mv_1 = p_0 + mv_0,$$

hence,

$$p_1 + \rho_1 v_1^2 = p_0 + \rho_0 v_0^2, \tag{3.13}$$

that is the forces exerted on each other by the gases on the two sides of the shock must be equal. Finally, conservation of energy tells us that the change in total energy per unit time per unit area of the shock surface must be equal to the work done by the gas per unit time per unit area, i.e.

$$\frac{1}{2}m(v_0^2 - v_1^2) + m(e_0 - e_1) = p_1 v_1 - p_0 v_0,$$

which by (3.12) can be expressed as

$$m\left(\frac{p_1}{\rho_1}+\frac{1}{2}v_1^2+e_1\right)=m\left(\frac{p_0}{\rho_0}+\frac{1}{2}v_0^2+e_0\right).$$

But for perfect gases, another of our assumptions,

$$e=\frac{p}{(\gamma-1)\rho}$$

and so we arrive at

$$m\left(\frac{\gamma p_1}{(\gamma-1)\rho_1}+\frac{1}{2}v_1^2\right)=m\left(\frac{\gamma p_0}{(\gamma-1)\rho_0}+\frac{1}{2}v_0^2\right). \tag{3.14}$$

Strictly speaking, the above equations do not apply to shocks only, but for any type of *surface of discontinuity*[2]. Equations (3.12)–(3.14) form a complete system of boundary conditions at a surface of discontinuity, and from them we can immediately deduce two types of surface of discontinuity. The first type is where there is no mass flux through the surface, i.e. $m = 0$. In which case, since ρ_0 and ρ_1 are not zero, it follows that $v_0 = v_1 = 0$. Condition (3.13) gives that $p_0 = p_1$. Thus the velocity and the gas pressure are continuous at the surface of discontinuity, while the density (and other thermodynamic quantities except the pressure) may be discontinuous. In multidimensional situations, such a surface discontinuity is called a *tangential discontinuity*[3] [16], and a particular case of it - relevant to our one-dimensional study - is that of a *contact discontinuity* (or just *contact*), where the velocity and pressure are continuous, but not the density. We will see such contacts appearing in some of our piston-driven shock simulations, and they will also be the driving force in our simulations in chapter 4.

In the second type of surface discontinuity, the mass flux is not zero, and hence v_0 and

[2]Any surface where the quantities concerned (such as velocity, pressure, density, etc.) change discontinuously as we cross such a surface.

[3]Tangential discontinuities are so called because although the velocity normal to the shock is continuous, the tangential velocities may be discontinuous.

v_1 are not zero. Energy condition (3.14) then becomes

$$\frac{\gamma p_1}{(\gamma-1)\rho_1} + \frac{1}{2}v_1^2 = \frac{\gamma p_0}{(\gamma-1)\rho_0} + \frac{1}{2}v_0^2. \tag{3.15}$$

Pressure, density, energy and fluid velocity are all discontinuous across the surface, and it this type of surface that is called a *shock wave*, or just a *shock*. The discontinuities in these variables are related by the conditions (3.12), (3.13) and (3.15).

The Mach number of the shock wave M_0 is defined as

$$M_0 = \frac{u_s}{c_0} = -\frac{v_0}{c_0}, \tag{3.16}$$

and so we can rewrite (3.12), (3.13) and (3.15) as the following shock jump conditions

$$\frac{\rho_1}{\rho_0} = \frac{(\gamma+1)\,M_0^2}{(\gamma-1)\,M_0^2+2}, \tag{3.17}$$

$$\frac{p_1}{p_0} = 1 + \frac{2\gamma}{\gamma+1}\left(M_0^2-1\right), \tag{3.18}$$

$$\frac{v_1}{v_0} = \frac{\rho_0}{\rho_1} = \frac{(\gamma-1)\,M_0^2+2}{(\gamma+1)\,M_0^2}, \tag{3.19}$$

$$\frac{T_1}{T_0} = \frac{p_1\rho_0}{p_0\rho_1}. \tag{3.20}$$

So, given γ and M_0, we can determine the state of ρ, p, v and T on one side of the shock from the state on the other side of the shock.

3.2 Numerical method

We shall solve equations (3.1), (3.2), (3.4), (3.6), (3.7) and (3.8) using the hierarchical adaptive code Cobra, which was developed by Mantis Numerics Ltd and is described fully by Sharpe and Falle [32]. Although Cobra is designed to solve a wide variety of fluid dynamics problems, its user module allows us to incorporate chemical kinetics and physical aspects peculiar to our model. Cobra allows us to use an arbitrary number of hierarchical Cartesian grids $G^0, \ldots, G^N$, with grid G^n having mesh spacing $h/2^n$, where h is the mesh spacing on the base grid G^0. Grids G^0 and G^1 cover the whole domain and the finer grids only cover regions where higher resolution is required, which is determined by an estimate of the truncation error calculated between the solutions on consecutive grids, hence explaining why G^1 also needs to cover the entire domain. If, from grid G^{n-1} to grid G^n, we get a truncation error in the values of the conserved quantities (e.g. density, fuel) or in the rate of change of the conserved quantities that is greater than given tolerances, then we refine to grid G^{n+1}.

Such an adaptive hierarchical grid ensures that areas of rapid change (e.g. shocks) are well refined. However, to guarantee maximum resolution around other areas of rapid change, we will always refine to the highest given grid level when any of the following conditions are satisfied:

1. $\left|\frac{Dy}{Dt}\right| > 0.01$, i.e. during reaction.

2. $f > 0.1$ AND $p > p_0$, i.e. whenever there is a significant amount of fuel behind the shock.

3. $y > 0.1$, i.e. whenever there is a significant concentration of chain carriers (which can only occur behind the shock).

Cobra uses an explicit Godunov scheme, designed for transient, compressible problems involving shocks, and is second order in both space and time.

For convenience, we shall transform to the piston frame by defining two new variables

$$X = x - u_p t, \qquad w = u - u_p \tag{3.21}$$

so that the piston is stationary at $X = 0$ and the post-shock gas speed is initially at rest, i.e. $w = 0$ initially. The boundary condition at the piston is $w(0,t) = 0$, i.e. the gas immediately in front of the stationary piston is also stationary. To express the solid and reflective nature of the piston, we designate the boundary type at the piston as a symmetry condition.

Although there are many parameters involved in this problem, we have already seen in the homogeneous problem that it is the value of T_B which mainly determines the nature of the reaction (between purely chain-branching and purely thermal). Hence we shall only consider varying values of T_B, while fixing the shock Mach number M_0, and keeping all other parameters as they were in the homogeneous study:

$$\varepsilon_I = \frac{1}{15}, \qquad \varepsilon_B = \frac{1}{5}, \qquad Q = 4, \qquad \gamma = 1.4, \qquad T_I = 3, \qquad M_0 = 1.5.$$

3.2.1 Grid resolution analysis

I have chosen the value $h = 0.001$ to be the base grid mesh spacing, i.e. 1000 points per unit X, which is sufficient to ensure a well-resolved induction zone behind the shock. However, to ensure that the whole numerical solution we obtain is independent of the grid spacing, we must choose the number of grid levels N such that the calculations are fully resolved. This will, of course, depend on the parameter set considered, but since we are only considering varying values of T_B, we need only analyse how this parameter would affect the value of N required. As described briefly in the introduction, a reaction wave can develop into a strong CJ detonation for both one-step and two-step kinetics before the

reaction wave collides with the leading shock. This CJ detonation, if it forms, is stronger than the CJ detonation that develops after collision with the leading shock, resulting in a much shorter reaction length and hence requiring the finest resolution. By determining the pre-collision CJ detonation reaction length we can get a good approximation of the highest resolution that will be required to ensure fully resolved calculations across the entire domain. We can thus determine a suitable value of N for that particular parameter set. For scenarios where no CJ detonation occurs before the reaction wave collides with leading shock, we shall still apply the same analysis, even though the value of N that results will be an overestimate of what is really required.

3.3 Numerical Solutions

Five values of T_B are considered: 0.5, 0.6, 0.8, 1.0 and 1.2. The value $T_B = 0.5$ represents a highly chain-branching reaction in the homogeneous constant volume scenario, whereas $T_B = 1.2$ represents a very weakly chain-branching reaction (and thus one resembling thermal reactions). The value of t_{ign} used in the variable scalings (3.9) is given with each figure to provide an idea of the time and distance scales for the value of T_B used.

3.3.1 $T_B = 0.5$

Figures 3.3 and 3.4 show the early evolution for the case $T_B = 0.5$. They show profiles of pressure, temperature and chemical mass fractions all against the distance X from the piston. The black profiles represent the first time step, and the chronological order of the remaining profiles should be self-evident. The pressure-specific volume phase plane diagrams (pV diagrams, where $V = \frac{1}{\rho}$ is the specific volume) are used to classify the evolution to detonation. Clarke et al. [5, 33, 35] have shown that straight lines with a negative slope in the pV diagrams represent quasi-steady wave phenomena, where the slope is proportional to the speed of the wave. We shall use this to identify shocks, fast

Figure 3.3: Piston-driven shock profiles for $T_B = 0.5$ at times 1.0, 1.8, 2.6, 3.4 and 4.2. Scaled with $t_{ign} = 0.1$.

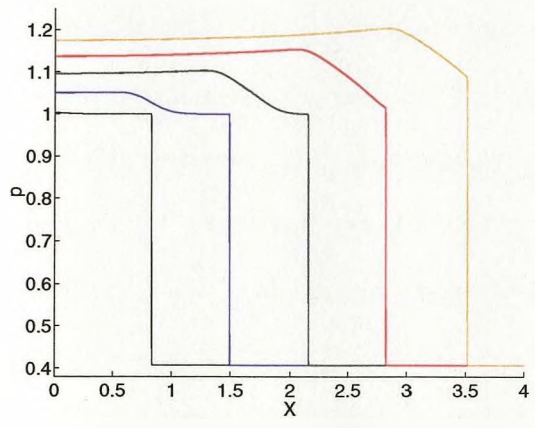

(a) Pressure profiles.

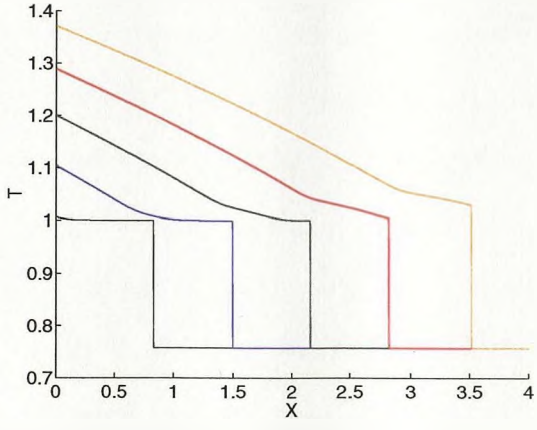

(b) Temperature profiles.

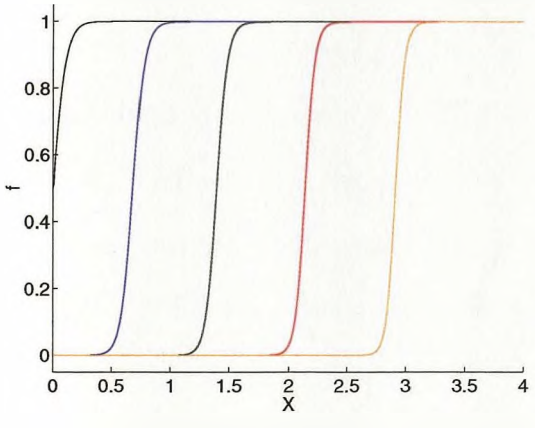

(c) Fuel profiles.

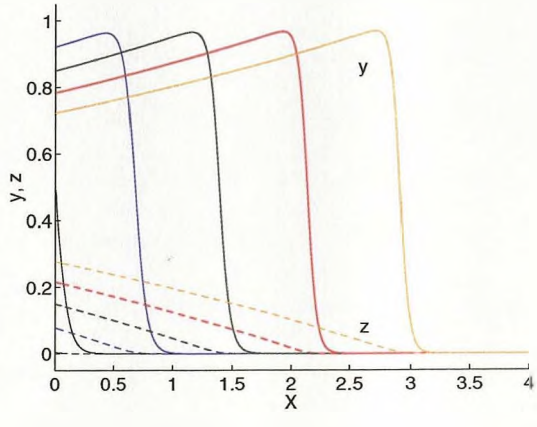

(d) Chain carrier and product profiles.

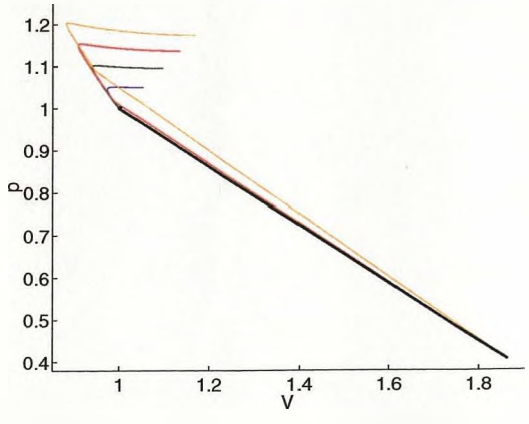

(e) pV diagrams.

flames and detonations, if and when they occur.

At $t = 1.0$ we see that the shock has just left the piston and that, as expected from our scalings in (3.9), the post-shock pressure and temperature are both unity. Also as expected from our scalings, the fuel f has just ignited at the piston (since it is here that the gas is shocked first) and chain carriers y are building up rapidly. In accordance with chain-branching kinetics, no products z, and hence no heat, have yet been produced. By the next time step, products are beginning to build up at the piston, and consequently, heat and pressure disturbances begin to propagate away from the piston (along positive characteristics) towards the shock at the sound speed of the undisturbed post-shock state. In contrast with one-step shock systems where the ignition point travels supersonically and with an initially infinite speed [20], here the ignition point (taken to be the point where $f = 0.5$) travels subsonically, and hence the disturbances quickly overtake the chain-branching explosion ignition point. At $t = 3.4$, the head of the compression wave catches up with the shock, leaving the chain-branching ignition point quite far behind. The fact that this compression wave reaches the shock before a secondary shock develops, makes this situation completely unlike what happens with one-step schemes where secondary shocks are always formed, unless the activation energy is rather low (i.e. the shock wave is sufficiently strong) [22].

Up to this point, the shock remains at the same strength, and this is represented in the pV plane by straight lines stretching from the bottom right corner (the unshocked gas) to a single point at $p = V = 1$. The steady nature of the shock is by virtue of an induction zone that is thermally neutral together with the fact that disturbances have not (up until now) had the chance to affect the shock. The induction zone lies along a curve with negative slope in the pV plane. Although these curves appear to lie on roughly straight lines, as do quasi-steady weak detonations [5], the induction zone is thermally neutral and so cannot be associated with reaction waves in the pV plane. Indeed, in section 3.5 we show that for chain-branching cases like this, the induction zone portions

Figure 3.4: Piston-driven shock profiles for $T_B = 0.5$ at times 5.0, 11.0, 17.0, 23.0 and 29.0. Scaled with $t_{ign} = 0.1$.

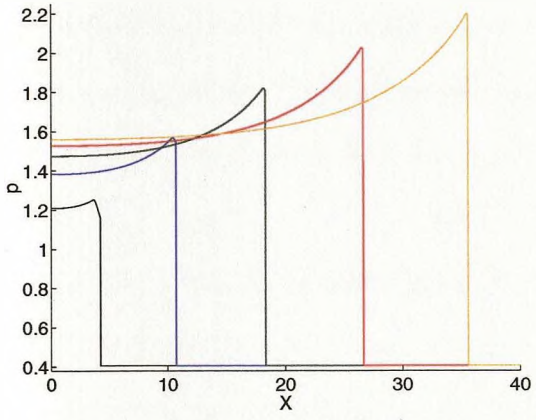

(a) Pressure profiles.

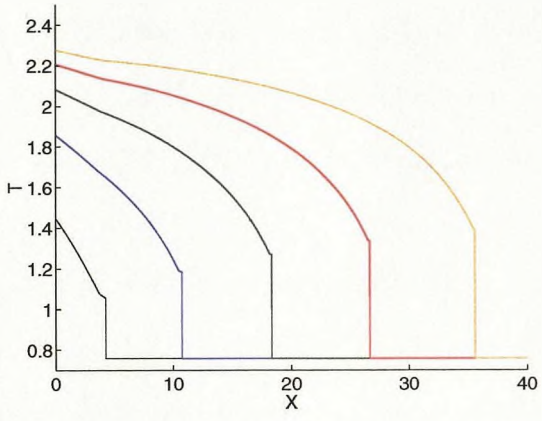

(b) Temperature profiles.

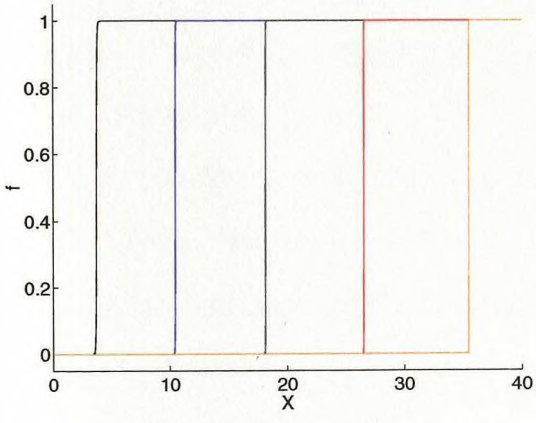

(c) Fuel profiles.

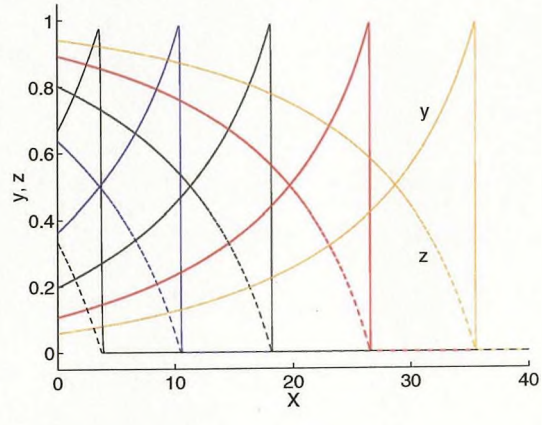

(d) Chain carrier and product profiles.

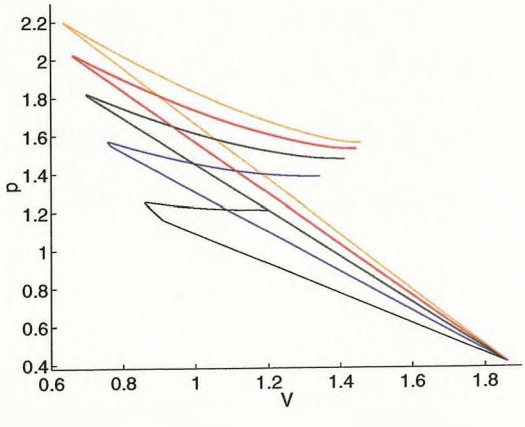

(e) pV diagrams.

of the pV curves are in fact parts of isentropes.

We see at $t = 4.2$ that the pressure disturbances have amplified the shock, and this is represented in the pV diagram by an upwards shift in the end point of the shock and a steepening of the slope. The pressure and pV profiles show the induction zone to be increasingly compressive, and the heat release zone gradually becoming increasingly expansive.

Figure 3.4 shows the shock rapidly increasing in strength, heating the gas in its wake to higher temperatures and thus shortening the induction zone until it becomes virtually no more than a single point in our pV diagrams from the third time step onwards. The closing in of the reaction wave on the shock is depicted in the pV plane by a gradual coalescing of the corresponding lines. Although not shown, eventually the two lines will be completely coupled in a single straight line, representing the birth of a quasi-steady strong CJ detonation.

This entire evolution of a highly chain-branching CJ detonation can be seen in Sharpe's simulations of the two-step (purely) chain-branching system [21]. The relevant case is that in which he considers slow heat release in the termination reaction zone (i.e. a small value of his k parameter). Although he uses larger Mach number and activation energy, we can still easily see that his pressure, temperature and pV profiles for this case compare qualitatively very well with the corresponding profiles in figures 3.3 and 3.4. A difference is that, since in the two-step model the branching zone is replaced by a discontinuity, the gradients in Sharpe's case are discontinuous at the pressure maximum, which separates the induction zone from the termination zone. In our case, the profiles remain smooth at the pressure maximum due to a finite, but thin, branching zone.

3.3.2 $T_B = 0.6$

Slightly increasing the branching crossover temperature T_B to 0.6, we begin to witness a qualitative change in the nature of the solution. The first three time steps in figure 3.5

Figure 3.5: Piston-driven shock profiles for $T_B = 0.6$ at times 1.0, 1.5, 2.0, 2.5 and 3.0. Scaled with $t_{ign} = 0.48$.

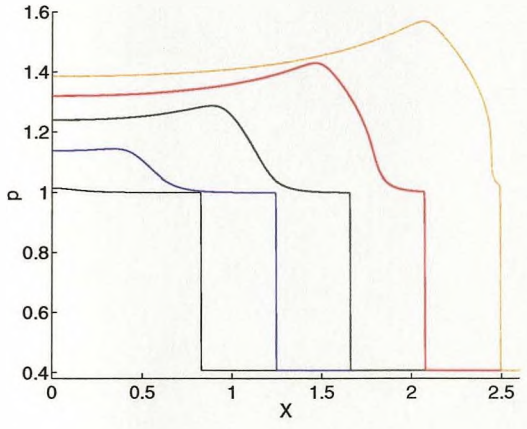

(a) Pressure profiles.

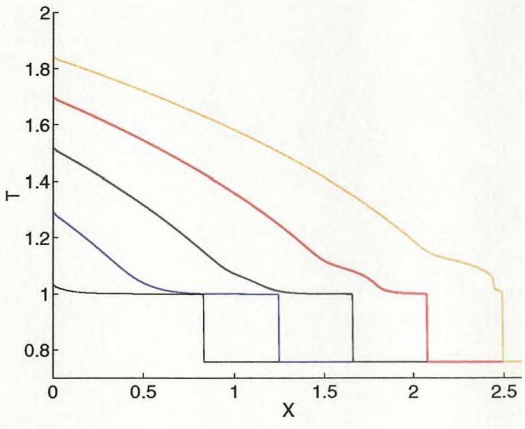

(b) Temperature profiles.

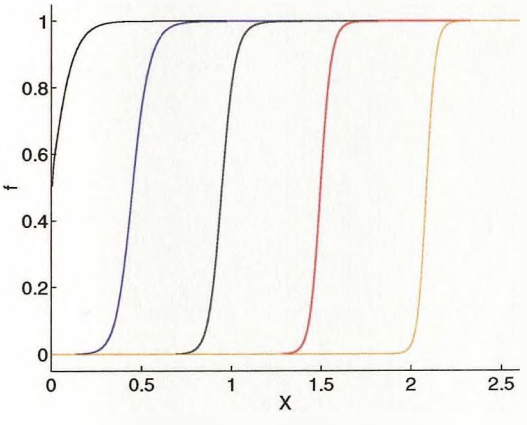

(c) Fuel profiles.

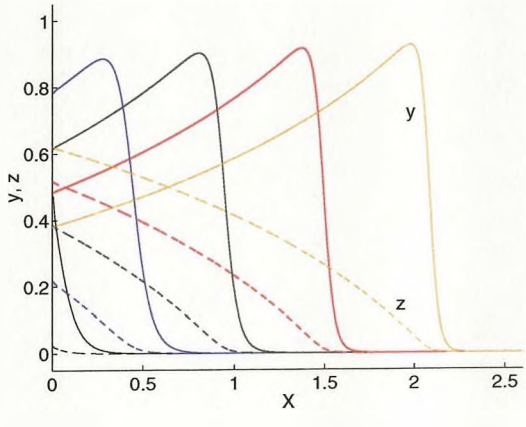

(d) Chain carrier and product profiles.

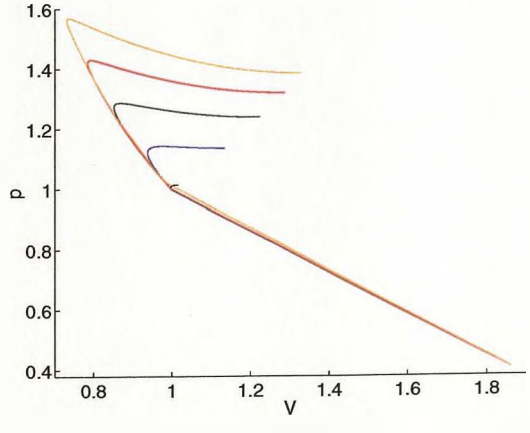

(e) pV diagrams.

Figure 3.6: Piston-driven shock profiles for $T_B = 0.6$ at times 3.05, 3.08, 3.11, 3.14 and 3.17. Profiles are zoomed in at wave collision except in pV figure. Scaled with $t_{ign} = 0.48$.

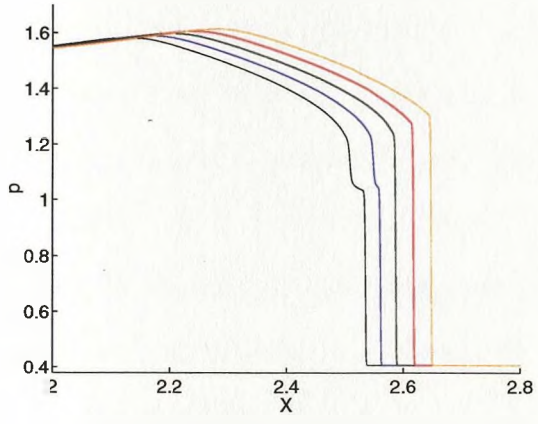

(a) Pressure profiles.

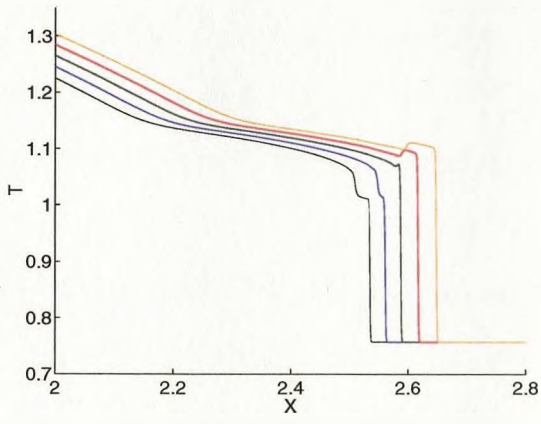

(b) Temperature profiles.

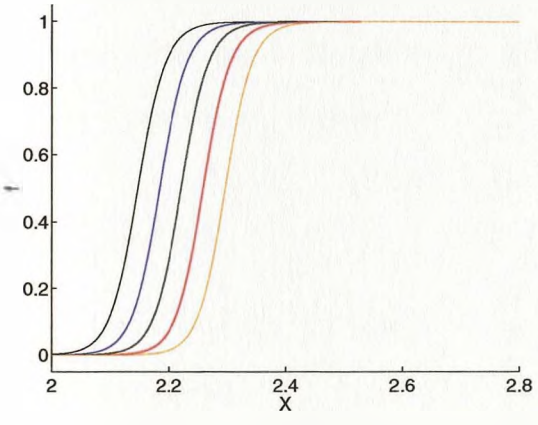

(c) Fuel profiles.

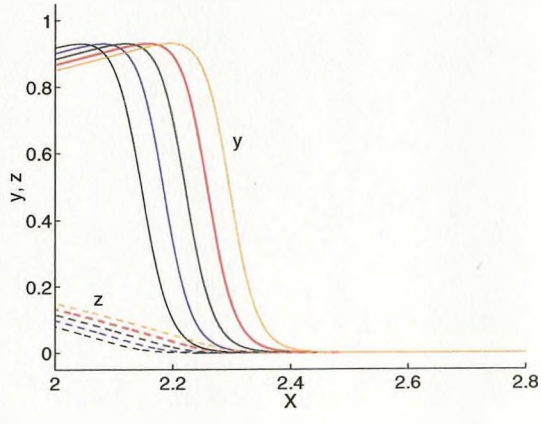

(d) Chain carrier and product profiles.

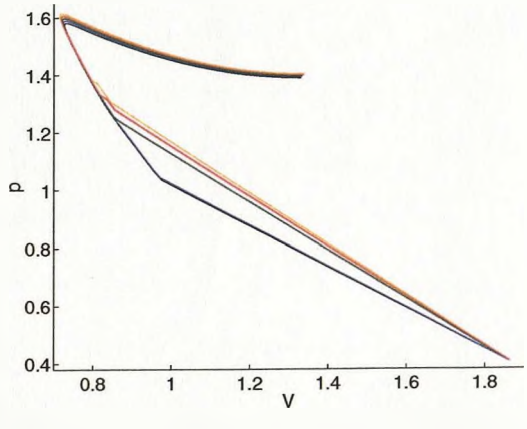

(e) pV diagrams.

are very similar to the early evolution in our $T_B = 0.5$ case, however the front of the compression wave steepens heavily, and eventually at $t = 3.0$ it becomes a very weak secondary shock located just behind the leading shock. It is so weak however, that it barely registers in the pV diagram as a straight line (stretching from $p = 1.1$ to $p = 1.2$ approximately), and hence it may be better described as a very strong compression wave at this point.

Figure 3.6 shows the very strong compression wave colliding with the leading shock, to form a new, much stronger, leading shock at $t = 3.11$. A structure similar to a contact forms at collision, and this is shown by a small and sudden rise in our temperature profiles at about $X = 2.6$ and a nearly horizontal line in our pV plane near to $V = 0.8$. A genuine contact would appear as a temperature discontinuity in the temperature profile and as a horizontal line in the pV diagram (which indicates a discontinuity in density and temperature but not in pressure).

3.3.3 $T_B = 0.8$

For $T_B = 0.8$, we notice in figure 3.7 that the pressure and temperature disturbances steepen more rapidly than for the previous case, so much so that a secondary shock (which is more powerful than the leading shock and which appears between the third and fourth times shown) forms much closer to the piston and further away from the leading shock than in the previous $T_B = 0.6$ case. A similar observation was noted in Sharpe's analysis of the two-step model [21] where, for the rapid heat release case (in which his k parameter is large), the secondary shock forms much nearer the piston and further away from the leading shock than for the moderate heat release case (in which $k = O(1)$).

It is worth noting here that, although the induction zone remains thermally neutral and void of products, we begin to witness a significant amount of product formulating in the branching zone at least initially (see the first three time steps in figure 3.7(d)), and hence we also get a significant amount of heat release according to equation (3.3). This heat

Figure 3.7: Piston-driven shock profiles for $T_B = 0.8$ at times 1.00, 1.25, 1.50, 1.75 and 2.00. Scaled with $t_{ign} = 3.801$.

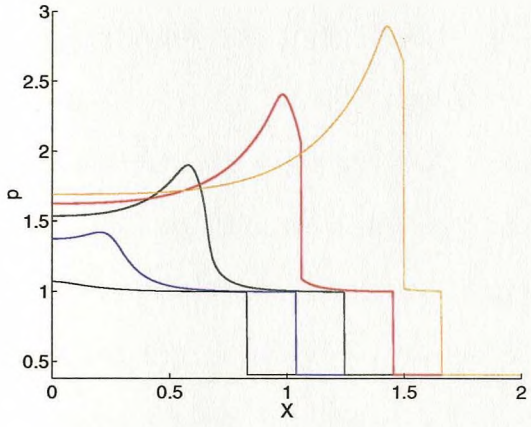

(a) Pressure profiles.

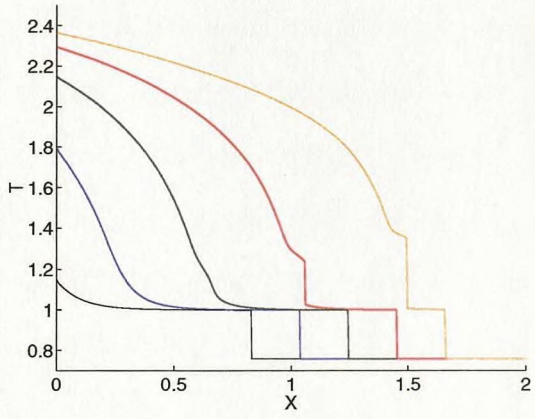

(b) Temperature profiles.

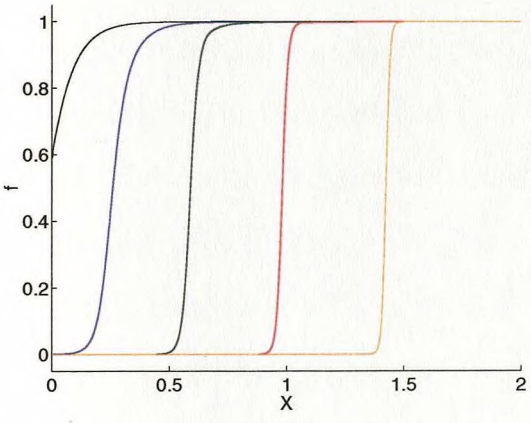

(c) Fuel profiles.

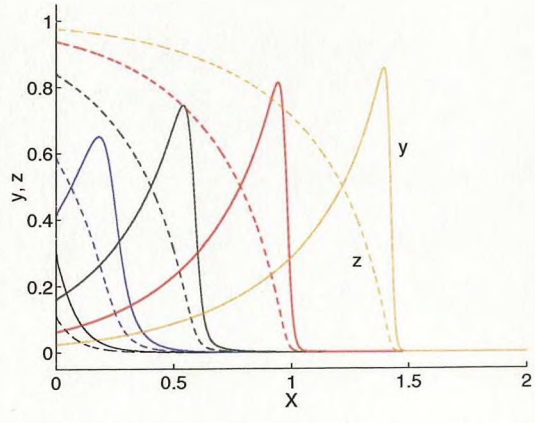

(d) Chain carrier and product profiles.

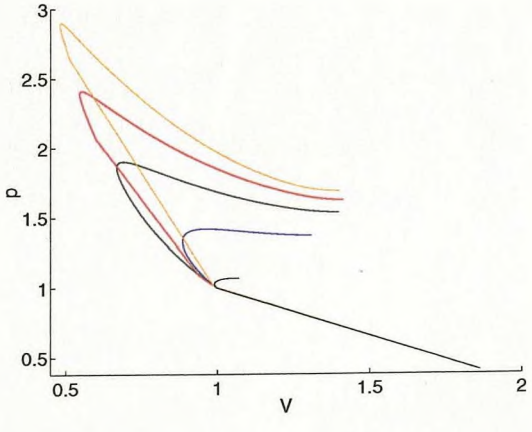

(e) pV diagrams.

release results in a rapid steepening of the pressure and temperature disturbances so that a powerful secondary shock eventually forms. The pV plane clearly shows this secondary shock as a straight line in the last two plots, and the steepening slope indicates that it is accelerating, due to the heat release from the expansive exothermic termination zone (the branching zone is now very thin). Before secondary shock formation, the compressive induction and branching zones are highly unsteady (apparent in the pV profiles as a highly curved section stretching from the leading shock wave to the pressure maximum, beyond which is the highly exothermic termination zone). After the secondary shock forms, these zones become thinner because of the secondary shock heating the gas to much higher temperatures, hence shortening the ignition times and increasing the peak value of the chain carrier concentrations.

The second time step in figure 3.8 shows that the secondary shock has just collided with the leading shock. The two straight lines of the first profile in the pV plane, representing the two shocks, merge in the second profile into one straight line which depicts a single transmitted shock that is much stronger than the pre-collision leading shock. We notice from comparing the shock profiles with the reactant profiles that the shock collision takes place inside the induction zone. A contact quickly develops, which is slower than the transmitted shock, and is clearly visible in the next time steps as a discontinuity downstream of the transmitted shock in the temperature profiles and as a horizontal line in the pV plane. Also at collision, a rarefaction or expansive wave forms and is shown moving slowly towards the piston in the pressure profiles. As is visible in the temperature profiles, the gas between the transmitted shock and the contact is now hotter in comparison to the trailing flow. As a result, a second ignition point starts to form in the last time step, and is manifested in the fuel profiles as a blip inside the original induction zone. The fuel just in front of the contact will soon ignite, giving a new reaction zone between the shock and contact. This new reaction zone however is interrupted by the passing contact, which drops the temperature suddenly back to pre-shock collision tem-

Figure 3.8: Piston-driven shock profiles for $T_B = 0.8$ at times 2.145, 2.155, 2.165, 2.175 and 2.185. Profiles are zoomed in at shock collision except in first pV figure. Scaled with $t_{ign} = 3.801$.

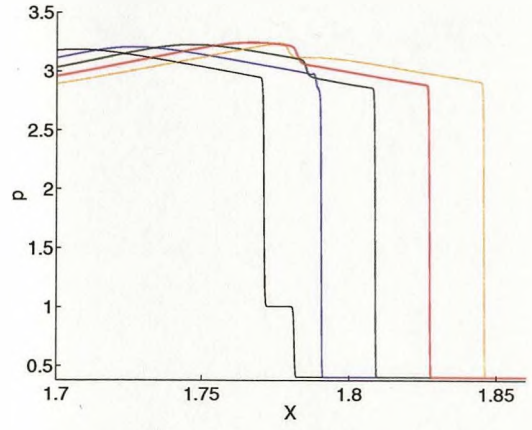

(a) Pressure profiles.

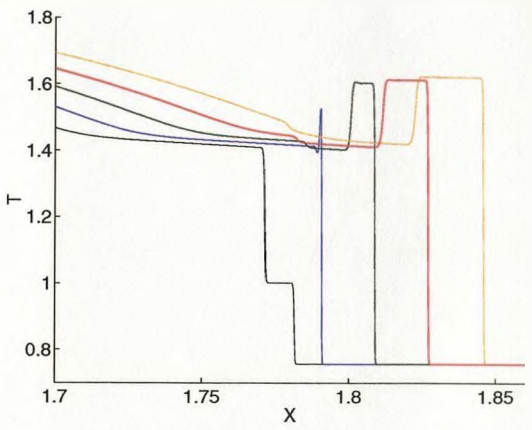

(b) Temperature profiles.

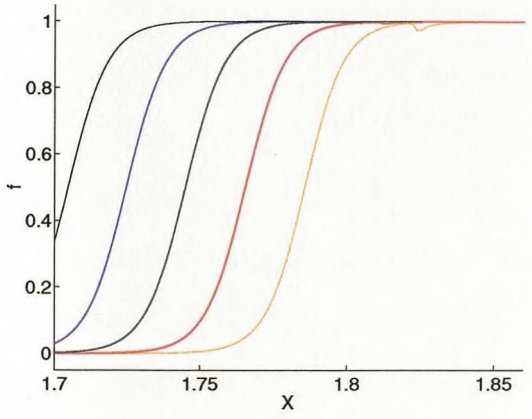

(c) Fuel profiles.

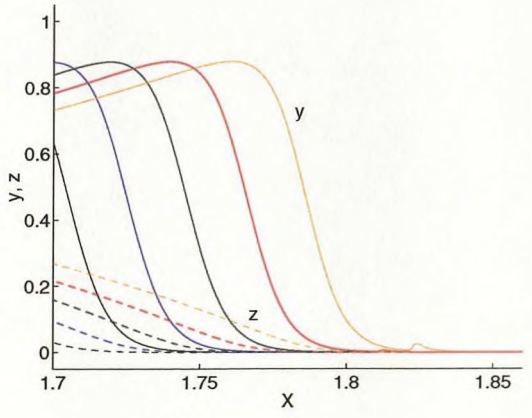

(d) Chain carrier and product profiles.

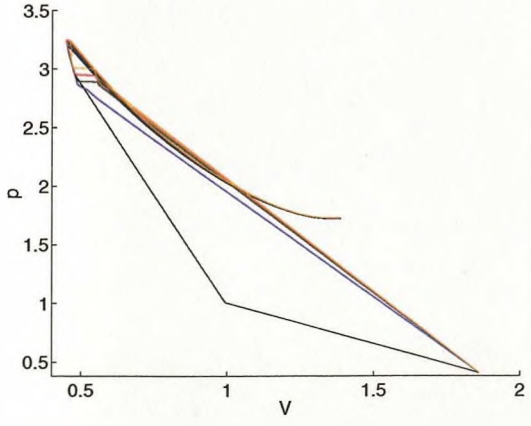

(e) pV diagrams.

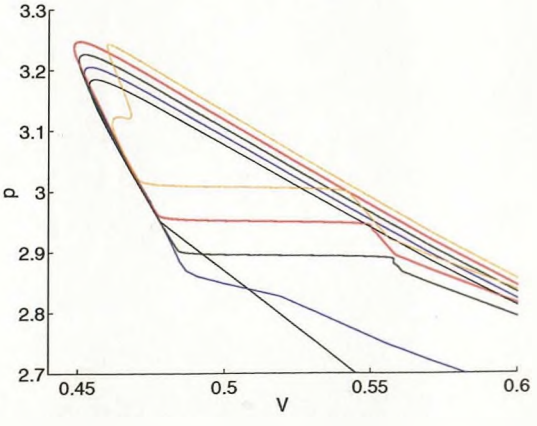

(f) pV diagrams zoomed in at contacts.

peratures. For this reason, this new reaction zone appears only as a blip in the chemical mass profiles. Downstream of the contact is the remainder of the original induction zone which was behind the secondary shock before collision.

3.3.4 $T_B = 1.0$

Increasing T_B further to 1.0, we expect to see both thermal and chain-branching effects to be present, at least initially (see figure 2.17).

Figure 3.9 shows that the secondary shock forms even closer to the piston and further away from the leading shock than in the previous $T_B = 0.8$ case. Pressure-mass fraction phase planes are used to show the location of events inside the reaction zone. For example, figure 3.9(f) shows the leading shock to exist where $f = 1$ and $y = z = 0$. The secondary shock forms at the start of the induction zone and certainly before the chain-branching explosion. This means that the secondary shock, which raises the temperature from near T_B to well above it, passes through a high concentration of fuel f, and hence is able to significantly affect the magnitude of the chain-branching reaction. We notice, for instance, that the rate of change of fuel and chain carriers increases significantly, and hence the value of the peak chain carrier mass fraction also increases significantly.

Initially, the pV diagrams have positive slope everywhere downstream of the leading shock, indicating that the induction zone is free of wave-like behaviour (the slope of a reaction wave in the pV plane is proportional to the negative square of the mass flux through the wave, and hence must be negative [33]), but also that it is now significantly thermal. Eventually, at $t = 1.21$, we begin to see the tell-tale signs of a weak detonation, a supersonic quasi-steady (shockless) reaction wave always witnessed during the evolution to a strong ZND detonation in one-step models. The straight line at the start of the induction zone extending to a short distance from the pressure maximum indicates the wave is quasi-steady, whereas the fact that f decreases as V decreases on the wave shows that the flow through the wave must be supersonic [5]. This, together with the fact

Figure 3.9: Piston-driven shock profiles for $T_B = 1.0$ at times 1.00, 1.07, 1.14, 1.21 and 1.28. Scaled with $t_{ign} = 34.64$.

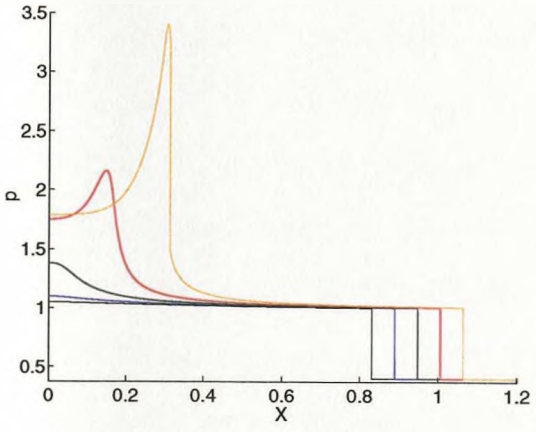

(a) Pressure profiles.

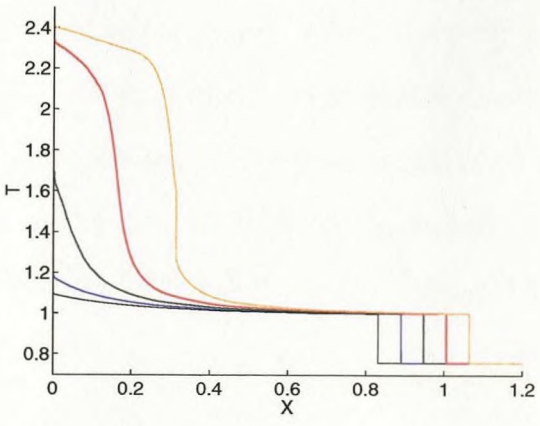

(b) Temperature profiles.

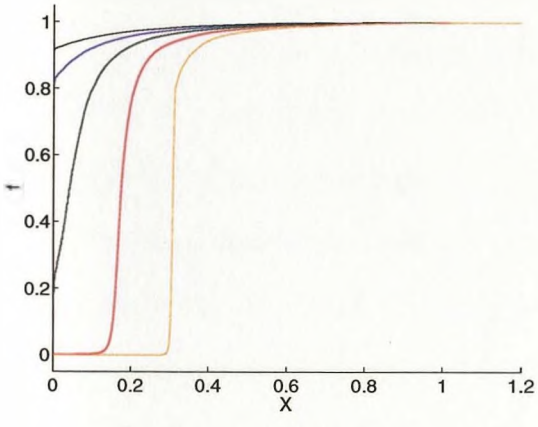

(c) Fuel profiles.

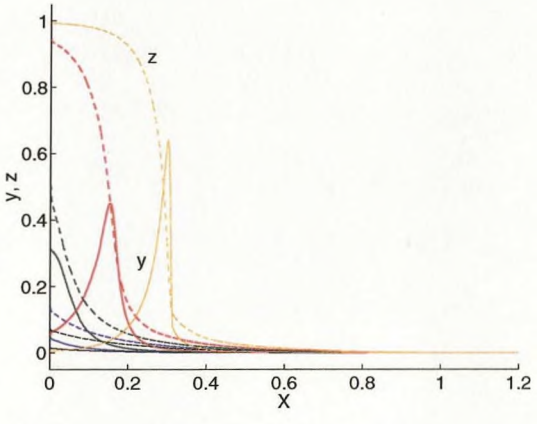

(d) Chain carrier and product profiles.

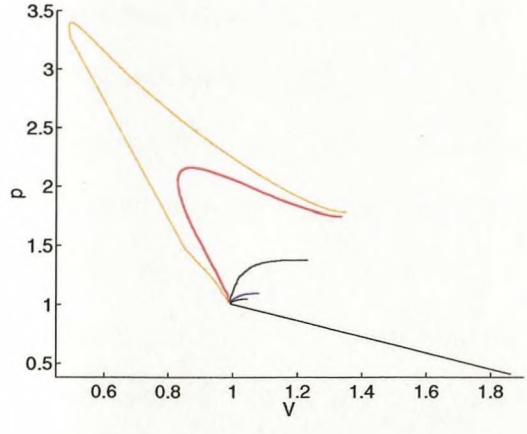

(e) pV diagrams.

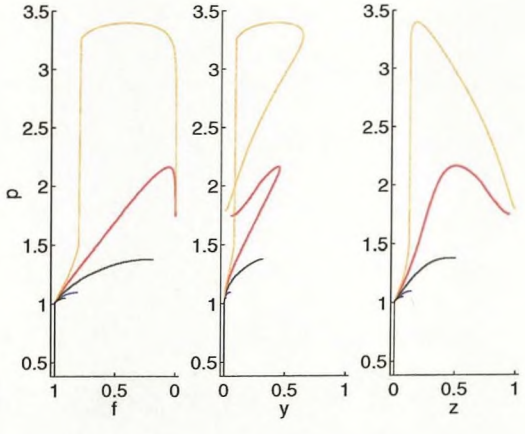

(f) Pressure against mass fractions.

that both pressure and density increase through the wave, means that it must be a weak detonation [5].

An important point to make here about this and other types of reaction waves (such as strong detonations and fast flames), is that heat must be released through the wave [33], otherwise the evolution is along an isentrope (cf. discussion on isentropes in sections 3.3.1 and 3.5). Heat release in our three-step model is proportional to the product mass fraction z (equation (3.3)), and we notice in figure 3.9(d) that there is a very substantial buildup of z very early on that is even greater than the buildup of chain carriers y (although both are building up substantially). This is unsurprising since $T \sim T_B$ early on, and hence $R_B \sim R_C$. Even in the last time step, we can see significant z ahead and within the growing branching explosion. This induction zone buildup of z and associated heat release is the main difference between this $T_B = 1$ case and the previous (highly chain-branching) $T_B < 1$ cases, and so the weak detonation is associated with the growth in z ahead, through which it is moving (see the last two p-z profiles in figure 3.9(f)).

In the last time step, this weak detonation is followed by the newly formed secondary shock, which in turn is followed by a highly unsteady, chemically active flow around the pressure maximum in which most of the fuel is consumed and in which the chain-branching explosion occurs (see the last profile in figure 3.9(f)). This is then followed by an expansive quasi-steady reaction wave, indicated by a straight line in the pV plane that heads down to about $p = 2.7$, which in turn is followed by an unsteady rarefaction wave that makes corrections to the gas velocity in order that the boundary condition at the piston, $w(0,t) = 0$, is met [5]. The quasi-steady reaction wave is actually a fast flame by virtue of it it being both expansive and subsonic (that it is subsonic is evident from the fact that, within it, f decreases as V increases [5]). The combination of the (secondary) shock wave, the unsteady region and the quasi-steady fast flame is known as the wave 'triplet', which has been shown to precede the formation of a strong ZND detonation [5, 34, 35, 36].

Figure 3.10: Piston-driven shock profiles for $T_B = 1.0$ at times 1.67, 1.68, 1.69, 1.70, 1.71 and 1.72. Profiles are zoomed in at shock collision except in first pV figure. Scaled with $t_{ign} = 34.64$.

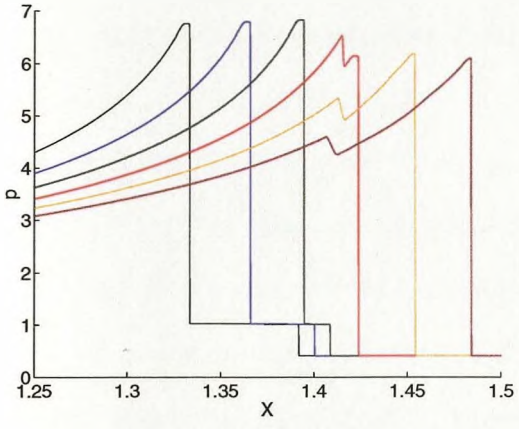

(a) Pressure profiles.

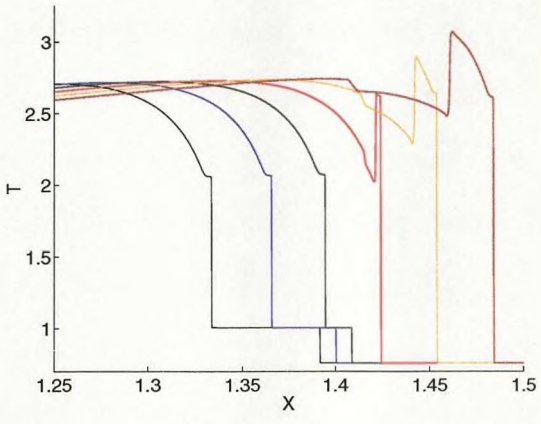

(b) Temperature profiles.

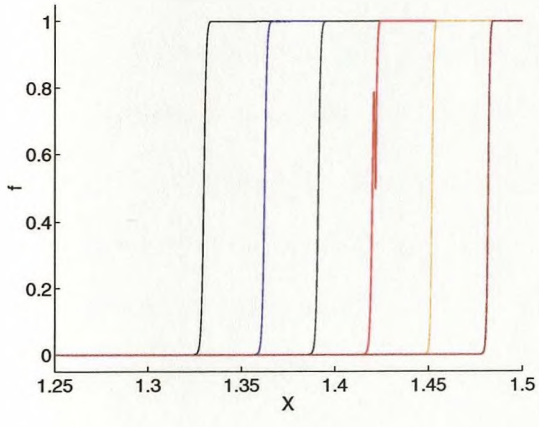

(c) Fuel profiles.

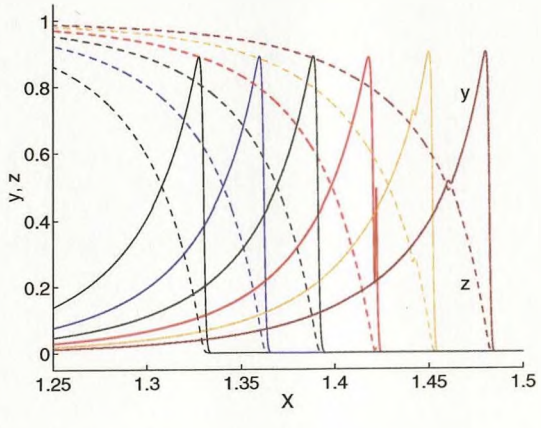

(d) Chain carrier and product profiles.

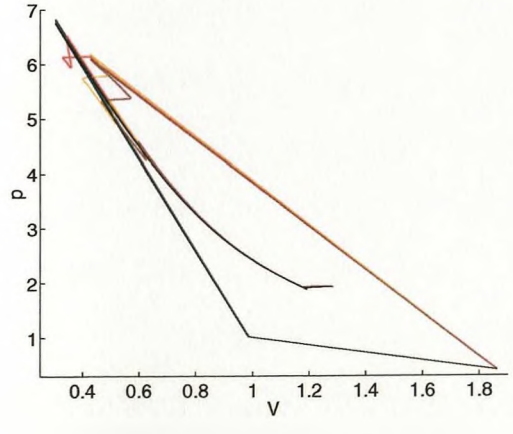

(e) pV diagrams.

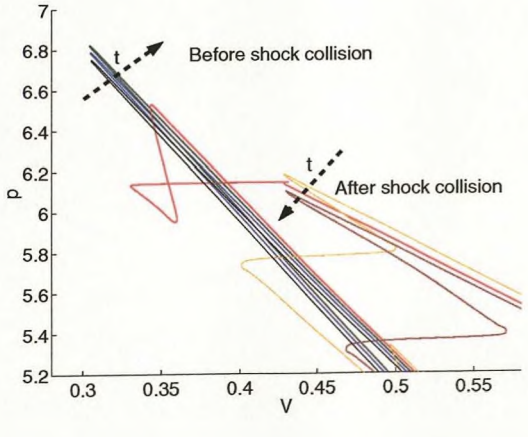

(f) pV diagrams zoomed in at contacts.

Figure 3.10 shows the evolution of the flow both just before and just after collision of the two shocks. Before collision, the pV diagrams in figure 3.10(f) reveal that the unsteady region around the pressure maximum is now very small and that the secondary shock is close to being fully coupled with the following fast flame (which, for $t = 1.67$, stretches from the top left corner down to about $p = 5.6$). Shock collision takes place just after $t = 1.69$, before the secondary shock can fully couple with the fast flame. Hence, the secondary shock has not reached the full CJ strength of a strong ZND detonation (note too that steady state calculations for this piston speed give the shock pressure in the steady CJ detonation to be 8.41, whereas our secondary shock pressure here is under 7). The transmitted shock is much stronger than in the previous $T_B = 0.8$ case, and hence a second ignition point develops very quickly close to the shock. The fourth time step shows this second ignition point and its associated branching zone as a large blip in fuel and chain carrier concentration. Eventually though, only one ignition point and branching zone remains owing to the complete consumption of fuel f at the contact and the disappearance of the induction and branching zones that were behind the contact initially. Therefore, the contact now lies in the temperature insensitive termination zone and hence the blip there virtually disappears.

In this $T_B = 1$ case, we have seen the appearance of weak detonations, a feature always existent in one-step systems but that does not appear in purely chain-branching models [21] and which did not appear also in our small T_B cases wherein chain-branching features prominently from the outset of the evolution (viz. the cases $T_B = 0.5, 0.6$ and 0.8). Based on our homogeneous study, a possible implication is that if we increase T_B further still, to values beyond the temperature of the initially shocked gas (unity here), then we might see the evolution proceed in a fashion that is even more accordant with one-step thermal kinetics than chain-branching kinetics.

3.3.5 $T_B = 1.2$

Figure 3.11 shows the evolution for $T_B = 1.2$ up to the development of a very strong secondary shock very close to the piston.

The pV profiles reveal that the flow downstream of the leading shock begins with an unsteady induction zone that, as expected from our homogeneous study and observed in one-step shock initiation models [5, 22], raises the pressure and temperature slightly (shown in the pV plane as a curved segment immediately following the leading shock). This is followed by a quasi-steady portion of a weak detonation[4], which lies on an almost straight line that starts at the end of the unsteady induction zone. The fact that the (magnitude of the) slope of this weak detonation is decreasing with time shows that it is decelerating. As in the previous $T_B = 1.0$ case, the weak detonation is followed by a highly unsteady domain around the pressure maximum.

We notice from the chain carrier profiles that, in this early evolution, only small chain-branching explosions take place, and these only occur well after the temperature exceeds T_B. We also note the very significant buildup of products z ahead of the weak detonation, through which the weak detonation is moving, as what occurs in one-step systems [22]. This buildup of z, which is greater than the buildup of chain carriers y, is expected since initially $T < T_B$ and hence $R_C \gg R_B$. The pressure-chain carrier plane shows that the secondary shock forms more or less where chain carriers reach their peak concentration, i.e. downstream of the (small) chain-branching explosion. The pV profile for $t = 1.302$ shows the spontaneous emergence of the secondary shock at the rear of the quasi-steady weak detonation and inside the head of the unsteady domain. This secondary shock grows in strength, resulting in the shrinking of the unsteady domain. In the last two time steps, we see from the expansive straight line regions of the pV profiles that the unsteady domain is followed by a quasi-steady fast flame. The expansive region of the pressure-fuel

[4]The quasi-steady weak detonation is only a portion of the complete weak detonation since not all the ambient reactant is consumed in the quasi-steady portion [5]. We see from figures 3.11(e) and 3.11(f) that a substantial amount of fuel is consumed in the induction zone adjacently ahead of the quasi-steady detonation and also in the region behind it.

Figure 3.11: Piston-driven shock profiles for $T_B = 1.2$ at times 1.290, 1.294, 1.298, 1.302 and 1.306. Profiles are zoomed in at secondary shock formation except in last two sub-figures. Scaled with $t_{ign} = 457.763$.

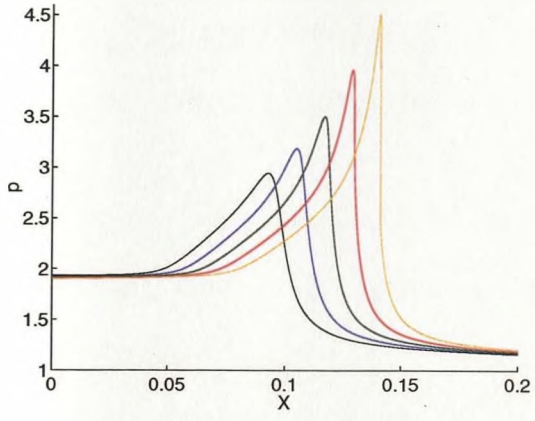

(a) Pressure profiles.

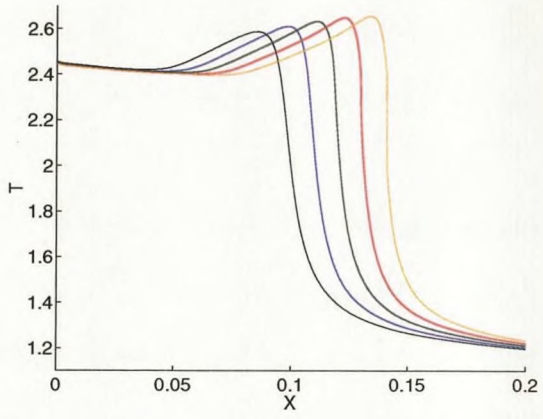

(b) Temperature profiles.

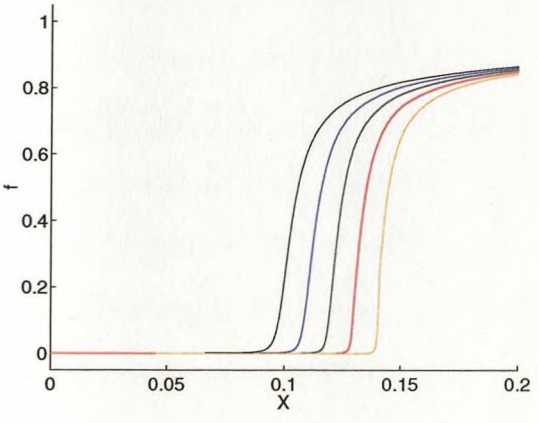

(c) Fuel profiles.

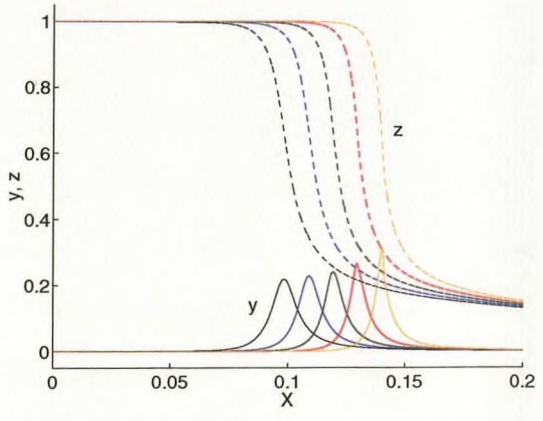

(d) Chain carrier and product profiles.

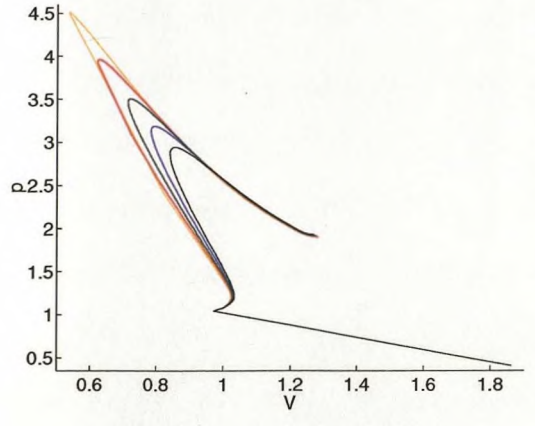

(e) pV diagrams.

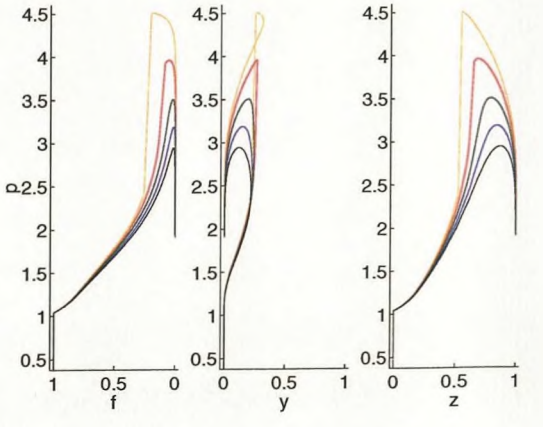

(f) Pressure against mass fractions.

profiles tells us that the fast flame consumes the last remnants of fuel, and that, finally, it is followed by a rarefaction wave which, as in the previous $T_B = 1.0$ case, is required to satisfy the piston boundary condition. Before these last two time steps (i.e. before the quasi-steady fast flame emerges), the pressure-fuel profiles show that all the fuel is consumed in the induction zone, in the quasi-steady weak detonation and in the unsteady domain.

At this stage, the flow consists of a leading shock wave, followed by an unsteady induction zone, which in turn is followed by a quasi-steady weak detonation. This is then followed by a wave triplet that was also seen in the previous $T_B = 1.0$ case, consisting of a powerful secondary shock, then an unsteady domain, followed by a quasi-steady fast flame. Finally, the flow is ended with a rarefaction wave. The wave triplet signals the beginnings of the appearance of a strong ZND detonation.

Figure 3.12 shows the secondary shock continuing to build up strength. The pressure-mass fraction diagrams clearly show that the secondary shock is accelerating towards the leading shock and so further towards the start of the induction zone, engulfing the weak detonation in the process (as predicted from one-step asymptotic theory [37]). Since the secondary shock now lies in gas that is predominantly made up of fuel, and since it raises the temperature to well above T_B and thus making $R_C \ll R_B$, it is able to magnify the rate of the chain-branching explosion and hence yield higher chain carrier peak values. The explosion structure behind the shock is thus no longer similar to that observed in one-step systems, but involves a very considerable amount of chain-branching instead.

The pV profiles show that the unsteady domain that existed between the secondary shock and the quasi-steady fast flame has become minutely small. The pV profiles together with the pressure-mass fraction profiles reveal that the reaction zone behind the secondary shock is now composed entirely of a quasi-steady fast flame. Also, while both the secondary shock and the fast flame are accelerating (the magnitude of their slopes is increasing in the pV plane), the fast flame is accelerating more rapidly and hence their

Figure 3.12: Piston-driven shock profiles for $T_B = 1.2$ at times 1.31, 1.33, 1.35, 1.37 and 1.39. Profiles are zoomed in at CJ detonation formation except in last two sub-figures. Scaled with $t_{ign} = 457.763$.

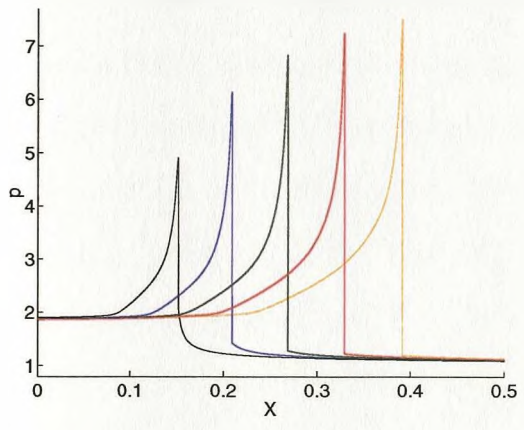

(a) Pressure profiles.

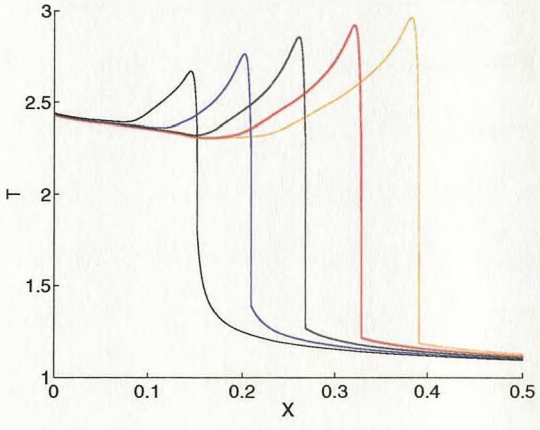

(b) Temperature profiles.

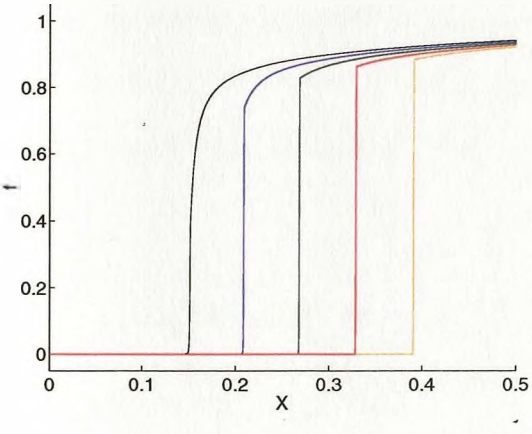

(c) Fuel profiles.

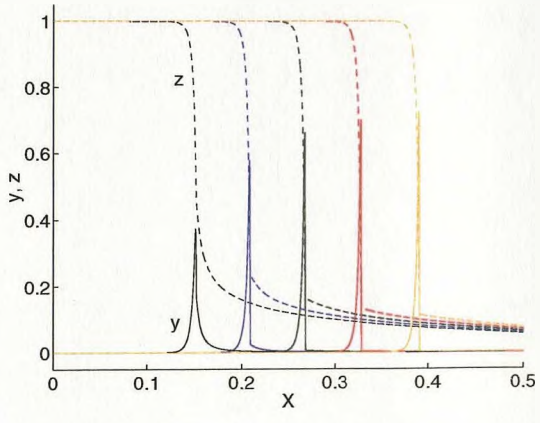

(d) Chain carrier and product profiles.

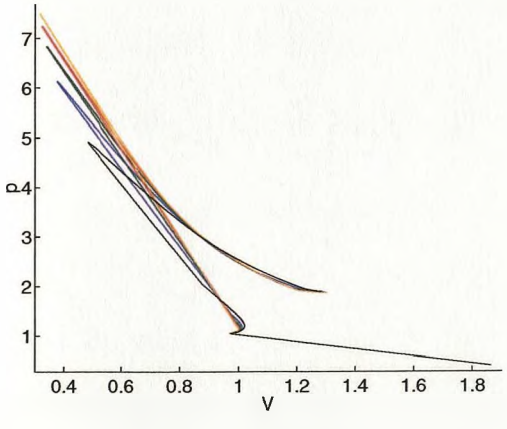

(e) pV diagrams.

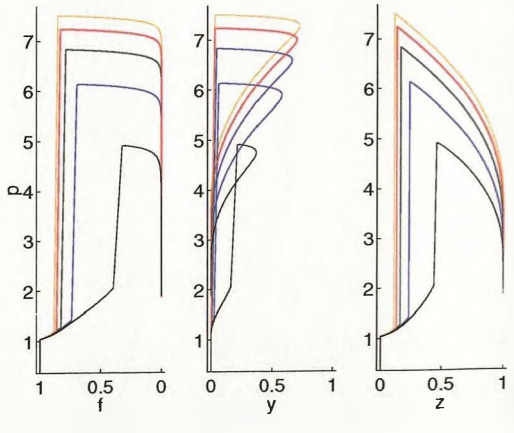

(f) Pressure against mass fractions.

sections of the pV profiles merge into a single line. This shows that the secondary shock is now fully coupled with the quasi-steady fast flame, indicating that a quasi-steady CJ detonation is born. The sharp maximum in the pressure profiles, known as the *von Neumann spike*, further attests to the coupling of the secondary shock with the fast flame and the creation of a strong ZND detonation [3]. Zooming into the spike reveals a three-stage structure, as observed by Short and Quirk [7], consisting of a very short but definite thermally neutral induction zone behind the shock, followed by a branching explosion zone, followed finally by an exothermic termination zone. In contrast, the detonation structure in one-step models can only have two stages at most, a definite induction zone and a reaction zone [22].

Apart from the detonation flow becoming chain-branching after the temperature exceeds T_B, the entire evolution of this $T_B = 1.2$ case is qualitatively identical to that observed in one of the one-step simulations undertaken by Sharpe [22] (viz. the case where his parameter values are: $Q = 4$, $\gamma = 1.4$, $M_0 = 1.5$ and $\epsilon = 1/15$).

3.4 Comparing our piston-driven shock simulations with those of other models

Using the parameter matches made in section 2.6, we can directly compare our (three-step) piston-driven shock simulations with those of the one-step and two-step models where it is appropriate to do so.

3.4.1 A comparison with the one-step model

Figures 3.13 and 3.14 show the results of the piston-driven shock simulations for the one-step model. The time-scale, t_{ign}, is the numerical time to ignition specific to the one-step model, i.e. the time it takes for half the fuel to be consumed in the one-step model. If we compare these one-step figures with figures from our three-step model that resemble thermal reactions the closest (i.e. figures 3.11 and 3.12 in which $T_B = 1.2$) then we notice

that they are virtually identical in the qualitative sense.

The development of the secondary shock in figure 3.13 involves the same phenomena as those of the three-step model, viz. the unsteady induction zone, the weak detonation and the wave triplet. Quantitatively, although the results from both models involve virtually the same values of pressure and temperature, we notice that they have very different time and distance scales, but this can be explained by the fact that $T_B = 1.2$ is not too far from unity, and hence from figure 2.17 we can expect this large discrepancy. Indeed, this discrepancy would disappear as we take $T_B \to \infty$ since then the three-step model would essentially become a one-step model owing to the virtual absence of the chain-branching reaction (cf. end of section 2.6.1). Also, we notice that the induction zone in the one-step model simulations has a noticeably higher fuel fraction than in the three-step model. Again, this can be explained by the absence of the chain-branching reaction in the one-step model, in the sense that chain-branching accelerates the consumption of fuel in the three-step model.

Figure 3.14 shows a qualitatively similar development of a CJ detonation using the one-step model to that of the three-step model in figure 3.12. Just as with the earlier evolution, the pV diagrams for both models in this latter phase are essentially the same, with the weak detonation becoming engulfed by the secondary shock, the unsteady domain at the pressure maximum becoming minutely small and the quasi-steady fast flame becoming fully coupled with the secondary shock, indicating the birth of the quasi-steady CJ detonation. The main qualitative difference between the two models is the detonation structure in the von Neumann detonation spike. Whereas in the three-step model we have seen that it consists of three stages, the absence of chain-branching in the one-step model means that the detonation structure only has two stages, a thermal induction zone followed by a thermal explosion.

Figure 3.13: One-step model: Piston-driven shock profiles at times 1.246, 1.249, 1.252, 1.255 and 1.259. Profiles are zoomed in at secondary shock formation except in last two sub-figures. Scaled with $t_{ign} = 1142.45$.

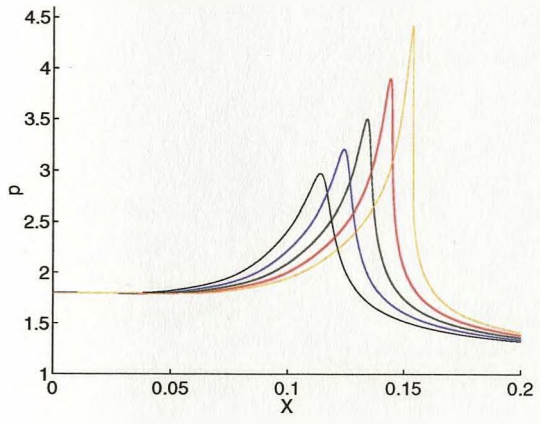

(a) Pressure profiles.

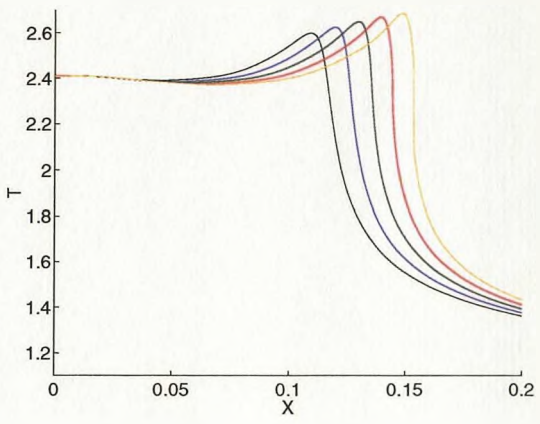

(b) Temperature profiles.

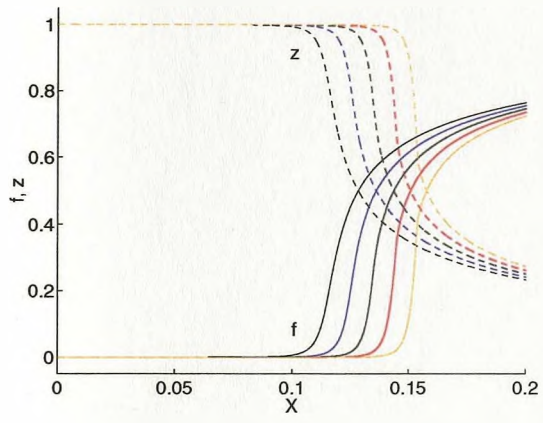

(c) Fuel and product profiles.

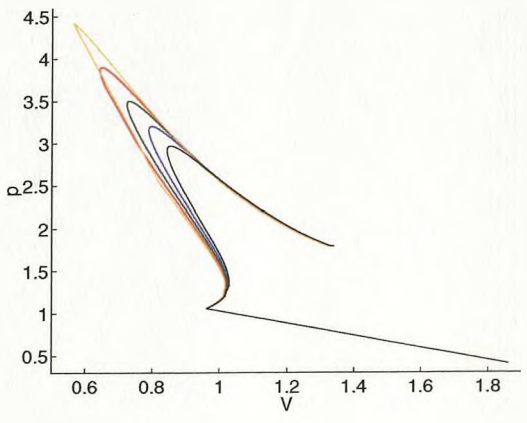

(d) pV diagrams.

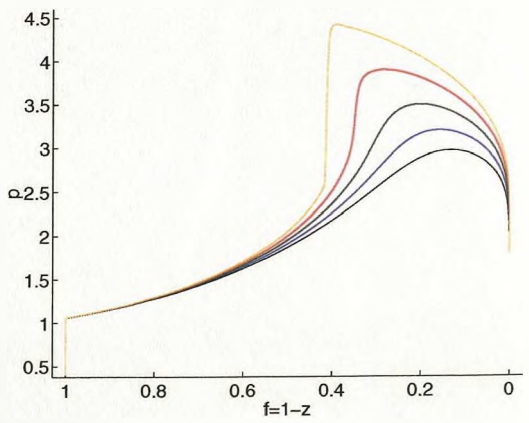

(e) Pressure against fuel.

Figure 3.14: One-step model: Piston-driven shock profiles at times 1.262, 1.277, 1.291, 1.304 and 1.318. Profiles are zoomed in at CJ detonation formation except in last two sub-figures. Scaled with $t_{ign} = 1142.45$.

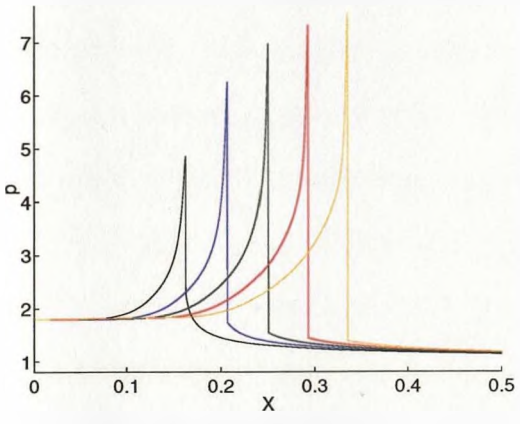

(a) Pressure profiles.

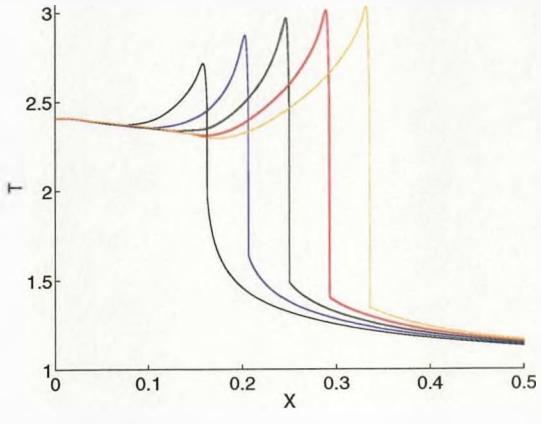

(b) Temperature profiles.

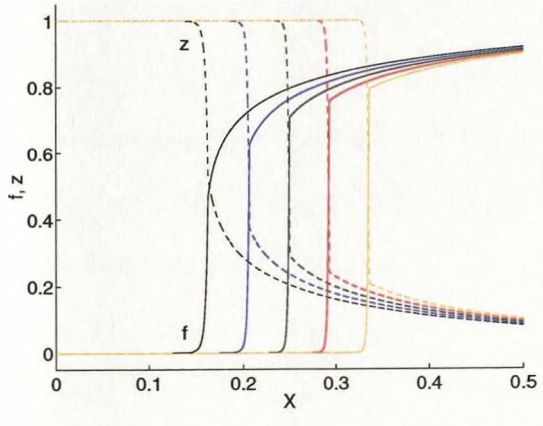

(c) Fuel and product profiles.

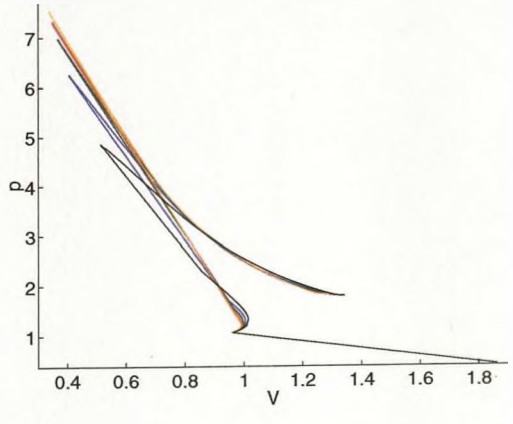

(d) pV diagrams.

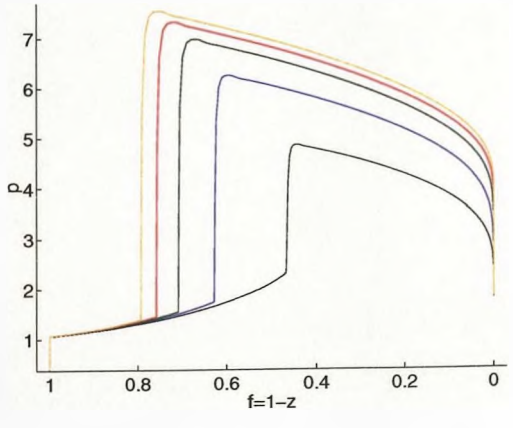

(e) Pressure against fuel.

3.4.2 A comparison with the two-step model

The two-step model, as we have already described for the homogeneous case in section 2.6, uses reaction progress variables as opposed to mass fractions. It is a simple method, in that the induction zone ends with a complete and instantaneous transformation from an all-fuel state to all-chain carrier state. This implies that the induction zone is completely thermally neutral and that the chain-branching explosion is infinitely thin, i.e. the model is purely chain-branching. Figure 3.15 compares the pressure, temperature and product profiles of the two-step case with those of the three-step case (where the two-step data was produced by Sharpe by applying the parameter matches in section 2.6 to the numerical code used in his two-step paper [21]) . The two-step λ progress variable for the termination reaction (see section 2.6) is considered equivalent to the three-step product fraction z, and so these are compared in the third sub-figure. Owing to the simplicity of this model, we cannot compare fuel or chain carrier profiles.

One immediate but expected difference is that the pressure profiles of the two-step model have discontinuous gradients owing to the Heaviside nature of the termination reaction. Generally, the two models compare well, especially during early time. We do however notice a slightly earlier emergence of a secondary shock in the two-step case, which appears at $t = 2.5$, whereas a similar profile for the three-step case appears at $t = 3.0$. Just before shock collision in the three-step case, a small contact appears in a spike in the last temperature profile of the two-step case, indicating shock collision has already (but only just) occurred for the two-step case. The product profiles show that the ignition point in the two-step moves well ahead of its three-step counterpart after the third time step (i.e. once the two-step secondary shock is formed). Profiles of all three sub-figures for the two models then begin to deviate quite noticeably, though the general form of the profiles is preserved.

Figure 3.15: Two-step model (- - -) against three-step model (—): Piston-driven shock profiles at times 1.0, 1.5, 2.0, 2.5 and 3.0. Scaled with $t_{ign} = 0.48$.

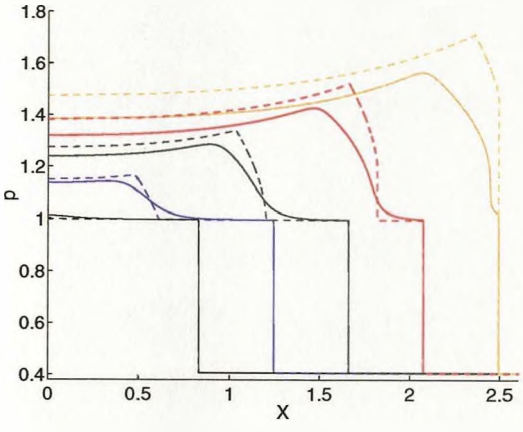

(a) Pressure profiles.

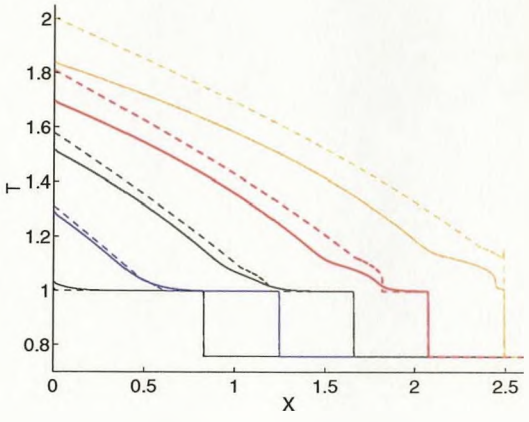

(b) Temperature profiles.

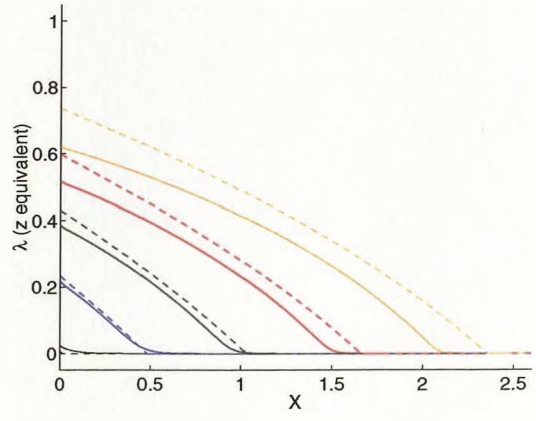

(c) Product profiles (λ treated as z).

3.5 Isentropicity of the induction zone in chain-branching reactions

In contrast with one-step thermal schemes, there is no heat release in the induction zone of chain-branching systems. This has been verified in our homogeneous and shock ignition cases for $T_B < 1$ when $T_B - 1 = O(1)$ (i.e. chain-branching values).

In the induction zone of our shock ignition case, and for chain-branching values of T_B,

we can therefore replace our energy equation (3.6) with the following adiabatic condition[5]

$$\frac{Ds}{Dt} = 0, \tag{3.22}$$

where s is the entropy, which upon integration through our thermally neutral induction zone gives

$$s = constant, \tag{3.23}$$

which is known as the *isentropic* condition [16]. This then allows us to integrate the definition of the sound speed c,

$$\left(\frac{\partial p}{\partial \rho}\right)_s = c^2 = \frac{\gamma p}{\rho}, \tag{3.24}$$

to give

$$p = C\rho^\gamma \tag{3.25}$$

where C is some constant. Before disturbances catch up with the shock, $p = \rho = 1$ at the shock front, and so we end up with the following isentrope:

$$p = \rho^\gamma = 1/V^\gamma. \tag{3.26}$$

If we plot this isentrope in the pV plane against pV data from chain-branching shock initiation cases, then, according to the above discussion, we should see the induction zone lying along the isentrope at least until the pressure disturbances have reached the shock. Figures 3.16 and 3.17 show two such plots, one for $T_B = 0.5$ and the other for $T_B = 0.6$, both of which are chain-branching values. We notice in figure 3.16(b) that the induction zones lie exactly on the isentrope for all the time steps except the last one where the shock and the induction zone have veered off slightly due to the amplification of the shock by pressure disturbances (which we saw in figure 3.3).

[5]This condition can only be valid between shocks, as s jumps across shocks.

Similarly for $T_B = 0.6$ in figure 3.17, we can clearly see that the isentrope is superimposed on the induction zones for all the time steps except the last one in which a very strong compression wave has collided with the shock (witnessed earlier in figure 3.6).

Figure 3.16: pV diagrams plotted against the isentrope for $T_B = 0.5$ at times 1.0, 1.8, 2.6, 3.4 and 4.2.

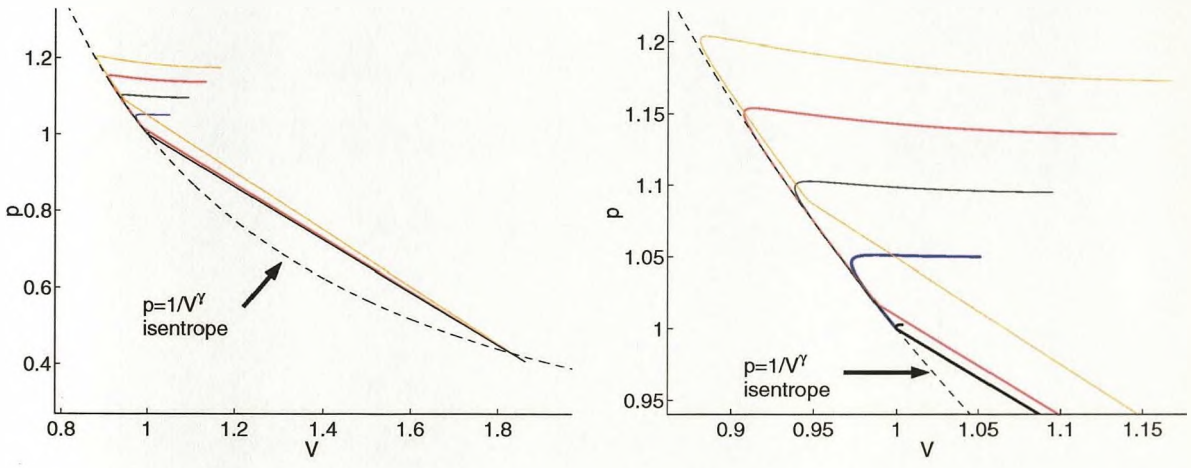

(a) Full flow profiles.

(b) Zoomed in at the induction zone.

Figure 3.17: pV diagrams plotted against the isentrope for $T_B = 0.6$ at times 1.0, 1.5, 2.0, 2.5 3.0 and 3.17

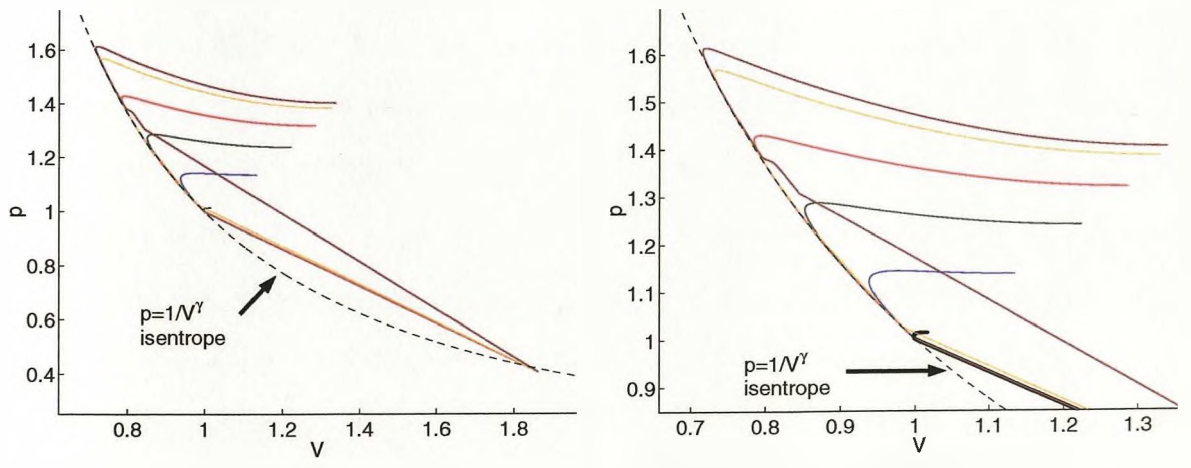

(a) Full flow profiles.

(b) Zoomed in at the induction zone.

Chapter 4

CONTACT-DRIVEN SHOCK-INDUCED INITIATION OF DETONATION WAVES

4.1 The mathematical model

In chapter 3, the mechanism driving the shock was a solid piston (or equivalent). Here, the solid piston is replaced with a contact surface - an acoustically permeable interface across which pressure and velocity remain continuous but a discontinuous drop in temperature and a corresponding discontinuous rise in density occur immediately behind it. As already mentioned in the introduction (chapter 1), the difference now is that acoustic disturbances emanating form the reaction zone ahead can be transmitted through the contact surface, whereas they were always reflected back into the reactive mixture in the piston case. Also mentioned, was the importance of this scenario to the problem of DDT, where an accelerated flame produces two weak shocks that eventually collide. The result is a Riemann problem whose solution involves a strong transmitted shock and a driving contact surface. Urtiew and Oppenheim [23] studied this shock merging problem experimentally, and were able to show that a detonation could be induced by the resulting contact-driven shock wave. Figure 4.1 shows schematics of the shock tube system both before and after the two shocks merge, together with representative profiles of the temperature, pressure and density. It is assumed that the leading shock, with known Mach number M_1, travels into

Figure 4.1: A schematic of the inert shock merging process in the shock tube, together with corresponding temperature, pressure and density profiles.

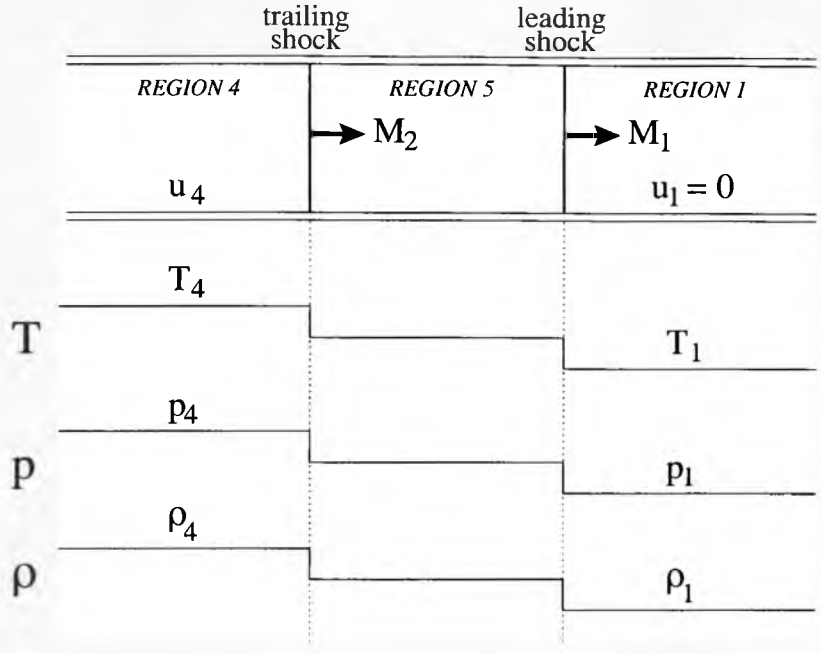

(a) Before merging.

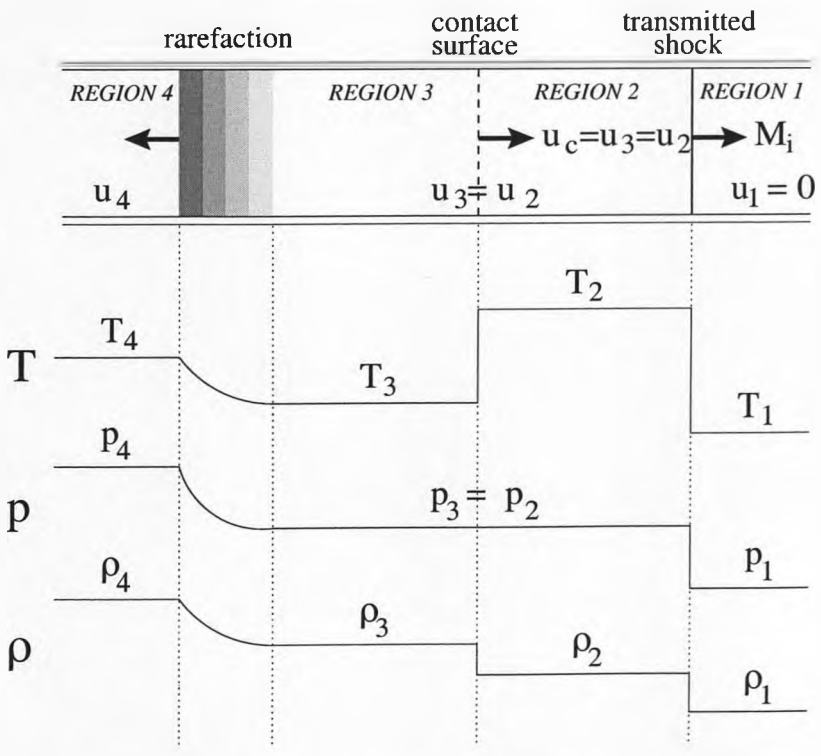

(b) After merging (in an inert material).

a region of stationary gas (region 1), whose known state is denoted by a '1' subscript, and hence $u_1 = 0$. This leading shock is followed by the trailing shock which has known Mach number M_2 and which leaves behind region 4 whose state can be determined from M_1, M_2 and the known state in region 1 by applying the shock jump conditions (3.17)–(3.20) twice. At some time $t = t_M$, the two shocks merge, subsequently resulting in the structure depicted in figure 4.1(b). This figure is in fact the schematic self-similar solution for an inert material, but since here we are investigating a reactive gas, this structure will evolve over time away from being self-similar. The figure shows that we now have a much stronger transmitted shock with Mach number M_i running into region 1. This transmitted shock leaves behind a new uniform region (region 2) of relatively high temperature that terminates at the contact surface (travelling at speed u_c, which is constant in the inert case). Behind the contact surface is a backward moving rarefaction that matches a new uniform region (region 3), which it leaves behind, to region 4. Once again we use the shock jump conditions (3.17)–(3.20) but this time to determine the region 2 state in terms of the unknown Mach number M_i and the known state in region 1. Pressure and velocity are continuous across a contact surface, i.e.

$$p_3 = p_2, \qquad u_3 = u_2 = u_c, \tag{4.1}$$

and so the region 3 state can be determined from the known state in region 4 using the isentropic relations across the rarefaction wave [24],

$$\frac{p_3}{p_4} = \left(\frac{\rho_4}{\rho_3}\right)^{-\gamma} = \left(\frac{T_3}{T_4}\right)^{\frac{\gamma}{\gamma-1}}, \qquad u_3 = u_4 + \frac{2}{\gamma-1}\sqrt{\frac{\gamma p_4}{\rho_4}}\left(1 - \left(\frac{p_3}{p_4}\right)^{\frac{\gamma-1}{2\gamma}}\right). \tag{4.2}$$

We can now form a nonlinear algebraic expression relating M_i with the known states in regions 1 and 4,

$$u_4 + \frac{2}{\gamma-1}\sqrt{\frac{\gamma p_4}{\rho_4}}\left(1 - \left[\frac{p_1}{p_4}\left(1 + \frac{2\gamma}{\gamma+1}(M_i^2 - 1)\right)\right]^{\frac{\gamma-1}{2\gamma}}\right) - \frac{2(M_i^2-1)}{(\gamma+1)M_i}\sqrt{\frac{\gamma p_1}{\rho_1}} = 0, \tag{4.3}$$

which we solve for M_i using the Newton-Raphson iteration method. Once M_i is known, actual values for the states in regions 2 and 3 can be determined as described above.

This shock merging formulation was previously used by Short and Dold [24] and then by Parkins [25] to study the evolution of the induction zone between a contact surface and a shock for the one-step thermal model, in the high activation energy asymptotic limit. Here, we will study this shock merging setup under the three-step and two-step chain-branching chemistry models.

We note from figure 4.1(b) that the temperature maximum occurs in region 2, i.e. between the transmitted shock and the contact surface. Short and Dold [24] show for the one-step model that this leads to a homogeneous constant volume ignition time which is very much smaller than ignition times in regions 3 and 4. It is therefore reasonable to consider all regions, apart from region 2, as chemically inert on the time scale of reaction in region 2. Disturbances resulting from chemical activity in region 2 will affect the shock Mach number M_i and can also travel through the contact surface into region 3 along negative characteristics. These disturbances cannot however affect the rarefaction wave (and consequently region 4 too) because the rear of the rarefaction travels at the local sound speed relative to the gas. In our asymptotic study therefore (where we solve for early time in the region ahead of the contact), although consideration needs to be given to changes in region 3, we can apply a radiation condition there [24]. Such a boundary condition need not be applied in our numerical simulations, where the entire flow domain is explicitly solved for.

Just as in the piston-driven case of chapter 3, transport effects are negligible, and so we shall continue to use the reactive Euler equations to model the gas dynamics, coupled to a set of chemical reaction rate equations. Unlike the piston case however, there is no symmetric rear boundary condition here.

Similarly to what we did in the piston case, where we transformed to the frame of the

driving piston, we shall transform to a frame moving at the initial speed u_c of the contact surface by defining a new velocity variable, v, and a new distance variable, X:

$$X = x - u_c t, \qquad v = u - u_c. \tag{4.4}$$

In the inert case, the contact and the gas in regions 2 and 3 would remain stationary relative to this frame. In the reactive case, they are only stationary before disturbances from the chemical activity can affect them.

The distance between the two weak precursor shocks can be chosen arbitrarily (since there is no reaction before they merge) and the position of the leading shock is then chosen such that the shocks merge (and therefore the contact is created) at $X = 0$ for convenience. In this case, the rear numerical boundary is placed sufficiently far behind $X = 0$ that it does not influence the computations for the time the simulation is run for.

4.2 Two-step asymptotic analysis of the ignition path

As discussed already on page 15 of the introduction, Short and Dold [24] and Parkins [25] have investigated the contact-driven shock case for the *one*-step model. Their high activation energy early time asymptotics have shown that the fuel is initially ignited (i.e. thermal runaway occurs) some distance d ahead of the contact surface, in contrast with piston-driven shock cases where the fuel is first ignited at the piston. To understand this phenomenon they explain that acoustic leakage takes place at the contact surface during the thermal induction phase. They also demonstrate that the distance d is larger with a weaker contact (i.e. with a contact of low acoustic impedance) and explain that this is so because more acoustic energy is leaked though the contact.

Here, we shall perform a similar asymptotic investigation of the contact-driven shock case but for a chain-branching model. However, a simpler two-step model will be used rather than the three-step model for a number of reasons. Firstly, we have seen that for

$T_B - 1 = O(1) < 0$, the three-step model is well represented by the two-step model in the homogeneous scenario and also, more relevantly, in the piston-driven shock scenario for early time. Secondly, it has already been shown by Sharpe [21] for the piston scenario that the two-step model is amenable to an early time asymptotic analysis, and hence we can perform a direct comparison between the asymptotic ignition paths of the piston and contact cases (here, "ignition path" refers to the locus in (X, t) space of the thin chain-branching explosion region). Finally, we do not require expressions for chemical species concentrations (which are possible through a three-step analysis) in order to determine the ignition path.

The analysis will be for the early time period immediately following the point in time when ignition first takes place. However, note that the analysis is early time on the time scale of the exothermic termination zone, but is $O(1)$ on the initial induction time scale, since, for $T_B < 1$, the homogeneous induction time is short.

Our aim in this section is therefore to extend the two-step analysis of Sharpe [21] in order to obtain insight into how the ignition path evolves initially, when compared with the piston scenario.

4.2.1 Governing equations for the two-step model

The two-step model is described fully in [21] (the homogeneous version was discussed in section 2.6). The equations governing the gas-dynamics are the Euler equations,

$$\frac{\partial \rho}{\partial t} + u\frac{\partial \rho}{\partial x} + \rho\frac{\partial u}{\partial x} = 0, \tag{4.5}$$

$$\frac{\partial u}{\partial t} + u\frac{\partial u}{\partial x} + \frac{1}{\rho}\frac{\partial p}{\partial x} = 0, \tag{4.6}$$

$$\frac{DT}{Dt} - \beta\frac{D\lambda}{Dt} - (\gamma - 1)\frac{p}{\rho^2}\frac{D\rho}{Dt} = 0, \tag{4.7}$$

where the polytropic equation of state $e = T/(\gamma - 1) - Q\lambda$ is used to write the internal energy e in terms of temperature T. These are coupled to two chemical reaction rate equations,

$$\frac{D\xi}{Dt} = k_1 \exp\left[\frac{1}{\varepsilon}\left(\frac{1}{T_s} - \frac{1}{T}\right)\right], \tag{4.8}$$

$$\frac{D\lambda}{Dt} = H(\xi)k_2(1-\lambda), \tag{4.9}$$

where T_s is the initial post-shock temperature (which is unity according to the non-dimensionalization in [21]), and all other parameters are as described in section 2.6. It is assumed that the activation temperature is high, i.e. $\varepsilon \ll 1$. Highly chain-branching reactions in our three-step model are achieved with $T_B - 1 = O(1) < 0$, which then forces a small induction-zone to termination zone ratio. Such ratios are achieved in the two-step model using a small ratio, k, of k_2 to k_1 [21], and as the non-dimensionalization in [21] gives $k_1 = 1$, then we may express this ratio by assuming $k = \varepsilon K$ where $K = O(1)$. Since Sharpe [21] non-dimensionalizes the variables with respect to the dimensional initial shocked state (as we do in all our shock related work in this thesis) then the initial shocked state is

$$\rho = 1, \quad p = 1, \quad T = 1, \quad u = u_c. \tag{4.10}$$

If we now apply the translations given in (4.4) then the contact is initially stationary and is formed at $X = 0$, and the gas velocity of the initially shocked state is given by $v = 0$.

As we are considering only early time behaviour to $O(\varepsilon)$, the $O(\varepsilon)$ early time contact surface boundary condition (to be discussed in section 4.2.2) can be applied to the fixed $O(1)$ contact surface position (i.e. $X = 0$) throughout this early time. If we were to apply this $O(\varepsilon)$ early time contact surface boundary condition to an $O(\varepsilon)$ corrected contact surface position, then the result would only be an $O(\varepsilon^2)$ correction.

Because the induction zone is thermally neutral for highly chain-branching values of T_B, acoustic leakage at the contact surface cannot take place until the induction time there has elapsed, since there are no pressure disturbances up to that point. Hence, just

like in piston-driven cases where ignition first takes place at the piston, here, ignition first takes place at the contact surface. Assuming that the two weak precursor shocks collide at $t = 0$, then with Sharpe's non-dimensionalization [21], the induction zone parameter ξ first reaches unity at time $t = 1$. It is therefore convenient to shift time by defining

$$\tau = t - 1 \tag{4.11}$$

so that ignition at the contact surface occurs at $\tau = 0$.

Since pressure and velocity must be continuous across the contact surface, the absolute boundary condition there can be written as

$$p^{b,c} = p^{a,c}, \qquad u^{b,c} = u^{a,c}, \tag{4.12}$$

where the superscript 'b' denotes the state behind the contact surface, the superscript 'a' denotes the state ahead of the contact surface and the auxiliary superscript 'c' denotes the state either immediately before or immediately after the contact surface.

4.2.2 The early time contact surface boundary condition

Since acoustic leakage occurs at the contact surface, we need to establish a boundary condition relating gas velocity and pressure at the contact to the level of acoustic leakage taking place.

The inert gas behind the contact surface will be perturbed by volumetric expansion caused by heat release in front of the contact surface. All dependant variables will therefore deviate from their initial state by an $O(\varepsilon)$ amount in this early time analysis. We may then define asymptotic expansions as follows:

$$p^b = 1 + \varepsilon p_1^b, \qquad \rho^b = \rho_i^b + \varepsilon \rho_1^b, \qquad T^b = T_i^b + \varepsilon T_1^b, \qquad v^b = \varepsilon v_1^b, \tag{4.13}$$

$$p_1^b,\ \rho_1^b,\ T_1^b,\ v_1^b = O(1),$$

where the subscript 'i' denotes initial values and the subscript '1' denotes perturbation variables. Since the evolution is entirely gas-dynamical and not chemical behind the contact, then $\lambda = 0$ there.

Substituting these expansions into the Euler equations (4.5)–(4.7) gives the following leading order equations:

$$\frac{\partial \rho_1^b}{\partial \tau} + \rho_i^b \frac{\partial v_1^b}{\partial X} = 0, \tag{4.14}$$

$$\frac{\partial v_1^b}{\partial \tau} + \frac{1}{\rho_i^b}\frac{\partial p_1^b}{\partial X} = 0, \tag{4.15}$$

$$\frac{\partial T_1^b}{\partial \tau} + \frac{(\gamma-1)}{(\rho_i^b)^2}\frac{\partial \rho_1^b}{\partial \tau} = 0. \tag{4.16}$$

By the ideal thermal equation of state (3.4), we can write $\rho_1^b \sim (p_1^b - \rho_i^b T_1^b)/T_i^b$, and hence (4.14) becomes

$$\frac{1}{T_i^b}\left(\frac{\partial p_1^b}{\partial \tau} - \rho_i^b \frac{\partial T_1^b}{\partial \tau}\right) + \rho_i^b \frac{\partial v_1^b}{\partial X} = 0, \tag{4.17}$$

and (4.16) becomes

$$\frac{\partial T_1^b}{\partial \tau} = \frac{(\gamma-1)}{\gamma \rho_i^b}\frac{\partial p_1^b}{\partial \tau}. \tag{4.18}$$

Substituting (4.18) into (4.17) gives

$$\frac{\partial p_1^b}{\partial \tau} + \gamma \frac{\partial v_1^b}{\partial X} = 0. \tag{4.19}$$

Hence, after defining

$$\chi = \frac{X}{\gamma^{\frac{1}{2}}}, \qquad \hat{U}_1 = (\gamma \rho_i^b)^{\frac{1}{2}} v_1, \tag{4.20}$$

we can write (4.15) and (4.19) in characteristic form as

$$\left(\frac{\partial}{\partial \tau} \pm \frac{1}{\sqrt{\rho_i^b}}\frac{\partial}{\partial \chi}\right)(p_1^b \pm \hat{U}_1^b) = 0. \tag{4.21}$$

When we come to actually solving the equations (which we do so in the region ahead of the contact), we will have to make use of a new scaling of gas velocity

$$U_1 = \gamma^{\frac{1}{2}} v_1. \tag{4.22}$$

Applying this scaling now to the characteristic equations (4.21) gives

$$\left(\frac{\partial}{\partial \tau} \pm \frac{1}{\sqrt{\rho_i^b}} \frac{\partial}{\partial \chi} \right) \left(p_1^b \pm \sqrt{\rho_i^b} U_1^b \right) = 0. \tag{4.23}$$

Therefore, at leading order, the positive characteristics in the (χ, τ) plane are straight lines with gradient $d\chi/d\tau = 1/\sqrt{\rho_i^b}$, representing waves travelling to the right at the initial sound speed (which is $1/\sqrt{\rho_i^b}$ in (χ, τ) coordinates), on which

$$\frac{d}{d\tau} \left(p_1^b + \sqrt{\rho_i^b} U_1^b \right) = 0. \tag{4.24}$$

Similarly, the negative characteristics are straight lines with gradient $d\chi/d\tau = -1/\sqrt{\rho_i^b}$, representing waves travelling to the left at the same initial sound speed, on which

$$\frac{d}{d\tau} \left(p_1^b - \sqrt{\rho_i^b} U_1^b \right) = 0. \tag{4.25}$$

Hence, the quantity $\sqrt{\rho_i^b}$ gives a measure of the rate of propagation of acoustic disturbances behind the contact surface.

The acoustic characteristic equations (4.23) are two linear advection equations and hence have solutions of the form

$$(p_1^b + \alpha_0 U_1^b) = C(\chi - \tau/\alpha_0), \tag{4.26}$$

$$(p_1^b - \alpha_0 U_1^b) = D(\chi + \tau/\alpha_0), \tag{4.27}$$

where α_0 is the (constant leading order) rate of propagation of acoustic disturbances (i.e. the acoustic impedance), given by

$$\alpha_0 = \sqrt{\rho_i^b}, \tag{4.28}$$

and which appears in Short and Dold's [24] analysis of the one-step contact-driven system. As already mentioned on page 15, α_0 is the (constant leading order) ratio of densities across the contact surface and controls the amount of acoustic leakage there. From (4.28), it can be seen that the piston-driven system can be recovered by taking the limit $\alpha_0 \to \infty$, which gives an infinite gas density behind the contact. As discussed on page 112, and also by Short and Dold [24], a radiation condition can be applied behind the contact surface since the rear of the rarefaction wave moves at the local sound speed of region 3. In other words, there will be no right travelling gas-dynamic waves behind the contact, and hence the function C in (4.26) can be set to zero. If we then apply the boundary condition (4.12) to (4.26) we finally arrive at the induction zone contact-surface boundary condition,

$$p_1^c = -\alpha_0 U_1^c, \tag{4.29}$$

where and p_1^c and U_1^c are the induction pressure and velocity perturbations at the contact surface.

4.2.3 The early time asymptotic ignition path

Having determined the early time boundary condition at the contact surface, we can now move on to an asymptotic analysis ahead of the contact surface, conducted in the same way as Sharpe's two-step asymptotic study for a piston-driven system [21].

The variables are expanded as

$$p = 1 + \varepsilon p_1, \qquad \rho = 1 + \varepsilon \rho_1, \qquad T = 1 + \varepsilon T_1, \qquad v = \varepsilon v_1, \qquad \lambda = \varepsilon \lambda_1, \tag{4.30}$$

$$p_1,\ \rho_1,\ T_1,\ v_1,\ \lambda_1 = O(1).$$

Applying the scalings

$$\chi = \frac{X}{\gamma^{\frac{1}{2}}}, \qquad U_1 = \gamma^{\frac{1}{2}} v_1, \tag{4.31}$$

and also the ideal thermal equation of state (3.4), the governing Euler equations (4.5)–(4.7) can be written in characteristic form as

$$\left(\frac{\partial}{\partial \tau} \pm \frac{\partial}{\partial \chi}\right)(p_1 \pm U_1) = \beta K H(\xi), \tag{4.32}$$

$$\frac{\partial T_1}{\partial \tau} = \frac{(\gamma - 1)}{\gamma}\frac{\partial p_1}{\partial \tau} + \frac{\beta K H(\xi)}{\gamma}, \tag{4.33}$$

where β was defined earlier in (2.15). Here, at leading order, the positive characteristics in the (χ, τ) plane are straight lines with gradient $d\chi/d\tau = 1$, representing waves travelling to the right at the initial sound speed (which is unity in (χ, τ) coordinates), on which

$$\frac{d}{d\tau}(p_1 + U_1) = \beta K H(\xi). \tag{4.34}$$

Similarly, the negative characteristics are straight lines with gradient $d\chi/d\tau = -1$, representing waves travelling to the left at the same initial sound speed, on which

$$\frac{d}{d\tau}(p_1 - U_1) = \beta K H(\xi). \tag{4.35}$$

Since the initial post-shock gas is stationary (as is the contact) in this frame of reference, the leading order particle paths are lines of constant χ, on which

$$\frac{d}{d\tau}\left(T_1 - \frac{(\gamma - 1)}{\gamma} p_1\right) = \frac{\beta K H(\xi)}{\gamma} \tag{4.36}$$

by equation (4.33). Along these particle paths, equation (4.8) gives the leading order rate

of change of the induction time parameter as

$$\frac{d\xi}{d\tau} = e^{T_1}. \tag{4.37}$$

If we suppose that the ignition point (i.e. the point where $\xi(\chi, \tau) = 1$) moves along the path $\tau = F(\chi)$ in (χ, τ) space, then $F(\chi)$ can be determined by integrating (4.37),

$$1 = \int_{\tau_s(\chi)}^{F(\chi)} e^{T_1} d\tau, \tag{4.38}$$

where τ_s is the time when the particle at position χ was shocked, and so T_1 must first be determined. Now, the first disturbance caused by the heat release in the termination zone will emanate from the contact surface at $(\chi = 0, \tau = 0)$ and will travel to the right at the unit sound speed, i.e. along the path $\tau = \chi$. An undisturbed part of the induction zone, region $\mathcal{U}$, therefore exists between this first characteristic and the shock ahead. Since, from Sharpe's analysis [21], the shock initially propagates along the path $\tau = \tau_s = \chi/M_s - 1$, where M_s is the post-shock flow Mach number with respect to the shock, then region $\mathcal{U}$ is given by

$$\frac{\chi}{M_s} - 1 \leq \tau < \chi, \tag{4.39}$$

and since $T_1 = 0$ in region $\mathcal{U}$ then (4.38) gives

$$\frac{(1 - M_s)\chi}{M_s} = \int_{\chi}^{F(\chi)} e^{T_1} d\tau. \tag{4.40}$$

Following region $\mathcal{U}$, lies a disturbed part of the induction zone, region $\mathcal{A}$, between the first positive characteristic and the ignition point, given by

$$\chi \leq \tau < F(\chi), \tag{4.41}$$

which in turn is followed by the exothermic termination zone, region $\mathcal{B}$, given by

$$F(\chi) \leq \tau. \tag{4.42}$$

As Sharpe [21] explains, since $T_1 \ll 1$ at early times, equation (4.40) gives the ignition path as $F(\chi) = \chi/M_s$ initially, i.e. it propagates at the initial shock speed and therefore subsonically with respect to the post-shock flow (as $M_s \leq 1$ by definition). Hence, the disturbances due to heat release in the exothermic region $\mathcal{B}$ will continually overtake the ignition path, thus increasing the temperature in region $\mathcal{A}$ of the induction zone and so accelerating the ignition path via equation (4.40). See figure 4.2 for a schematic diagram of the ignition path and the location of regions $\mathcal{U}$, $\mathcal{A}$ and $\mathcal{B}$.

Figure 4.2: Schematic diagram of the (χ, τ) plane showing the location of regions $\mathcal{U}$, $\mathcal{A}$ and $\mathcal{B}$ in relation to the ignition path (—), the initial shock path (– · –), the first positive characteristic from the exothermic termination zone (· · ·, positive gradient) and the first negative characteristic from the disturbed shock (· · ·, negative gradient).

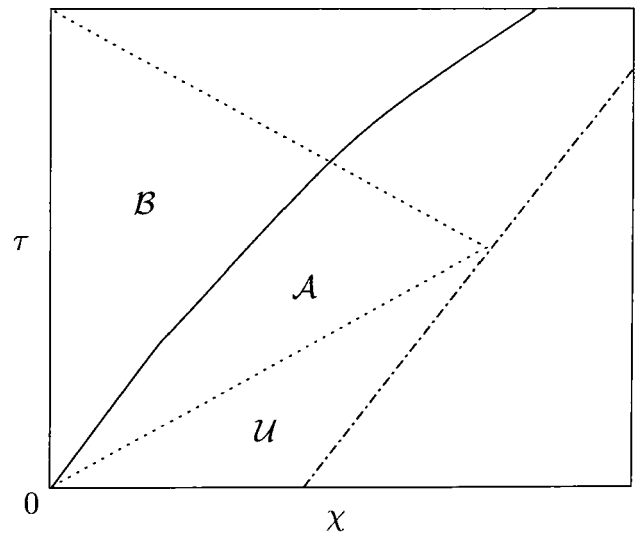

Once the first disturbance reaches the shock, the shock will accelerate, and information form the disturbed shock will therefore propagate backwards towards the contact at unit speed along the negative characteristic $\tau = 2M_s/(1 - M_s) - \chi$. Since we are only considering early time ($\tau \ll 1$) however, we need only construct the flow field in the region

unaffected by disturbances to the shock speed, i.e. $\tau < 2M_s/(1 - M_s) - \chi$.

Consider the negative and positive characteristics that respectively enter or leave a point on the contact path ($\chi = 0$) at some time τ_c (with $0 \leq \tau_c \leq 2M_s/(1 - M_s)$). The negative characteristic, $\tau = \tau_c - \chi$, starts at the shock path in region $\mathcal{U}$ where $p_1 = U_1 = 0$, and so integrating (4.35) gives $p_1 - U_1 = 0$ everywhere in regions $\mathcal{U}$ and $\mathcal{A}$. The negative characteristic intersects the ignition path at (χ_-, τ_-), where

$$\chi_- + F(\chi_-) = \tau_c, \qquad \tau_- = F(\chi_-). \tag{4.43}$$

In region $\mathcal{B}$, equation (4.35) can be integrated to give

$$p_1 - U_1 = \beta K(\tau - \tau_-) \tag{4.44}$$

after matching with the solution in region $\mathcal{A}$. At the contact, $\tau = \tau_c$ and gas velocity is given by the contact boundary condition (4.29), so that equation (4.44) then gives

$$p_1(0, \tau_c) - \frac{-p_1(0, \tau_c)}{\alpha_0} = \beta K(\tau_c - \tau_-),$$

and so

$$p_1(0, \tau_c) = \frac{\beta K(\tau_c - \tau_-)}{1 + \frac{1}{\alpha_0}} \tag{4.45}$$

is the pressure boundary condition at the contact.[1]

The positive characteristic which originates at the point $(0, \tau_c)$ on the contact path, is given by $\tau = \tau_c + \chi$ and intersects the ignition path at (χ_+, τ_+), where

$$F(\chi_+) - \chi_+ = \tau_c, \qquad \tau_+ = F(\chi_+). \tag{4.46}$$

[1] As expected, the pressure at the piston in Sharpe's study [21] is recovered by taking $\alpha_0 \to \infty$.

In region $\mathcal{B}$, equation (4.34) can then be integrated to give

$$p_1 + U_1 = \beta K \left(\tau + \frac{\tau_- - \alpha_0 \tau_- - 2\tau_c}{1 + \alpha_0} \right) \tag{4.47}$$

after employing the contact boundary condition (4.45). In region $\mathcal{A}$, equation (4.34) can be integrated to give

$$p_1 + U_1 = \beta K \left(\tau_+ + \frac{\tau_- - \alpha_0 \tau_- - 2\tau_c}{1 + \alpha_0} \right) \tag{4.48}$$

after matching with the solution in region $\mathcal{B}$. But since $p_1 - U_1 = 0$ everywhere in region $\mathcal{A}$, then

$$p_1 = U_1 = \frac{\beta K}{2} \left(\tau_+ + \frac{\tau_- - \alpha_0 \tau_- - 2\tau_c}{1 + \alpha_0} \right). \tag{4.49}$$

Since $T_1 = p_1 = 0$ at the shock, integrating equation (4.36) along the particle paths gives the temperature in region $\mathcal{A}$ as

$$T_1 = \frac{(\gamma - 1)}{\gamma} p_1. \tag{4.50}$$

Hence, given $F(\chi)$, we can construct the solution at any point (χ, τ) in region $\mathcal{A}$ from equations (4.49) and (4.50) by determining the appropriate value of τ_c for the positive characteristic that passes through that point.

In order to determine the solution at any point (χ, τ) in region $\mathcal{B}$, we also need to consider the negative characteristic which passes through the point. The positive characteristic through (χ, τ) leaves the contact at time $\tau_c = \tau - \chi$, while the negative characteristic through (χ, τ) intersects the ignition path at (χ'_-, τ'_-), where

$$\chi'_- + F(\chi'_-) = \chi + \tau, \qquad \tau'_- = F(\chi'_-). \tag{4.51}$$

Integrating equation (4.35) along this negative characteristic gives

$$p_1 - U_1 = \beta K (\tau - \tau'_-) \tag{4.52}$$

after matching with the solution in region $\mathcal{A}$. Adding equations (4.47) and (4.52) gives the pressure solution as

$$p_1 = \beta K \tau + \frac{\beta K}{2}\left(\frac{\tau_- - \alpha_0 \tau_- - 2\tau_c}{1+\alpha_0} - \tau'_-\right), \tag{4.53}$$

while subtracting gives the gas velocity solution as

$$U_1 = \frac{\beta K}{2}\left(\frac{\tau_- - \alpha_0 \tau_- - 2\tau_c}{1+\alpha_0} + \tau'_-\right). \tag{4.54}$$

Integrating equation (4.36) then gives the temperature solution in region $\mathcal{B}$ as

$$T_1 = \frac{(\gamma-1)}{\gamma} p_1 + \frac{\beta K}{\gamma}\left[\tau - F(\chi)\right] \tag{4.55}$$

after matching with the solution in region $\mathcal{A}$.

So, given the ignition path $F(\chi)$, the flow field can now be determined everywhere in the region unaffected by disturbances to the shock speed, i.e. $\tau < 2M_s/(1-M_s) - \chi$. As Sharpe [21] explains, a simple iterative method can be used to determine $F(\chi)$. The initial ignition path, $F(\chi) = \chi/M_s$, is used as a first guess. Equations (4.43), (4.46) and (4.51) then respectively give

$$\chi_- = \frac{(\tau-\chi)M_s}{1+M_s}, \qquad \chi_+ = \frac{(\tau-\chi)M_s}{1-M_s}, \qquad \chi'_- = \frac{(\tau+\chi)M_s}{1+M_s}, \tag{4.56}$$

and so equations (4.49) and (4.50) give

$$p_1 = U_1 = \frac{\beta K M_s(M_s+\alpha_0)}{(1-M_s^2)(1+\alpha_0)}(\tau-\chi), \qquad T_1 = \frac{\beta K M_s(\gamma-1)(M_s+\alpha_0)}{\gamma(1-M_s^2)(1+\alpha_0)}(\tau-\chi) \tag{4.57}$$

in region $\mathcal{A}$, and equations (4.53), (4.54) and (4.55) give

$$p_1 = \frac{\beta K M_s}{(1+M_s)(1+\alpha_0)}(\alpha_0\tau + \chi), \qquad U_1 = \frac{\beta K\left[\chi(1+\alpha_0) - M_s(\tau-\chi)\right]}{(1+M_s)(1+\alpha_0)},$$
$$T_1 = \frac{\beta K M_s(\gamma-1)(M_s+\alpha_0)}{\gamma(1-M_s^2)(1+\alpha_0)} + \frac{\beta K}{\gamma}\left(\tau - \frac{\chi}{M_s}\right) \tag{4.58}$$

in region $\mathcal{B}$. Although in Sharpe's region $\mathcal{B}$ solution, p_1 is independent of χ and U_1 is independent of τ [21], we note in (4.58) that this is no longer true for the contact-driven case, where the solutions are dependent on both distance and time.

The following improved estimate of $F(\chi)$ is achieved by substituting (4.57) into (4.40):

$$F(\chi) = \chi + \frac{1}{A}\ln\left[1 + \frac{A(1-M_s)}{M_s}\chi\right], \text{ where } A = \frac{\beta K M_s(\gamma-1)(M_s+\alpha_0)}{\gamma(1-M_s^2)(1+\alpha_0)}. \tag{4.59}$$

As expected, allowing $\alpha_0 \to \infty$ leads us to Sharpe's expression for the asymptotic ignition path for the *piston*-driven shock case [21]. Further iterations to improve $F(\chi)$ are possible, but they will require equations (4.43), (4.46) and (4.51) to be solved numerically. Anyhow, Sharpe [21] finds that this first iteration is sufficient for a quantitatively converged solution at early times.

Figure 4.3 shows the asymptotic ignition path (4.59) plotted for two sets of the heat release parameters Q and K. For comparative purposes, both sub-figures also show Sharpe's ignition path expression for the piston case. Even though in figure 4.3(a) we have set $\alpha_0 = 1$ (the smallest possible value, meaning that all backward-moving acoustic disturbances pass through the contact), the ignition path does not diverge much at all from Sharpe's ignition path for the piston case (where all backward-moving acoustic disturbances are reflected back into the reactive gas). Figure 4.3(b) shows the ignition paths for a relatively higher rate of heat release. We immediately notice that, although the ignition path initially travels at the same velocity as the shock, it quickly accelerates due to the overtaking disturbances originating from the now more intense exothermic termination zone. There is also a larger deviation from the piston case's ignition path than with the

Figure 4.3: Asymptotic ignition paths, $F(\chi)$, for the 2-step contact-driven shock case (—) for two sets of heat release parameters. Also shown are Sharpe's asymptotic ignition path for the 2-step *piston*-driven shock case [21] (- - -), the initial shock path (— · —·), the first positive characteristic from the exothermic termination zone (· · ·, positive gradient) and the first negative characteristic from the disturbed shock (· · ·, negative gradient). The value used for the initial transmitted shock Mach number is the same as the value which shall be used in the three-step numerical simulations, i.e. $M_i = 2.89$. It is then deduced that $M_s = 0.48$.

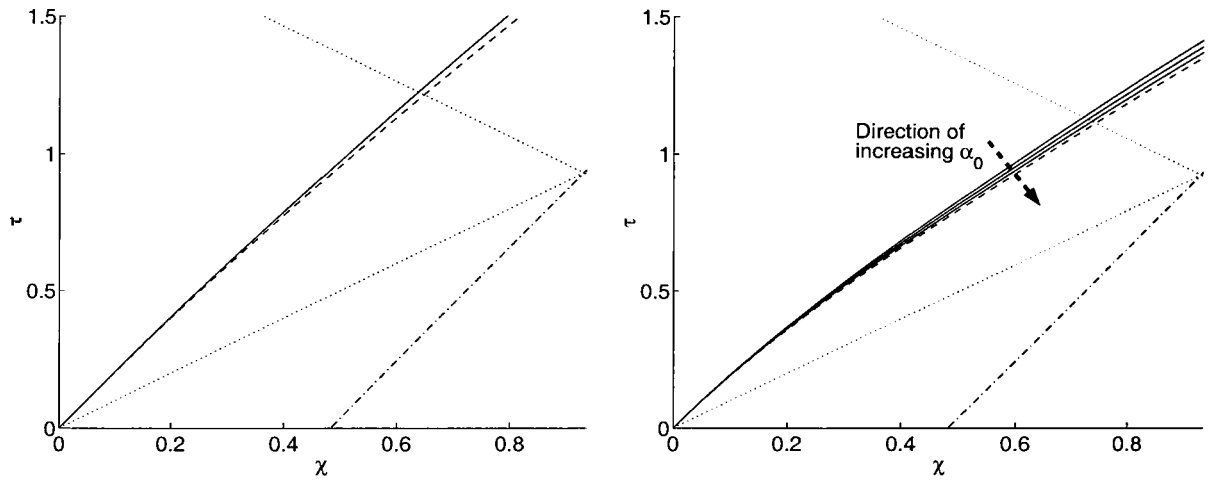

(a) $Q = 4$, $K = 2.5$, $\alpha_0 = 1$.

(b) $Q = 10$, $K = 5$, $\alpha_0 = 1$, 2 and 5.

lower heat release values used in figure 4.3(a), and as such we are able to plot the ignition paths clearly for three increasing values of α_0 starting from the smallest value of unity. As can be seen, when we increase α_0, the resulting ignition path tends to the ignition path of the piston case. This is as expected, since a larger α_0 means a higher density of material behind the contact surface and so a more reflective boundary condition. What may seem surprising is that even with these higher heat release parameter values and for $\alpha_0 = 1$, the deviation from the piston case's ignition path is still not very large. This can be explained by the fact that, regardless of the rate of heat release, the induction zone will always remain thermally neutral in chain-branching reactions, and hence acoustic leakage at the contact surface cannot take effect until only after the elapse of the ignition time of the particle at the contact surface. Also, the fact that we have only considered the early time evolution, and certainly the period of time before the first positive characteristic

can affect the shock velocity (i.e. below the line of the first negative characteristic in figure 4.3), then there is not much available time for acoustic leakage to affect the ignition path considerably. Therefore, the implication for our three-step numerical simulations is that, for chain-branching values of T_B (e.g. $T_B = 0.8$ in our chosen list of values), there should be little difference in the early time behaviour of the ignition path between the piston and contact cases, although the ignition path in the contact case will lag slightly behind.

4.3 Numerical Solutions

We shall produce numerical solutions for the three-step contact-driven case using the same method as that used for the piston-driven case (outlined in section 3.2). As in the piston case, we shall vary T_B, while keeping the rest of the parameters constant as follows:

$$\varepsilon_I = \frac{1}{15}, \qquad \varepsilon_B = \frac{1}{5}, \qquad Q = 4, \qquad \gamma = 1.4, \qquad T_I = 3, \qquad M_1 = M_2 = 1.7. \tag{4.60}$$

Solving equation (4.3) using the above values of M_1 and M_2 gives the initial transmitted shock Mach number as $M_i = 2.89$.

We shall use the same reactive Euler equations, (3.1), (3.2), (3.4) and (3.6), to model the gas dynamics, coupled to the same conservation of chemical species equations, (3.7) and (3.8) as those used in the piston-driven case. All variables and constants are non-dimensionalized with respect to the initial shocked state (i.e. with respect to region 2 of the inert case), so that we may apply the same scalings as those of the piston-driven case, (3.9), by replacing the '$\star$' subscript with a '2' subscript. Hence, the initial shocked state is

$$\rho = 1, \quad p = 1, \quad T = 1, \quad u = u_c. \tag{4.61}$$

The scalings (3.9) also give that time, t, is scaled with respect to the homogeneous,

constant volume (numerical) ignition time appropriate to region 2. We shall further rescale the origin of the time variable, t, but keeping the same name, such that the two weak precursor shocks merge at the reference time $t = t_M = 0$. Therefore, just as in the piston case, the homogeneous, constant volume ignition time appropriate to the initial post-shock or region 2 state is given by $t = 1$.

4.3.1 $T_B = 0.8$

Figure 4.4 shows the complete profiles for the initial stages of evolution of the chain-branching $T_B = 0.8$ case after the merging of the two weak precursor shocks. The temperature profiles show a strong transmitted shock travelling into region 1, which leaves behind a relatively hot and rapidly evolving region 2 that terminates at the contact surface (visible as a temperature discontinuity and as a horizontal line in the pV profiles). The contact surface (which initially lies at $X = 0$ and remains extremely close to it for the first two times shown) leaves behind region 3, which is evolving quite noticeably though not as significantly as region 2. The pressure profiles confirm pressure to be continuous at the contact surface, and show the rarefaction wave separating region 3 from region 4.

At $t = 1.0$ (the ignition time for the homogeneous, constant volume problem), the temperature and pressure profiles do not look qualitatively very different from the schematic diagrams of the inert case in figure 4.1(b), apart from the appearance of pressure and temperature disturbances near the contact surface. We notice that the fuel has just ignited at the contact surface owing to the onset of a chain-branching explosion there, and that, consequently, temperature and pressure disturbances begin to emerge from this region, as they did in the piston-induced case of chapter 3. A crucial difference though, is that here, some of these disturbances travel backwards along negative characteristics owing to the acoustic permeability of the contact surface. This can clearly be seen in the pressure profiles as a compression wave, and also in the temperature profiles as a weak thermal wave, travelling into region 3 at the same (sound) speed as the rarefaction wave. Both

Figure 4.4: Contact-driven shock profiles for $T_B = 0.8$ at times 1.0, 1.2, 1.4, 1.6 and 1.8. Scaled with $t_{ign} = 3.801$.

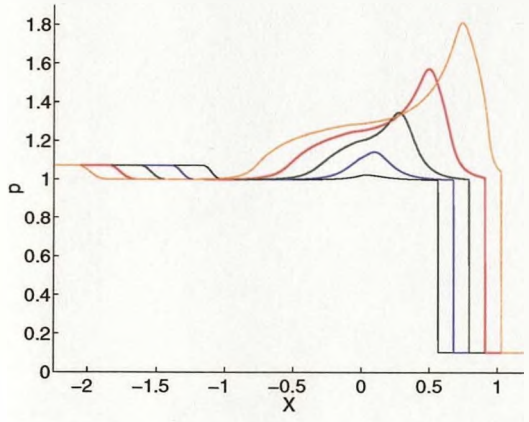

(a) Pressure profiles.

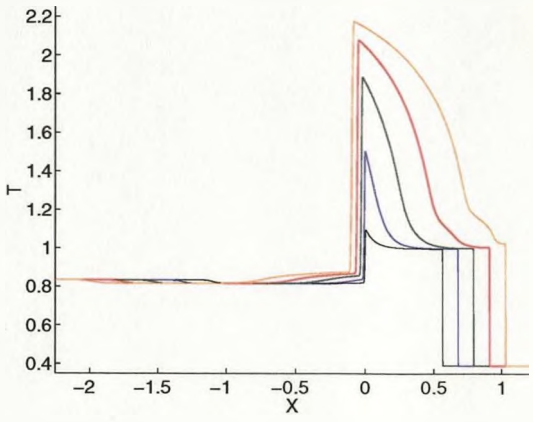

(b) Temperature profiles.

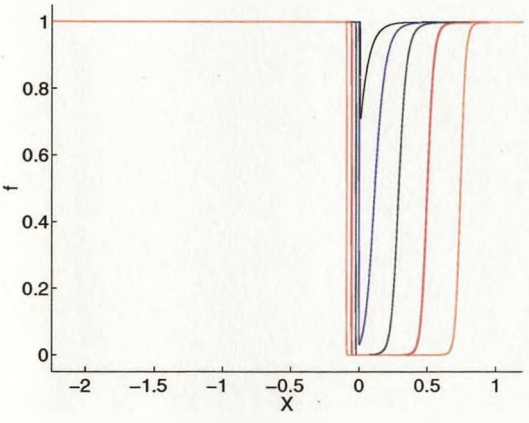

(c) Fuel profiles.

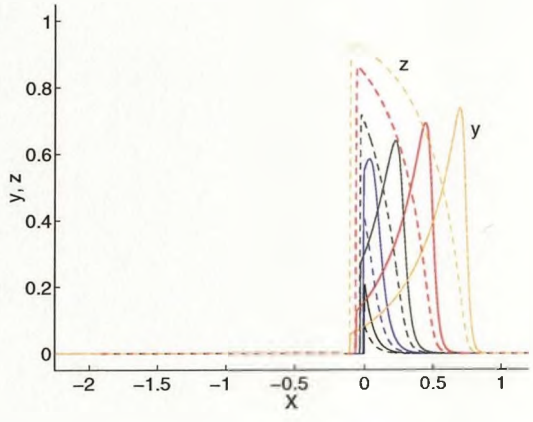

(d) Chain carrier and product profiles.

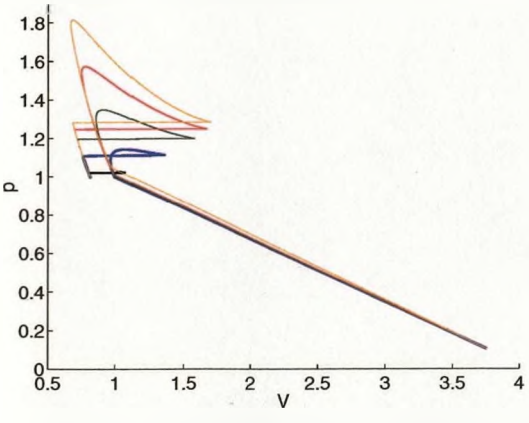

(e) pV diagrams.

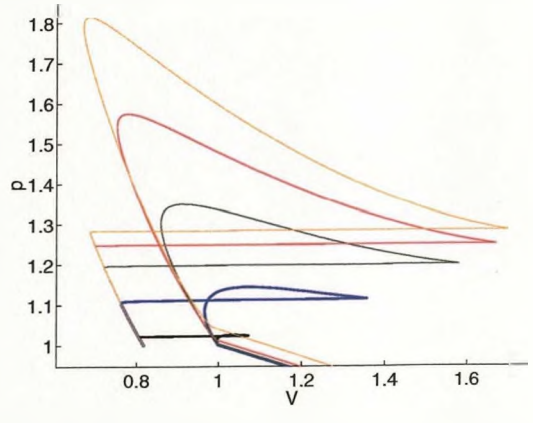

(f) pV diagrams zoomed in behind shock.

Figure 4.5: Contact-driven shock profiles for $T_B = 0.8$ at times 1.79, 1.83, 1.87, 1.91 and 1.95. Profiles are zoomed in between the contact and the shock except in pV figure. Scaled with $t_{ign} = 3.801$.

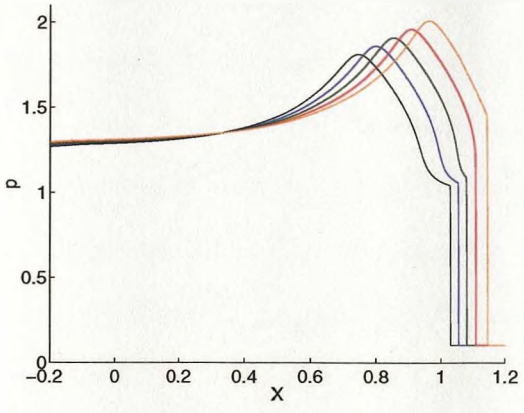

(a) Pressure profiles.

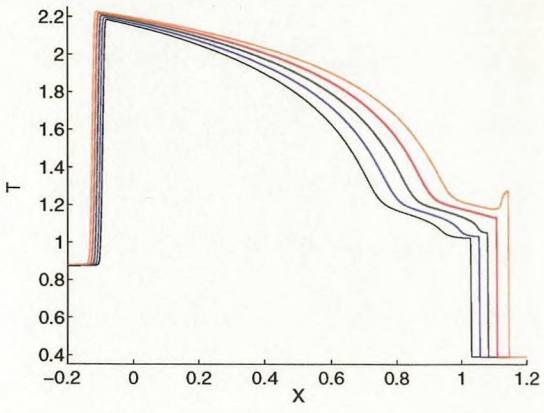

(b) Temperature profiles.

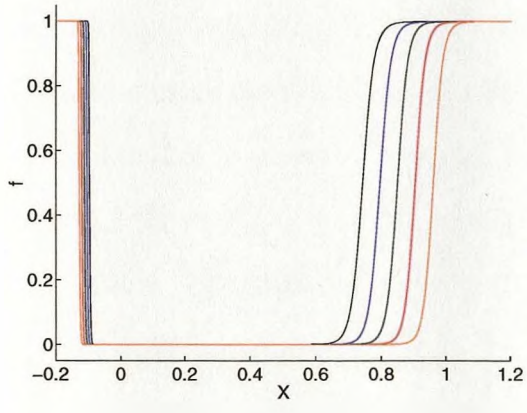

(c) Fuel profiles.

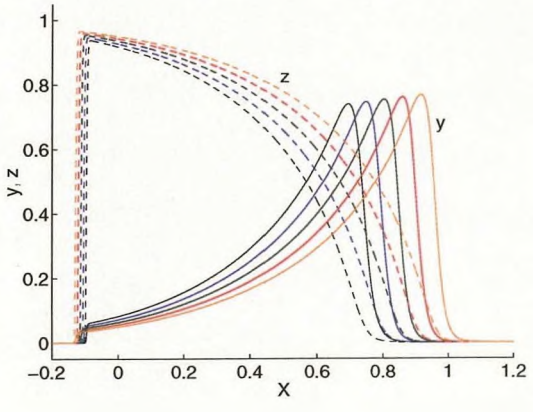

(d) Chain carrier and product profiles.

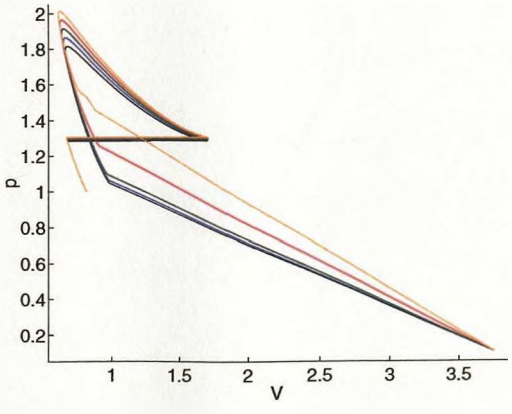

(e) pV diagrams.

the left and right moving waves become stronger as more heat is released in the reaction zone ahead of the contact. Due to the action of thermal expansion in the induction zone, the contact can be seen moving slowly backwards as it increases in strength, meaning it is decelerating in the shock tube frame (it would remain at the constant speed u_c if the gas was inert). Decelerating contacts (or decelerating impact interfaces) are observed in shock experiments with solid explosives, and can be used as an indicator for the occurrence of reaction [26]. The disturbances travelling along positive characteristics to the right are rapidly increasing in strength, and are manifested in a strong compression wave that overtakes the subsonic chain-branching explosion ignition point (where the pressure is a maximum) and is about to collide with the shock in the last time step (the weakly compressive head of the compression wave has actually already reached the leading shock and amplified it a little - see the last pV profile). The reaction is shown clearly to proceed in a chain-branching fashion from the outset, with a well-defined, thermally neutral and product-free induction zone followed by a strong and short branching explosion.

Figure 4.5 shows that before the strong compression wave can develop into a secondary shock, it collides with the shock wave ahead, producing a much stronger shock that can be seen accelerating in the pV diagrams. Eventually, although not shown, the expansive heat releasing reaction zone will couple with the shock wave, resulting in a quasi-steady CJ detonation.

4.3.2 $T_B = 1.0$

For $T_B = 1.0$, figure 4.6 shows a very strong secondary shock that begins to develop between the second and third time steps. In contrast with the previous, highly chain-branching $T_B = 0.8$ case, the induction zone here is not void of products z, but in fact has a higher proportion of products than chain carriers y initially. This induction zone buildup of z and associated heat release means that the reaction bears some resemblance to thermal reactions, which is unsurprising as $R_B \sim R_C$ in the early part of the evolution. The pV

Figure 4.6: Contact-driven shock profiles for $T_B = 1.0$ at times 1.212, 1.312, 1.412, 1.512 and 1.612. Profiles are zoomed in between the contact and the leading shock except in pV figure. Scaled with $t_{ign} = 34.64$.

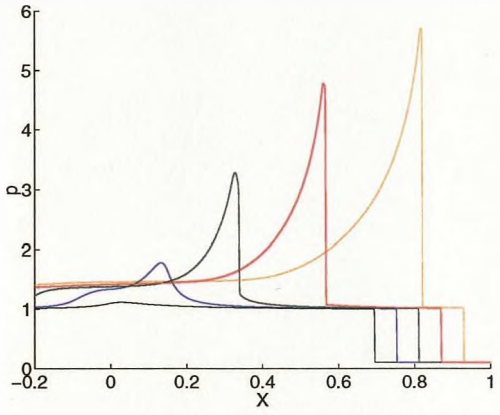

(a) Pressure profiles.

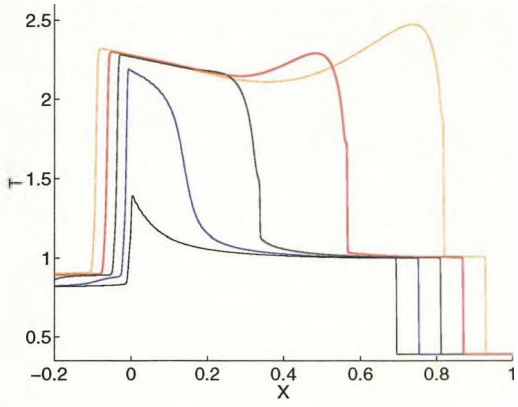

(b) Temperature profiles.

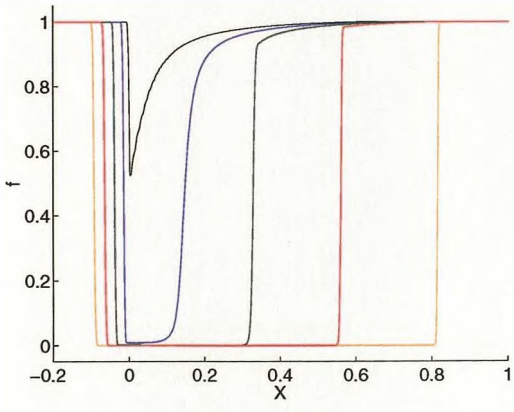

(c) Fuel profiles.

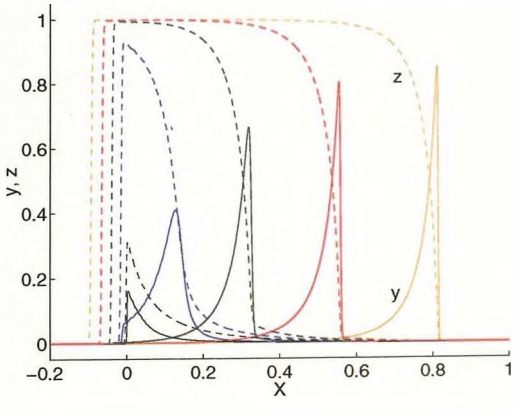

(d) Chain carrier and product profiles.

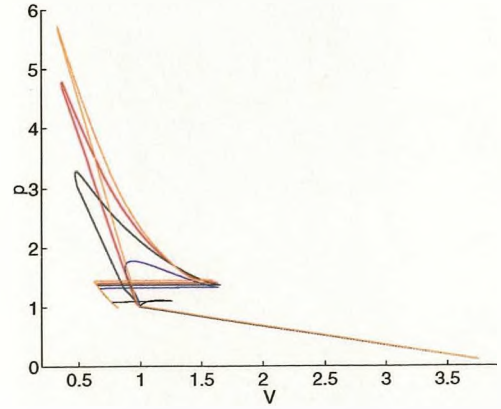

(e) Complete pV diagrams.

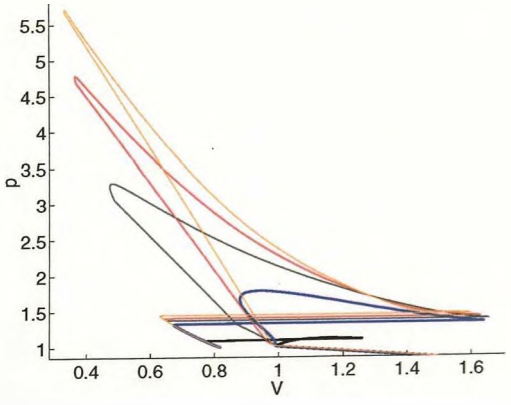

(f) pV diagrams zoomed in behind main shock.

Figure 4.7: Contact-driven shock profiles for $T_B = 1.0$ at times 1.64, 1.67, 1.70, 1.73 and 1.76. Profiles are zoomed in at shock collision except for pV figure. Scaled with $t_{ign} = 34.64$.

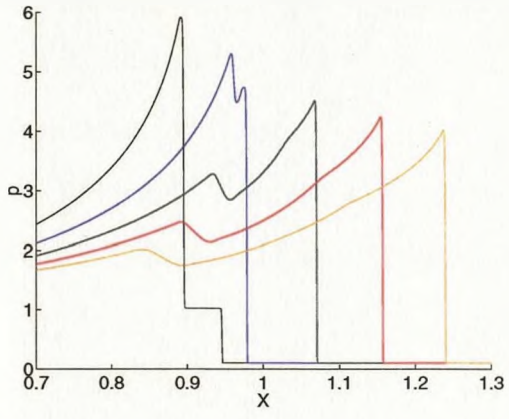

(a) Pressure profiles.

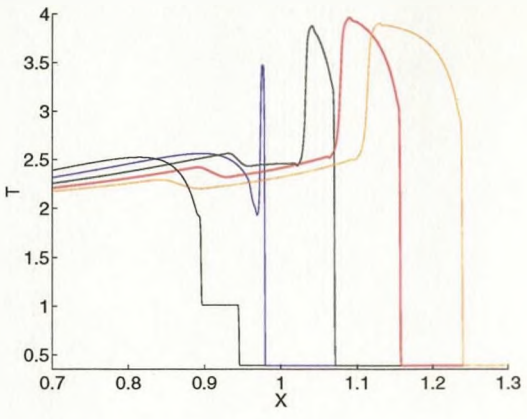

(b) Temperature profiles.

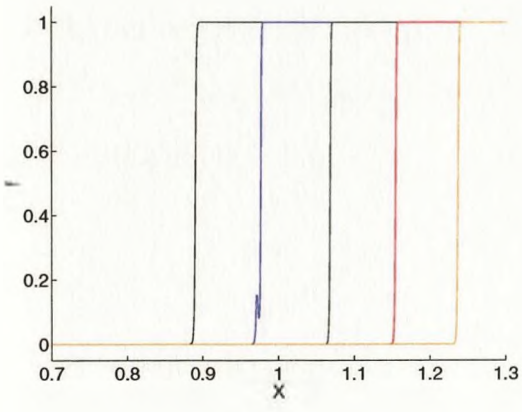

(c) Fuel profiles.

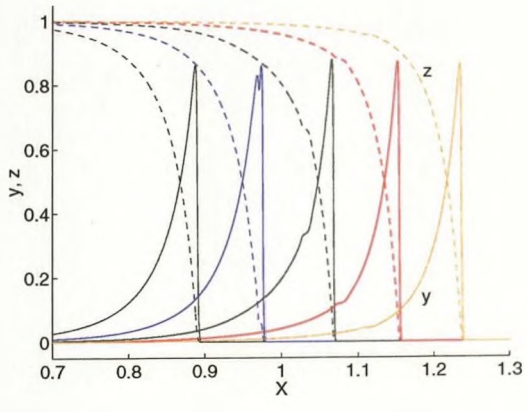

(d) Chain carrier and product profiles.

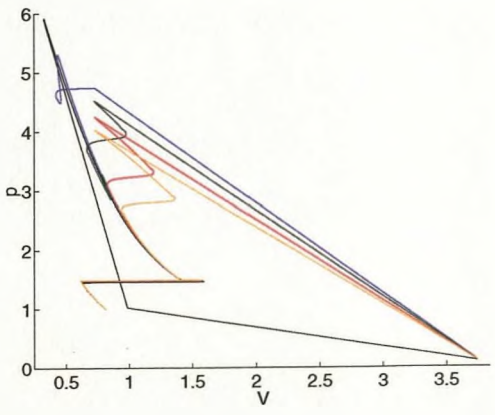

(e) pV diagrams.

diagrams indicate that a quasi-steady weak detonation is travelling through this growth in z, and subsequently, a secondary shock can be seen forming and growing in strength and velocity. Eventually, there is no reaction taking place ahead of the accelerating secondary shock, with all reaction taking place behind it in a highly chain-branching fashion (as the temperature increasingly becomes greater than T_B at the secondary shock). The pV diagrams shows the reaction wave coming close to coupling with the secondary shock, although a CJ detonation does not form before the two shocks collide.

Figure 4.7 gives a close-up view of the shock collision process, where the collision can be see to take place just before the second time step. As expected, the temperature profiles shows that a second contact forms at collision. However, the high temperature region generated ahead of the contact cannot influence the reaction rates significantly because the contact was formed downstream of the induction zone where most of the fuel has already been depleted (only a small blip in fuel and chain carrier fractions can be seen in the second time step).

4.3.3 $T_B = 1.2$

As we have already observed in our homogeneous and piston studies, the value $T_B = 1.2$ leads to initial behaviour that is more synonymous with thermal reactions than chain-branching reactions. Figure 4.8 shows the evolution of the flow around the contact surface during ignition and the associated thermal runaway. We immediately notice one major qualitative difference that sets this $T_B = 1.2$ case apart from all previous cases, that is the spatially non-monotonic structure of the fuel fraction f. Rather than the usual monotonic decrease of f as we approach the contact surface from the reacting gas on the right, the f minimum moves away from the contact surface into this reacting gas (figure 4.8(c) shows this to begin between the fifth and sixth time steps). Numerical results by Short and Dold [24] and analytical results by Parkins [25] (in the limit of high activation energy) show thermal runaway for the thermal one-step model to take place

Figure 4.8: Contact-driven shock profiles for $T_B = 1.2$ at times 1.440, 1.445, 1.450, 1.455, 1.460, 1.465, 1.470 and 1.475. Profiles are zoomed in at thermal runaway. Scaled with $t_{ign} = 457.763$.

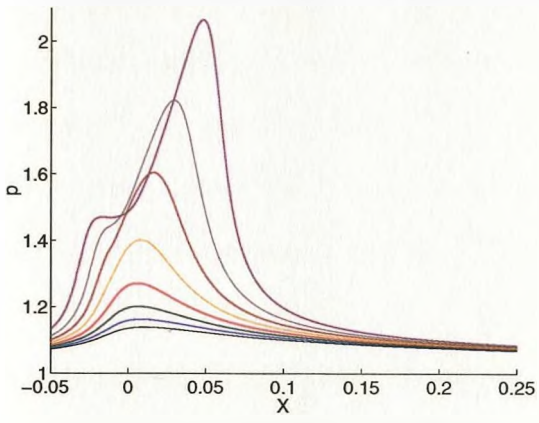

(a) Pressure profiles.

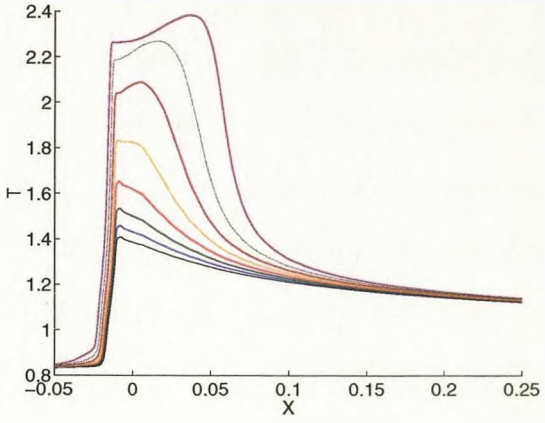

(b) Temperature profiles.

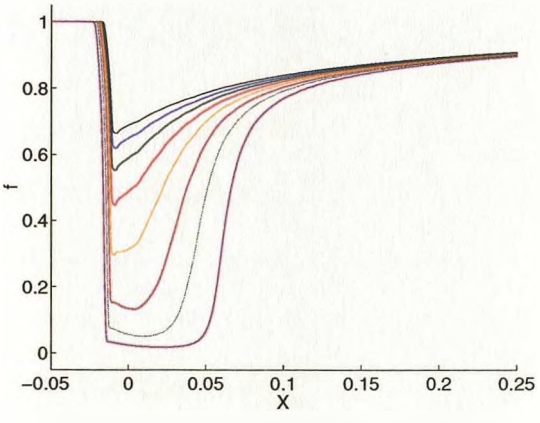

(c) Fuel profiles.

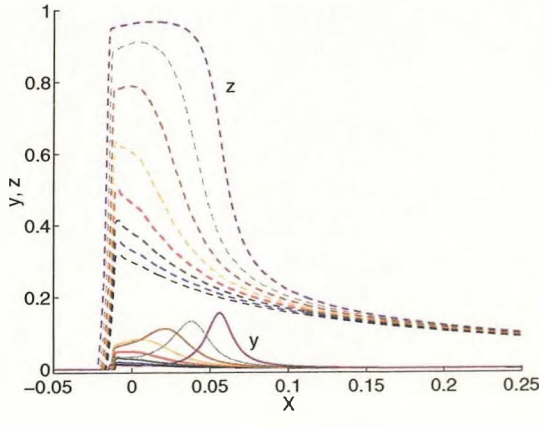

(d) Chain carrier and product profiles.

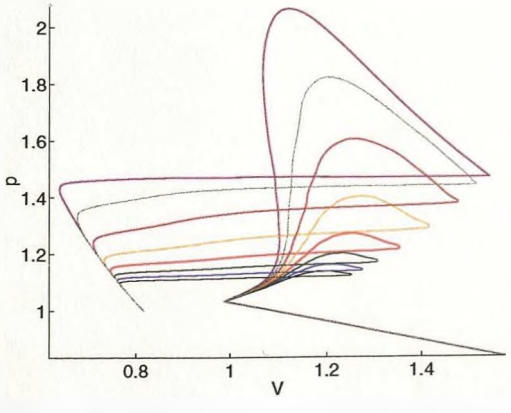

(e) pV diagrams zoomed in behind shock.

upstream of the contact surface owing to acoustic leakage at the contact surface. In our finite activation energy three-step temperature profiles, we notice that although thermal runaway begins at the contact surface, the temperature maximum moves away from it and thus thermal runaway is completed away from the contact surface. Short and Dold [24] explain that the acoustic leakage allows a rate of expansion of material that is largest at the contact surface (which can be seen in our pressure profiles). This causes a faster deceleration of the contact surface as thermal runaway is approached, allowing a faster rise in temperature away from the contact surface. The fact that this movement of the temperature maximum occurs whilst there is still ample fuel at the contact explains why the fuel minimum also moves ahead of the contact.

4.4 A comparison with piston-driven shocks

In order to see directly how using a contact surface to drive a shock differs from using a piston, we can compare profiles from both simulations using the same parameter set and for the same set of times. We shall use the parameter set (4.60) used in the above contact simulations. Hence, for a valid comparison, the initial Mach number of the shock wave in the piston case is set at the value of the initial Mach number of the transmitted shock wave in the contact case ($M_i = 2.89$), and so the contact surface initially travels at the same speed as the steady piston. The term "rear boundary" refers to the piston face in the piston case and to the contact in the contact case.

4.4.1 $T_B = 0.8$

Figure 4.9 shows the piston profiles and the contact profiles for the chain-branching $T_B = 0.8$ case superimposed on the same axes. The vertical dotted line at $X = 0$ shows the position of the piston and also of the contact when it is initially formed (at $t = 0$). The four time steps chosen where taken from the contact profiles in figures 4.4 and 4.5. The

Figure 4.9: Comparing contact-driven shock profiles (- - -) with piston-driven shock profiles (—) for $T_B = 0.8$ at times 1.19 (black), 1.79 (blue), 1.87 (green) and 1.95 (red). Profiles are zoomed in between the contact and the leading shock. Scaled with $t_{ign} = 3.801$.

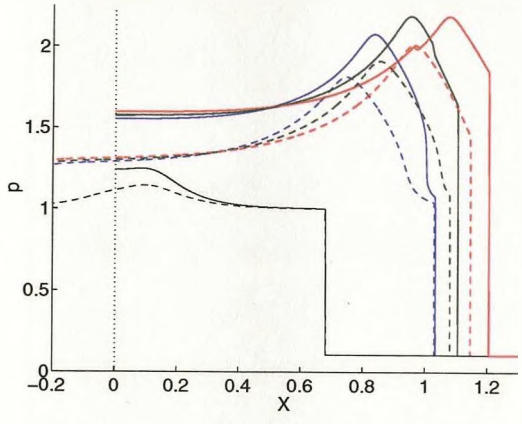

(a) Pressure profiles.

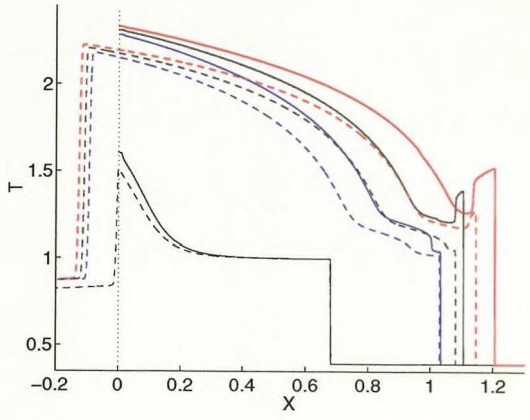

(b) Temperature profiles.

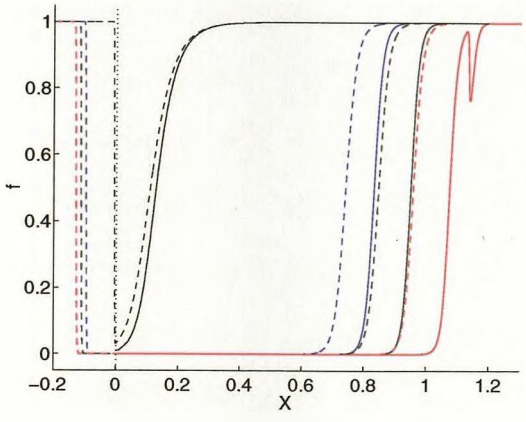

(c) Fuel profiles.

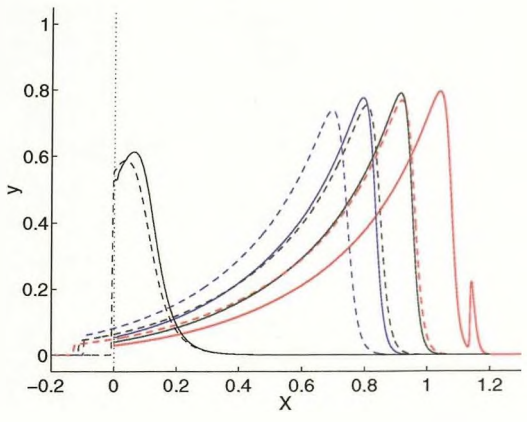

(d) Chain carrier profiles.

first time step gives a snapshot from the early evolution. From it we notice that, as expected, the contact surface remains virtually at the same position where it originated, i.e. at $X = 0$. More importantly, although the chain-branching ignition point is lagging behind that of the piston-driven case, the deviation is not very significant in this early time since acoustic leakage cannot occur in a chain-branching induction zone (which is thermally neutral by nature). This was predicted by the two-step chain-branching asymptotic ignition paths (e.g. figure 4.3).

In the second time shown, although a strong compression wave exists in the contact-driven case (as we have already seen), a small but noticeable secondary shock is observed in the piston-driven case. The acoustic leakage (which is now very noticeable) at the driving contact means that less energy can travel to the right than in the piston case where all disturbances are forced along positive characteristics. Hence, the compression wave in the contact case cannot steepen quickly enough to develop into a secondary shock before it reaches the leading shock. The acoustic leakage also means that the pressure and temperature are significantly lower for the contact case than for the piston case at their respective rear boundaries. The overall temperature in the piston case is thus higher than in the contact case, and so its induction zone is significantly shorter (the fuel is igniting upstream of where it is igniting for the contact case). The third time step shows that, in the piston case, the secondary shock has already collided with the leading shock, creating a stronger and faster transmitted shock and a small contact. In the contact case, the strong compression has yet to merge with the leading shock and so the leading shock lags behind the stronger transmitted shock of the piston case. In the last time step, the compression wave has finally merged with the leading shock to create a stronger shock, while in the piston case, the strong shock has triggered a second ignition point that will soon consume all the fuel at the newly formed contact.

4.4.2 $T_B = 1.0$

Figure 4.10 shows two time-steps for $T_B = 1.0$, where as before, the piston profiles and the contact profiles are superimposed on the same axes and the dotted line at $X = 0$ shows the piston and initial contact point. We can expect a greater discrepancy between the piston profiles and the contact profiles than in the previous $T_B = 0.8$ case since now thermal effects are present early on and so acoustic leakage at the contact is significant even in the induction zone. The first time step shows that while a strong secondary shock has already formed in the piston case, there is only a compression wave in the contact

Figure 4.10: Comparing contact-driven shock profiles (- - -) with piston-driven shock profiles (—) for $T_B = 1.0$ at times 1.312 (black) and 1.612 (blue). Profiles are zoomed in between the contact and the leading shock. Scaled with $t_{ign} = 34.64$.

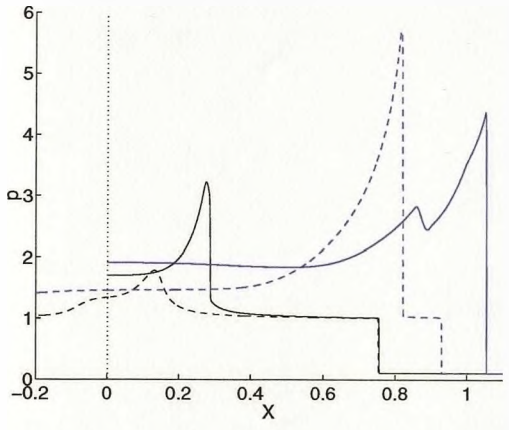

(a) Pressure profiles.

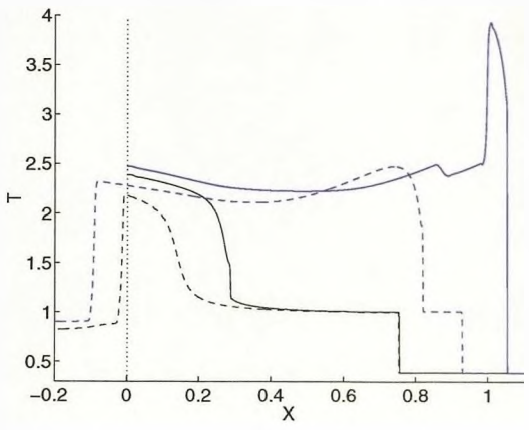

(b) Temperature profiles.

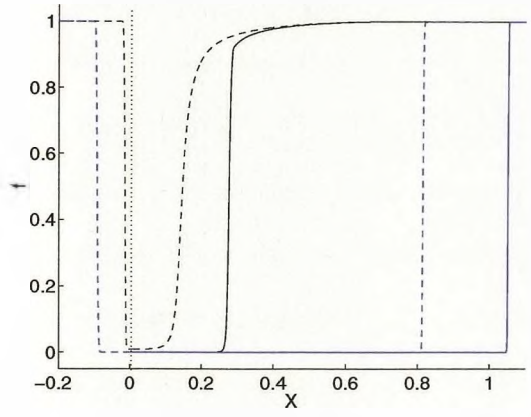

(c) Fuel profiles.

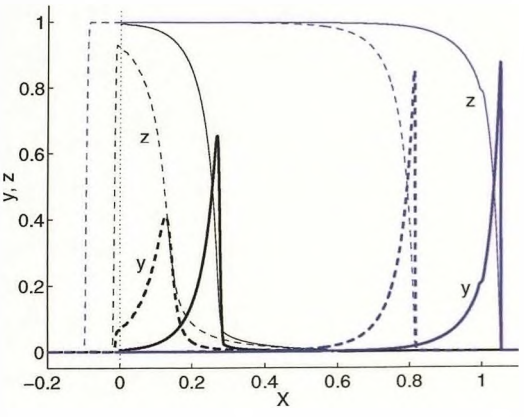

(d) Chain carrier and product profiles.

case. The temperature and pressure at the rear boundary are much lower for the contact case than for the piston case, and the two fuel ignition points are thus considerably far apart (much more so than with the previous value of $T_B = 0.8$). The chain-branching explosion is also much thinner in the piston case, and yields a far higher chain carrier maximum, since the temperatures are higher and thus further above T_B. The second of the two time steps shows that the secondary shock in the piston case has already collided

with its leading shock and created a strong contact in the process. Meanwhile, although the compression wave in the contact case has developed into a secondary shock, it is still some distance away from reaching its leading shock. The undisturbed leading shock can be seen lagging quite far behind the amplified and accelerated transmitted shock of the piston case.

4.4.3 $T_B = 1.2$

In this weakly chain-branching case, thermal effects are quite prominent, especially those concerning heat release in the induction zone. With a contact-driven shock, we have already seen a large amount of acoustic leakage during the evolution to thermal runaway in figure 4.8. This led to the T maximum, and consequently the f minimum, moving away from the contact into the interior of the gas, just as what occurs with one-step thermal models. Figure 4.11 shows the evolution to thermal runaway for the piston-driven case, using the same value $T_B = 1.2$ as in figure 4.8. The first thing to note is that an earlier set of times is used in the piston case because thermal runaway, or ignition, at the rear boundary takes place earlier. Although not shown, by $t = 1.440$ (the first time step in the contact case) a strong CJ detonation will have already developed in the piston case due to the faster evolution. Qualitatively, we notice that, in contrast with the contact case, the T maximum never leaves the piston face except only after virtually all the fuel is depleted there. Consequently, the f minimum also does not leave the piston face and hence f cannot develop non-monotonically. These differences are due to the completely reflective nature of the piston face, which prevents any leakage of disturbances and so serves to enhance reaction in the gas ahead.

In contact-driven cases where $T_B < 1$, i.e. highly chain-branching values (such as $T_B = 0.8$ considered in section 4.3.1), there is no heat release in the induction zone and hence no acoustic leakage there. Therefore, the induction zone remains void of any gas-dynamical evolution, and so the T maximum remains at the contact surface at least until

Figure 4.11: Piston-driven shock profiles for $T_B = 1.2$ at times 1.304, 1.308, 1.312, 1.316, 1.320, 1.324, 1.328 and 1.322, to be compared with the contact-driven profiles in figure 4.8. Profiles are zoomed in at thermal runaway. Scaled with $t_{ign} = 457.763$.

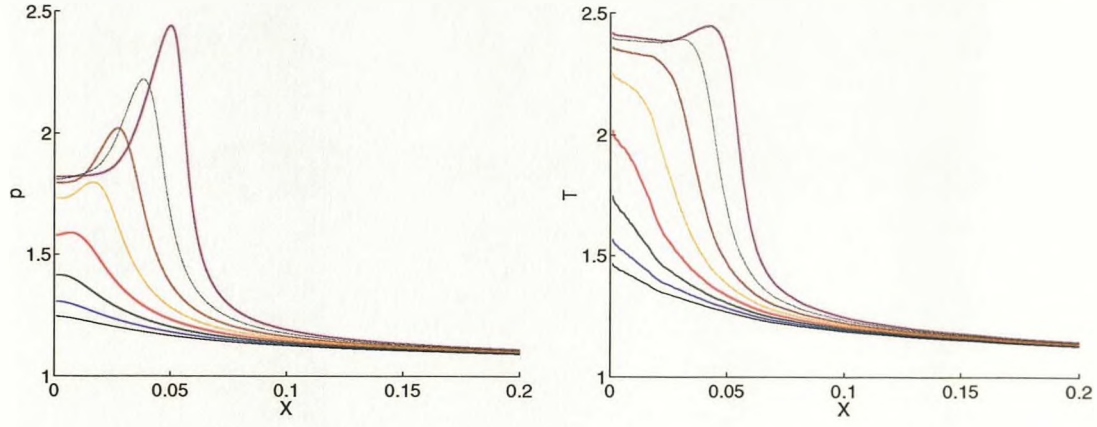

(a) Pressure profiles.

(b) Temperature profiles.

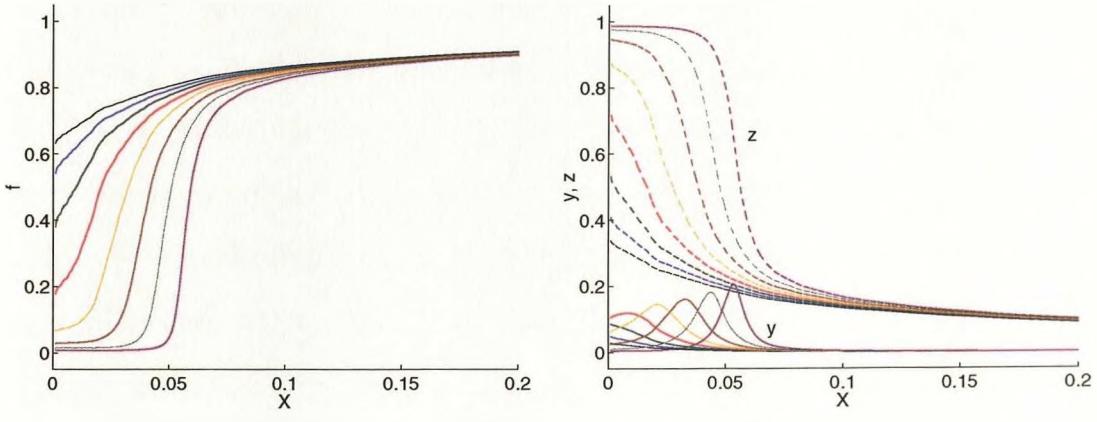

(c) Fuel profiles.

(d) Chain carrier and product profiles.

the fuel is depleted there, completely unlike what occurs with one-step thermal models.

Chapter 5

CONCLUSIONS AND FURTHER WORK

5.1 Conclusions

The main aim of this work is to show that a three-step chain-branching scheme can be used to not only model chain-branching reactions but also thermal reactions that are normally modelled by a one-step scheme, as well as intermediate thermal-chain-branching effects. We have seen that the crucial parameter is the chain-branching crossover temperature T_B. If for a period of time the ambient temperature is above T_B then the reaction can potentially proceed in a chain-branching fashion, assuming there is ample fuel left. If the temperature is below T_B then chain-branching cannot occur rapidly.

For the homogeneous, closed vessel scenario, complete numerical solutions were given for various values of T_B. For $T_B < 1 = T(0)$, we achieved the three distinct temporal zones characteristic of chain-branching explosions. The smaller the value of T_B, the more well-defined the zones became, in the sense that the induction zone released less heat and witnessed virtually no change from the initial state. Also, the chain-branching explosion was faster, occurred earlier, resulted in a higher peak chain carrier concentration and hence produced less heat and fewer products for smaller T_B. The products are then formed and the heat is released in the final chain-termination stage. Our leading order

asymptotic study revealed that the fuel ignites (i.e. the chain-branching explosion occurs) at

$$t = t_{ign} = \exp\left[\frac{1}{\varepsilon_B}\left(1 - \frac{1}{T_B}\right)\right]\left\{\frac{1}{\varepsilon_B}\left(\frac{1}{T_B} - 1\right) - \frac{1}{\varepsilon_I}\left(\frac{1}{T_I} - 1\right)\right\},$$

with the exponential factor confirming that smaller T_B or ε_B results in a shorter ignition time. In terms of the accuracy of our asymptotic solutions, the crucial parameter is e_B, an exponential encompassing both T_B and ε_B. Smaller T_B or ε_B gave a better match between our numerics and asymptotics, as expected.

For $T_B > 1$, the temperature must first exceed T_B before any chain-branching, if at all, can take place. Our numerical calculations showed that the larger T_B is, the more the reaction looks like a thermal explosion since the branching rate R_B becomes more suppressed and branching crossover occurs much later when little fuel remains. For the larger values of T_B, R_B is so small that the only reactions which take place are the initiation reaction which converts fuel into chain carriers and the exothermic termination reaction which quickly converts any chain carriers produced into stable products, and hence no build-up of chain carriers is possible. Increasing T_B to higher values yields little or no change in the solutions. The asymptotic study uncovered the following leading order expression for the fuel ignition time (i.e. the time the thermal explosion occurs):

$$t = t_{ign} = \frac{\varepsilon_I}{\beta}\exp\left[\frac{1}{\varepsilon_I}\left(1 - \frac{1}{T_I}\right)\right],$$

which confirms the exponential dependency of the ignition time on ε_I. The absence of T_B in this expression implies that branching plays no part in determining the leading order ignition time, and hence the $T_B > 1$ case mimics the one-step thermal model in this regard.

Further analysis of the asymptotic solutions for both the $T_B < 1$ and $T_B > 1$ cases revealed that these solutions are only valid when $T_B - 1 = O(1)$ (see figure 2.17). Parameter matching between the leading order asymptotic solutions of this and two other

commonly used models later verified that, assuming $T_B - 1 = O(1)$, the solutions of the three-step model are indeed well described by the one-step thermal system for $T_B > 1$ and the two-step chain-branching system for $T_B < 1$.

With piston-driven shock-induced ignition in a tube, gas dynamics (through the Euler equations) coupled with the same chemical equations as used in the homogeneous study now govern the evolution of the solution. Again, the crucial parameter is T_B as compared to the initial shock temperature (unity in our scalings), which, for chain-branching values, is analogous to the parameter k used by Sharpe [21] that controls the ratio of the length of the induction zone to that of the chain-termination zone. For the chosen set of parameters, high resolution numerical simulations show that the $T_B = 0.5$ case (a strongly chain-branching value) results in a compression wave, formed from the pressure disturbances originating in the exothermic reaction zone, which travels towards the shock at the local sound speed, overtakes the subsonic chain-branching ignition point and eventually reaches the shock before it is able to develop into a secondary shock. This situation is therefore very much like the small k case in Sharpe's two-step chain-branching study [21], but is completely unlike what usually occurs with a one-step scheme, where a locally-supersonic weak detonation always forms and then a secondary shock develops soon after (unless the activation energy is rather low). Slightly increasing T_B results in the formation of a secondary shock, but such a shock collides with the leading shock before it can develop into a strong detonation. Larger values of T_B mean that the secondary shock forms much earlier and much closer to the piston (a similar effect is observed when increasing Sharpe's k parameter [21]). For $T_B = 1.0$, we begin to observe characteristics typical of one-step thermal models, in particular the appearance of a supersonic weak detonation and also the induction zone buildup of products and associated heat release. Although a secondary shock subsequently forms, it cannot develop into a strong detonation before colliding with the leading shock. For $T_B = 1.2$ however, the induction zone is

more thermal, and a strong CJ detonation is born before shock collision, as is typically witnessed with one-step thermal schemes.

When using a contact surface, as opposed to a piston, to drive the shock, acoustic leakage at the contact surface means that the reaction ahead cannot be as vigorous as it would with a piston-driven system. A two-step early time asymptotic analysis confirms that, in a chain-branching system, the early time ignition point moves at a slightly slower speed with the contact-driven shock. Numerical solutions of the three-step model show that, with the contact-driven case, the overall temperatures and pressures are lower at the various stages of the evolution, and that the evolution therefore takes place on a longer time scale, e.g. the development of a secondary shock will be delayed or may not even have enough time to develop at all. This leakage of energy, however, has its greatest effect on systems that are thermal rather than chain-branching in nature. Since the induction zone releases heat in thermal regimes, acoustic leakage at the contact surface takes place very early on while there is still ample fuel there (in contrast, acoustic leakage in chain-branching systems can only occur after induction zone, which is thermally neutral). Therefore, we noticed in our $T_B = 1.2$ case that the temperature maximum, and consequently the fuel fraction minimum, moved away from the contact into the interior of the reactive gas, similarly to what occurs with one-step thermal models, and that thermal runaway was delayed as compared to the piston-driven case.

5.2 Further work

Our three-step model assumes that the initiation and branching reactions are thermally neutral, with all the heat release occurring in the termination reaction. This is a reasonable assumption since, for example, only 5% of the overall heat release in Hydrogen-Oxygen systems occurs in the branching reactions. In actual fact, the overall initiation and branching reactions in Hydrogen-Oxygen systems are slightly endothermic, and so a

more accurate model can be devised by accommodating this fact. One would intuitively expect that, due to the consequent drop in temperature in the induction zone, the time to ignition would be slightly delayed and the maximum achievable temperature would slightly decrease. Also due to this endothermicity, we would expect a slight evolution in the induction zone even when using chain-branching values of T_B. It would be especially interesting to see the outcome of the contact-driven shock case to see what effect this would have on the gas-dynamical evolution that results from acoustic leakage.

Possibilities for related work include looking into the direct initiation of detonations using the three-step model, as opposed to shock-induced detonations. The source of ignition would be a blast wave propagating into the surrounding reactive gas to generate a spherical CJ detonation if the source energy is sufficiently high. Such work would extend the work by Short and Sharpe [39]. Using our parameter matches, we could also perform a comparison of results from the three-step model with results from the one-step purely thermal model and the two-step purely chain-branching model.

Another scenario worth investigating is ignition due to an initial small spatial non-uniformity in temperature or fuel/chain carriers, and the role of T_B in such scenarios.

Appendix A

Extra details on working out for $T_B < 1$

A.1 Determining leading order gauge functions for section 2.3.2

Let

$$f = 1 + gF, \qquad y = 0 + hY, \qquad T = 1 + k\theta, \qquad t = j\tau,$$

$$F,\ Y,\ \theta,\ \tau = O(1),$$

where the gauge functions g, h, k and j must be chosen for a leading order balance. The exponential factors in (2.10) and (2.11) become

$$\exp\left[\frac{1}{\varepsilon_I}\left(\frac{1}{T_I} - \frac{1}{1+k\theta}\right)\right] \sim \exp\left[\frac{1}{\varepsilon_I}\left(\frac{1}{T_I} - 1 + k\theta\right)\right] = e_I \exp\left(\frac{k\theta}{\varepsilon_I}\right)$$
$$\sim e_I\left(1 + \frac{k\theta}{\varepsilon_I}\right) \sim e_I,$$

$$\exp\left[\frac{1}{\varepsilon_B}\left(\frac{1}{T_B} - \frac{1}{1+k\theta}\right)\right] \sim \exp\left[\frac{1}{\varepsilon_B}\left(\frac{1}{T_B} - 1 + k\theta\right)\right] = e_B \exp\left(\frac{k\theta}{\varepsilon_B}\right)$$
$$\sim e_B\left(1 + \frac{k\theta}{\varepsilon_B}\right) \sim e_B.$$

Hence, to leading order

$$\frac{g}{j}\frac{dF}{d\tau} = -e_I - hYe_B \qquad \Rightarrow h = \frac{e_I}{e_B},\ \frac{g}{j} = e_I$$

(we cannot neglect the first term on the right-hand side, since it represents the vital initiation reaction),

$$\frac{h}{j}\frac{dY}{d\tau} = e_I + hYe_B - hY \qquad \Rightarrow \frac{h}{j} = e_I \Rightarrow j = \frac{1}{e_B} \Rightarrow g = \frac{e_I}{e_B},$$

$$\frac{k}{j}\frac{d\theta}{d\tau} = \beta hY \qquad \Rightarrow k = hj = \frac{e_I}{e_B^2}.$$

A.2 Non-uniformity "initiation=branching" for section 2.3.2

$$\exp\left[\frac{1}{\varepsilon_I}\left(\frac{1}{T_I}-1\right) - \frac{1}{\varepsilon_B}\left(\frac{1}{T_B}-1\right) + \frac{1}{\varepsilon_I}\left(1-\frac{1}{1+\frac{1}{e_B}\hat{\theta}}\right) - \frac{1}{\varepsilon_B}\left(1-\frac{1}{1+\frac{1}{e_B}\hat{\theta}}\right)\right] = O(1)$$

$\Rightarrow$

$$\frac{1}{\varepsilon_I}\left(\frac{1}{T_I}-1\right) - \frac{1}{\varepsilon_B}\left(\frac{1}{T_B}-1\right) + \frac{1}{\varepsilon_I}\left(1-\frac{1}{1+\frac{1}{e_B}\hat{\theta}}\right) - \frac{1}{\varepsilon_B}\left(1-\frac{1}{1+\frac{1}{e_B}\hat{\theta}}\right) \to 0$$

$\Rightarrow$

$$\frac{1}{\varepsilon_I T_I} - \frac{1}{\varepsilon_B T_B} - \frac{1}{\varepsilon_I\left(1+\frac{1}{e_B}\hat{\theta}\right)} + \frac{1}{\varepsilon_B\left(1+\frac{1}{e_B}\hat{\theta}\right)} \to 0$$

$\Rightarrow$

$$\left(\frac{1}{\varepsilon_B}-\frac{1}{\varepsilon_I}\right)\left(\frac{1}{1+\frac{1}{e_B}\hat{\theta}}\right) \to \frac{1}{\varepsilon_B T_B} - \frac{1}{\varepsilon_I T_I}$$

$\Rightarrow$

$$1+\frac{1}{e_B}\hat{\theta} \to \frac{\frac{1}{\varepsilon_B}-\frac{1}{\varepsilon_I}}{\frac{1}{\varepsilon_B T_B}-\frac{1}{\varepsilon_I T_I}} = \frac{\frac{\varepsilon_I}{\varepsilon_B}-1}{\frac{\varepsilon_I}{\varepsilon_B T_B}-\frac{1}{T_I}} = \frac{1-\frac{\varepsilon_I}{\varepsilon_B}}{\frac{1}{T_I}-\frac{\varepsilon_I}{\varepsilon_B T_B}}$$

$\Rightarrow$

$$\hat{\theta} \to \left(\frac{1 - \frac{\varepsilon_I}{\varepsilon_B}}{\frac{1}{T_I} - \frac{\varepsilon_I}{\varepsilon_B T_B}} - 1 \right) e_B = \lambda e_B \text{ (λ is the } O(1) \text{ bracketed factor)}$$

but (2.45) then gives that $\hat{\tau} = O(e_B)$.

Bibliography

[1] M.A. Birkan and D.R. Kassoy, *The Unified Theory for Chain Branching Thermal Explosions with Dissociation-Recombination and Confinement Effects.* Combustion Science and Technology 44:223–256, 1984.

[2] B.F. Gray and C.H. Yang, *On the unification of the thermal and chain theories of explosion limits.* J. Phys. Chem. 69:2747–2750, 1965.

[3] J.A. Barnard and J.N. Bradley, *Flame and Combustion.* J.W. Arrowsmith Ltd, Bristol, Second Edition, 1985.

[4] R.A. Strehlow, *Combustion Fundamentals.* McGraw-Hill, 396–405, 1984.

[5] G. Singh and J.F. Clarke, *Transient phenomena in the initiation of a mechanically driven plane detonation.* Proc. R. Soc. Lond. A 438:23–46, 1992.

[6] J.W. Dold and A.K. Kapila, *Comparison Between Shock Initiations of Detonation Using Thermally-Sensitive and Chain-Branching Chemical Models.* Combustion and Flame 85:185–194, 1991.

[7] M. Short and J.J. Quirk, *On the nonlinear stability and detonability limit of a detonation wave for a model three-step chain-branching reaction.* J. Fluid Mech. 339:89–119, 1997.

[8] M. Short, A.K. Kapila and J.J. Quirk, *The chemical-gas dynamic mechanisms of pulsating detonation wave instability.* Phil. Trans. R. Soc. Lond. A 357:3621–3637, 1999.

[9] N.N. Semenov, *Chemical Kinetics and Chain Reactions.* Oxford University Press, 1935.

[10] D.A. Frank-Kamenetskii, *Diffusion and heat Exchange in chemical kinetics.* Princeton University Press, Princeton, 1955.

[11] A.K. Kapila, *Homogeneous branched-chain explosion: Initiation to completion.* Journal of Engineering Mathematics 12:221–235, 1978.

[12] D.R. Kassoy, *Extremely rapid transient phenomena in combustion, ignition and explosion.* SIAM-AMS Proceedings 10:61–72, 1976.

[13] L.L. Bonilla, A.L. Sánchez and M. Carretero, *The Description of Homogeneous Branched-Chain Explosions with slow Radical Recombination by Self-Adjusting Time scale.* SIAM J. APPL. MATH. 61 (2):528–550, 2000.

[14] P.A. Blythe, M. Short and A.K. Kapila, *Homogeneous ignition for a three-step chain-branching reaction model.* In review with the Journal of Engineering Mathematics since Nov 17, 2004.

[15] A.G. Gaydon and I.R. Hurle, *The Shock Tube in High-Temperature Chemical Physics.* Chapman and Hall Ltd., 1963.

[16] L.D. Landau and E.M. Lifshitz, *Fluid Mechanics 2nd edition. Course of Theoretical Physics, Volume 6.* Pergamon Books Ltd, 1987.

[17] The Centre for Explosion Studies, *http://neumann.dph.aber.ac.uk/research/research.html.* University of Wales, Aberystwyth.

[18] G.E. Abouseif and T.Y. Toong, *On direct initiation of gaseous detonations.* Combustion and Flame 45:39–46, 1982.

[19] T.L. Jackson and A.K. Kapila, *Shock-Induced Thermal Runaway.* SIAM J. APPL. MATH. 45 (1):130–137, 1985.

[20] J.W. Dold, A.K. Kapila and M. Short, *Theoretical Description of Direct Initiation of Detonation for One-Step Chemistry.* Dynamic Structure of Detonation in Gaseous and Dispersed Media 109–141, A.A. Borissov (ed.), Kluwer Academic Publishers, 1991.

[21] G.J. Sharpe, *Shock-induced ignition for a two-step chain-branching kinetics model.* Physics of Fluids 14:4372–4388, 2002.

[22] G.J. Sharpe and M. Short, *Shock-induced ignition of thermally sensitive explosives.* IMA Journal of Applied Mathematics 69:493–520, 2004.

[23] P.A. Urtiew and A.K. Oppenheim, *Detonative ignition induced by shock merging.* Eleventh Symposium (International) on Combustion, The Combustion Institute 1966:665–670, 1966.

[24] M. Short and J.W. Dold, *Unsteady gasdynamic evolution of an induction domain between a contact surface and a shock wave. I: Thermal runaway.* SIAM J. APPL. MATH. 56 (5):1295–1316, 1996.

[25] C.J. Parkins, *Shock-generated ignition. Newtonian asymptotics for the induction domain between a contact surface and a shock.* SIAM J. APPL. MATH. 61 (2):701–729, 2000.

[26] R.L. Gustavsen, S.A. Sheffield, R.R. Alcon and L.G. Hill, *Shock Initiation of New and Aged PBX 9501 Measured with Embedded Electromagnetic Particle Velocity Gauges.* 23rd Aging, Compatibility and Stockpile Stewardship Conference, 14 Nov 2000–16 Nov 2000, Livermore, CA (United States), 2000.

[27] R.L. Gustavsen, S.A. Sheffield and R.R. Alcon, *Shock ignition of "virgin" and "recycled" PBX 9502 measured with embedded electromagnetic particle velocity gauges.* CP706, Shock Compression of Condensed Matter - 2003:973–976, American Institute of Physics, 2004.

[28] W. Fickett and W.C. Davis, *Detonation: Theory and Experiment.* Dover Publications, 1979, reprinted 2001.

[29] A.K. Kapila, *Asymptotic treatment of chemically reacting systems.* Pitman Advanced Publishing Program, 1983.

[30] D.R. Kassoy, *The supercritical spatially homogeneous thermal explosion: initiation to completion.* Quart. J. Mech. Appl. Math. 30 (2):71–89, 1997.

[31] C. Campbell and D.W. Woodhead, *The ignition of gases by an explosion wave. Part I. Carbon monoxide and hydrogen mixtures.* J. Chem. Soc. 1927:1572–1578, 1927.

[32] G.J. Sharpe and S.A.E.G. Falle, *One-dimensional nonlinear stability of pathological detonations.* J. Fluid Mech. 414:339–366, 2000.

[33] J.F. Clarke and N. Nikiforakis, *Remarks on diffusionless combustion.* Phil. Trans. R. Soc. Lond. A 357:3605–3620, 1992.

[34] J.F. Clarke, D.R. Kassoy and N. Riley, *On the direct initiation of a plane detonation wave.* Proc. R. Soc. Lond. A 408:129–148, 1986.

[35] J.F. Clarke, D.R. Kassoy, N.E. Meharzi, N. Riley and R. Vasantha, *On the evolution of plane detonations.* Proc. R. Soc. Lond. A 429:259–283, 1990.

[36] N. Nikiforakis and J.F. Clarke, *Numerical Studies of the Evolution of Detonations.* Mathl. Comput. Modelling 24 (8):149–164, 1996.

[37] M. Short and J.W. Dold, *Weak detonations, their paths and transition to strong detonation.* Combust. Theory Modelling 6:279–296, 2002.

[38] J.W. Meyer and A.K. Oppenheim, *On the shock-induced ignition of explosive gases.* Thirteenth Symposium (International) on Combustion, The Combustion Institute 1971:1153–1164, 1971.

[39] M. Short and G.J. Sharpe, *Failure and ignition limits of three-step chain-branching detonations.* Submitted, 2004.